Spring 2020

Highly Transmissive Scalable Colored Coatings for Architectural Photovoltaic Panels

Akbar Ali Syed
Old Dominion University, asyed002@odu.edu

HIGHLY TRANSMISSIVE SCALABLE COLORED COATINGS FOR ARCHITECTURAL PHOTOVOLTAIC PANELS

by

Akbar Ali Syed

B.Tech., ECE, April 2017, V. R Siddhartha Engineering College

A Thesis Submitted to the Faculty of
Old Dominion University in Partial Fulfillment of the
Requirements for the Degree of

MASTER OF SCIENCE

ELECTRICAL AND COMPUTER ENGINEERING

OLD DOMINION UNIVERSITY
May 2020

Approved by:

Dr. Hani Elsayed Ali (Director)

Dr. Helmut Baumgart (Member)

Dr. Gon Namkoong (Member)

ABSTRACT

HIGHLY TRANSMISSIVE SCALABLE COLORED COATINGS FOR ARCHITECTURAL PHOTOVOLTAIC PANELS

Akbar Ali Syed
Old Dominion University, 2020
Director: Dr. Hani Elsayed Ali

Highly transmissive coatings were developed by fabricating thin films using SiO_2 and SiO_2/TiO_2 core/shell nanoparticles on glass substrates and on the photovoltaic cell glass covers. This coating is to maintain an attractive color appearance of the exterior surface for architecturally integrated photovoltaics and can be coated on fabricated photovoltaic panels. The color and optical properties of the nanoparticle coating was investigated for different nanoparticle diameters of 200-400 nm for SiO_2 nanoparticles and core/shell nanoparticles having SiO_2/TiO_2 structure with 300 ± 11 nm diameter, and $SiO_2/TiO_2/SiO_2$ structure with 506 ± 13 nm diameter. We describe controlled coating of glass surfaces by the nanoparticles to form an ordered structure on the surface with selective reflection and high transmission in the photon energy range needed for photovoltaic panels, while reflecting a selected part of the spectra to achieve a certain color. The effect of the concentration of colloidal solution based on the size of nanoparticles was examined and properties of the coating fabricated on glass slides were studied. An optical spectrometer was used to measure the transmission and reflectance of the coating. Scanning electron microscopy was used to observe the stacking of the nanoparticles, while atomic force microscopy was used to determine the roughness of coating deposited on glass slides.

The nanoparticle coating was fabricated on Si photovoltaic cells to observe the effect of the coating on the solar cell performance using a solar cell simulator. The solar cells coated using commercial 200 nm, 300 nm, and 400 nm nanoparticles showed blue, pink, and green colors

respectively, and the solar cells coated using $SiO_2/TiO_2/SiO_2$ nanoparticles showed pink color. The solar cell power loss observed is 5.47 %, 15.61 %, and 10.73 % for coatings done using 200, 300, and 400 nm particles respectively, and ~ 11. 01 % power loss was observed with three coats of $SiO_2/TiO_2/SiO_2$ nanoparticles.

This thesis is dedicated to my parents, siblings, friends, and colleagues whose continuous support and encouragement has helped to guide and motivate me throughout this process.

ACKNOWLEDGEMENTS

I would like to express my acknowledgement to several people, without whose continuous support and encouragement it was impossible for me to travel this long journey.

First and foremost, I express my whole-hearted gratitude to Dr. Hani E. Elsayed-Ali, my M.S. supervisor for his guidance and motivation throughout my graduate studies. I thank him for offering me the opportunity to work under his supervision and conduct research that ultimately concluded into this thesis report. He has taught me the methodology to carry out the research and present the research works as clearly as possible. It was a great privilege and honor to work under his guidance.

I am grateful to Dr. Helmut Baumgart, and Dr. Gon Namkoong for their willingness to serve on my thesis committee and spending their valuable time for reviewing the thesis.

A special thanks to Dr. Gon Namkoong for allowing me to work on solar simulator without which my thesis would be incomplete. I would like to offer special thanks to Tanzila Tasnim Ava for allocating her valuable time to help and train me on solar cell testing.

I would like to offer special thanks to Dr. Wei Cao for training and assistance that makes me able to work on various instruments and enlightening me the first glance of research instruments.

I wish to extend a heartfelt thank you to my parents, Syed Abdul Khader Jelani and Syeda Jasmine Sultana for their support and everlasting encouragement. Your inspiration always helps me in my professional and personal life. A big thank you to my siblings, Syeda Gousia Sultana and Syeda Sarah for their encouragement and persistent belief in me. I'm grateful to my brother-in-law, Siraj Ahmed for his intense support and advice. I'm truly blessed to have all of you in my life and I love you all immensely.

Table of contents

Page

LIST OF TABLES

LIST OF FIGURES

Figure Page

Figure Page

CHAPTER 1

INTRODUCTION

1.1 ARCHITECTURAL SOLAR CELLS

Building-integrated photovoltaics (BIPV) are solar cells used in parts of the building envelopes, such as traditional building material, roofs, skylights and facades. These are increasingly integrated as a main or ancillary power source into the construction of new buildings, while existing buildings may also be retrofitted with BIPV modules [1]. With the increasing need for solar energy, photovoltaic panels can be integrated into the building design for which photovoltaics can be made aesthetically appealing. The solar elements are appealingly and clearly used as architectural components. This can only be done if the creation of the photovoltaic system is part of the building's design.

Architectural photovoltaic can be used in many applications, such as in the elevation of buildings rather than on the rooftop. Other uses of colored photovoltaics are in automobiles and devices such as cell phones and solar cells used for streetlights. For most current solar cells, its incorporation in the building siding is still unusual due to the black or dark blue color of the absorber [2].

1.2 CURRENT TECHNOLOGIES IN BUILDING ARCHITECTURAL PHOTOVOLTAICS

The colored PV is manufactured with multilayer interference coating tailored to reflect a narrow band portion of the spectrum [3]. In the field of innovative solar solutions (ISSOL) under Kromatix™, commercial PV panels with color treated glass have been launched [4]. Its approach consists in applying a multi-layer coating on inner side of a glass window by low pressure plasma processes that reflects a narrow spectral band of visible light, while the outer side of the glass is treated to prevent glare reflections resulting in a diffuse surface encapsulating solar cell in this

glass window. Different colors such as grey, blue, bluish-green, bronze, and brass are currently available with 90 ± 1 %, 88 ± 1 %, 88 ± 1 %, 89 ± 1 %, and 86 ± 1 % solar transmittance respectively [5]. These coatings are expensive to produce and show narrow angle of reflection.

The Swiss firms SOLAXESS and ISSOL are manufacturing white solar cells and other colored solar cells. White color solar cells are achieved using tempered laminated glass and contain 6 layers of different materials on top of the solar cells – back encapsulate for laminated glass, laminated glass, back encapsulate for reflector, reflector, front encapsulate for reflector, and a last layer of Ethylene tetrafluoroethylene (ETFE). Other colors are achieved by adapting the combination of the filters on the micro-structured surface [6]. These solar cells use high-efficiency single-crystalline silicon (Si) solar cells, which are considerably more expensive than the polycrystalline silicon solar cells or copper indium gallium selenide (CIGS) solar cells. In standard test conditions, this product has an efficiency of 90 watts peak per square meter (Wp / m_2): irradiance of 1000 W / m_2, 25° C and AM 1.5. In comparison to commercial, crystalline Si solar cells that produce 215 Wp / m_2 in standard terms, this approach suffers from reduced efficiency reported with 40% loss of efficiency.

Recently, solar cells with a bright-green color were developed based on silicon heterojunction integrated light scattering dielectric nano-scatterer arrays. In this approach, dense arrays of crystalline silicon nanocylinders were made onto module cover slides using substrate-conformal soft-imprint lithography [7]. This is a promising technology but requires integration of the nano-scatters with the solar cell at the significant cost of lithography and several fabrication steps. Colored PV were produced by encapsulating the PV in a colored semitransparent thin film, which results in low efficiency [8]. Another approach of coating the solar cell with assembled Ag plasmonic structures was discussed, where monocrystalline solar cells were used for the

fabrication. Thin films of Ag were deposited on the solar cell using DC sputtering and thermally annealed at 300° C to convert the thin film into coating of Ag nanoparticles [9]. This approach scatters light at narrow band and suffers from ohmic dissipation in the nanoparticles.

In our work, we demonstrate optical coating using silica and multi-shell nanoparticles to provide an opaque colored appearance but transmissive coating. This coating can be applied similar to that of paint and can be made into any color depending on the size of nanoparticles used. In this work we have used commercially available 200, 300, and 400 nm silica particles to achieve blue, pink, and green colors respectively. Also, an approach to attain optical coating using multi-shell nanoparticles with 300 ± 11 nm, and 506 ± 13 nm diameters are used to achieve blue, and pink colors respectively.

1.3 THESIS OBJECTIVES AND ORGANIZATION

The aim of this thesis is to develop highly-transmissive colored thin films using the scalable and cost-effective fabrication technique of roll-to-roll coating of silica nanoparticles and SiO_2/TiO_2 multi-shells. Blue, green, and pinkish-violet colors are fabricated using commercial nanoparticles of 200, 400, and 300 nm diameters respectively. Also, blue and pink colors are fabricated using multishell nanoparticles with increasing number of shells SiO_2, SiO_2/TiO_2, and $SiO_2/TiO_2/SiO_2$ respectively.

In Chapter 2, an overview of physics behind structural color is described with introduction explaining structural colors occurring in nature and efforts to develop them, thin film and multilayer interference, effect of photonic crystal structure in formation of structural color with based on Braggs and Mie theories.

In Chapter 3, optimization of solution is discussed for two groups of solutions, each with three different concentrations, one containing viscosity enhancing reagent, and the other without

any viscosity enhancing reagent to compare the stacking of nanoparticles and color formed in each case.

In Chapter 4, the optimized solution chosen is used to fabricate thin films using different diameters, and to study the optical losses caused by increase in number of layers on glass slides and solar cells.

In Chapter 5, the performance of coated solar cells is tested and compared with the performance of uncoated solar cells to check the total power loss caused due to fabrication of thin film on solar cell covers.

In Chapter 6, multi-shelled nanoparticles are deposited, and the effect of growth of TiO_2 shell is studied on the core, core/shell, and core/shell/outer shell terminated with SiO_2 showing the optical results and loss when fabricated on glass slide, and on solar cell.

Chapter 7 covers conclusion and a summary of the work along with the future scope of developing colored photovoltaics using SiO_2 and multi-shelled nanoparticles.

CHAPTER 2

STRUCTURAL COLOR

2.1 INTRODUCTION

The structural color in nature emerges mainly from the optical interference of light, which are reflected or refracted in regularly textured materials. Owing to the Bragg interference, natural opals consisting of stacked silica spheres acquire their characteristic iridescence [10]. Sub-micrometer sized structures reflect or scatter light so that waves of certain frequencies can interfere constructively in forming color. Opals naturally formed consist of a periodic set of monodisperse silica (SiO_2) spheres with sub-micrometer scale diameters. Examples of the naturally occurring structural colors, are morpho-butterflies, bird feathers, scales of longhorn beetles [11-15].

Considering one of the best examples for structural coloring in nature, 'Morpho-butterfly', the wings of grown M. butterfly contain alternately arranged scales of slender shapes which causes light interference within the lamella on the scale. The scales have normal and slightly slender shapes or irregular ridges which cancels out further interferences of light and forms diffuse and uniformly-distributed reflected light. Also, the multi-layers present in lamella are a reason for high reflectivity [16].

2.2 THIN FILM AND MULTILAYER INTERFERENCE

Thin film interference

Let us consider a light wave is incident on a surface having refractive index n_2 and n_3 and the film thickness is *t*. Let the sample be in air with refractive index n_1. Now, the light reflected from any of these layers might interfere with the light that has already reflected from other layers [17]. Fig. 2.1 shows a schematic of a light wave incident on a film. Here, the incident light is only partially reflected from the top surface and the remainder light enters the film and it is partially

reflected from the bottom surface and this light will emerge from the top of the film and would interfere with the light ray reflected from the top.

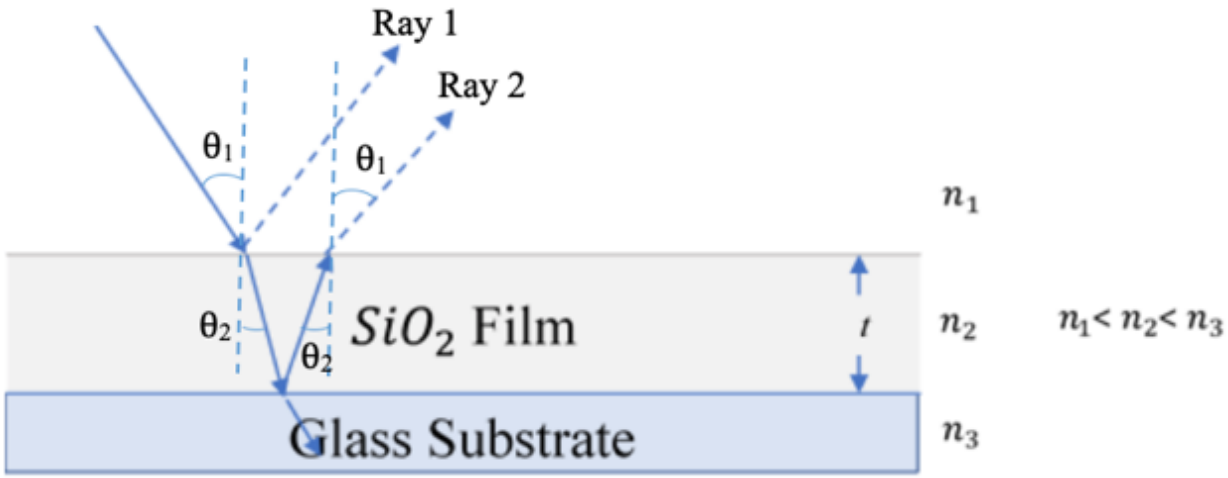

Fig. 2.1. Schematic showing the interaction of light ray from air to film and to glass substrate showing the transmission, refraction and reflection.

In Fig. 2.1, the waves that are reflected from the surface may or may not undergo phase shift depending upon the index of refraction of the two layers. If the index of refraction before the interface is lower than that of index of refraction after the interface, then there is 180° phase shift [17]:

$$n_1 < n_2 \qquad \Delta\emptyset = 180° \qquad \text{(Eqn. 2.1)}$$

When the index of refraction before the interface is higher than that of index of refraction after the interface then there is no phase shift [17]. The two rays reflected from the bilayer travel different distances. The extra distances travelled *d* is [18]:

$$t = d / \cos\theta \quad \text{for light ray travelling from front to back surface} \qquad \text{(Eqn. 2.2)}$$

$$2t = 2d / \cos\theta \quad \text{for light ray travelling round trip} \qquad \text{(Eqn. 2.3)}$$

For, the extra path travelled by the wave is:

$$\lambda_{film} = \frac{\lambda_{vacuum}}{n} \quad \text{(Eqn. 2.4)}$$

where *n* is the index of refraction of the material in which the light ray travels.

From Fig. 2.1, we can write Eqn. 2.4 as;

$$\Delta wavelength = 2tn_2/(\lambda) \quad \text{(Eqn. 2.5)}$$

where, Δwavelength is the number of extra wavelengths travelled [17]. For the destructive interference to occur, the rays must be 180° out of phase, and should not undergo any phase shift in case of constructive interference. For destructive interference to occur the number of waves difference must be 1/2 [18]:

$$t = \frac{\lambda}{4n_2} \quad \text{(Eqn. 2.6)}$$

Eqn. 2.6 gives the relation for destructive interference which may occur when the difference is 1.5, 2.5, 3.5, ….. :

$$t = \frac{(m+\ 1/2)}{2}\frac{\lambda}{n_2}, \quad m = 0,1,2,3\ldots \quad \text{(Eqn. 2.7)}$$

Similarly, constructive interference occurs when the difference between the waves is of integer multiples of wavelength:

$$t = \frac{m\lambda}{2n_2}, \quad m = 0,1,2\ldots. \quad \text{(Eqn. 2.8)}$$

For antireflective coatings, the reflection is minimum. To maximize the amount of destructive interference, the amplitudes of ray 1 and ray 2 must be same [17]. For non-reflective coatings the coating material generally has refraction index less than that of glass, thus having $\lambda/2$ shift [19]. The minimum film thickness is:

$$t = \frac{1}{4}\frac{\lambda}{n_2} \quad \text{(Eqn. 2.9)}$$

Multilayer interference:

Multilayers are stacks of different thin films. If we consider two layers A and B with different thicknesses and refractive indices, then if the refractive index of B is greater than refractive index of A it can be thought of as similar to antireflection coatings and the phase shift will be 180° [20]. For the multilayers, the transmission and reflection can be calculated using transfer matrices by using a numerical iterative method [21]. If we consider a multilayer film, then the theory uses total electric and magnetic fields and boundary conditions of each layer in a transfer matrix to determine the reflection from coated surface [22, 23, 24]. The total reflection can be given as [22, 25]:

$$2(n_A d_A cos\theta_A + n_B d_B cos\theta_B + n_C d_C cos\theta_C) = m\lambda \qquad \text{(Eqn. 2.10)}$$

n_A, n_B, n_C and d_A, d_B, d_C are the refractive indices and thicknesses of films A, B, C respectively. The total reflection can be given in terms of refractive indices as;

$$R = \frac{n_A n_C n_B^2 - (n_A n_C)^2}{n_A n_C n_B^2 + (n_A n_C)^2} \qquad \text{(Eqn. 2.11)}$$

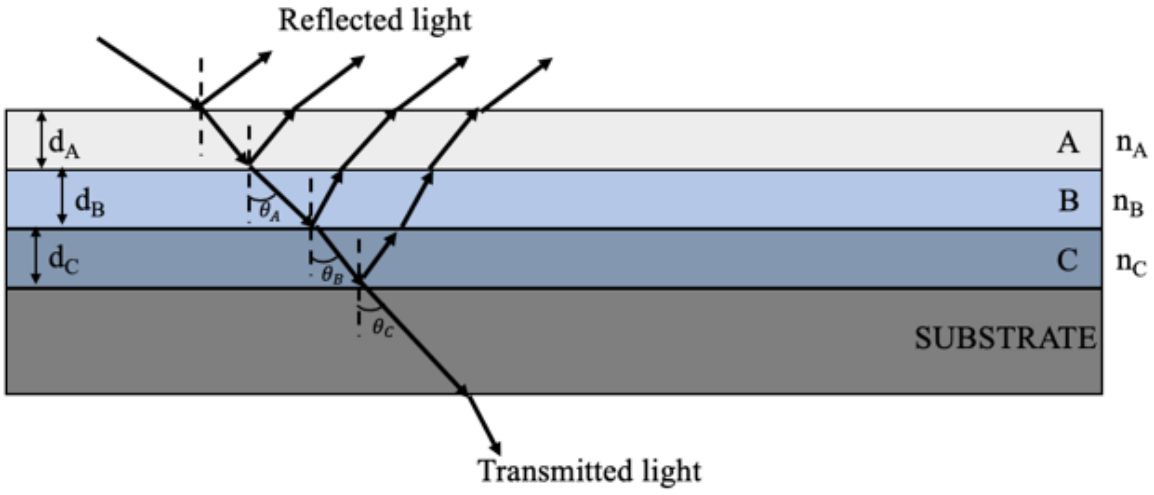

Fig. 2.2. Schematic showing the multilayer interference of light ray passing through three different films A, B, and C having refractive indices $n_A, n_B,$ and n_C respectively.

Eqn. 2.11 gives the total reflection of the multilayer film, without considering the absorption. The addition of thin films as stacked on one another to form multilayer films causes either narrowband or broadband multilayers. For the narrowband multilayers, the reflected light consists of narrow range of frequencies and would depend on the base layer to produce bright light or a white color of reflected light depending upon the absorption of light in base layer. If the base layer is dark or if it is consistently such that it can absorb all the light incident on it then it would produce bright colors [21].

2.3 PHOTONIC CRYSTALS

The periodical modulation of the refractive index of a dielectric creates a restricted gap in the structure of the photonic band which excludes optical modes within a limited frequency range. Such photonic crystals are attractive optical materials to monitor the flow of light and manipulate it. They can be used as reflective coatings, paint and ink color pigments, light propagation waveguides, and highly reflective mirrors in laser cavity [26].

The formation of optical band gaps requires contrasting refractive indices of the various components [27]. Propagation of photons in the photonic materials is controlled due to the periodic modulation in dielectric constant allowing for manipulation and control the light in three dimensions of space [28-30].

It remains a major challenge to use modern micro-lithography to produce three-dimensional (3D) periodic structures with feature sizes equivalent to the wavelength of the visible light. An alternative approach is to make 3D photonic band gap crystals. Sphere ranges from a few nano to a few hundred micrometers of monodispersed particles. The resulting highly ordered, regular structures can diffract light strongly with a stop band in their transmission spectrum when these spherical particles are assembled into 3D crystalline arrays [31]. The position of the stop

band can be tuned by changing the sizes of nanoparticles, and this tuning can range from UV to near IR [32]. Forbidden frequencies for the transmission of light in the photonic crystal, called photonic bandgaps, are induced by Mie scattering and Bragg's interference [33]. A commonly used way to attain 3D photonic crystals, is by self-assembly of sub-micrometer particles, which have the ability to prohibit propagation of light in UV and IR regions and allow them to exhibit structural colors. The diffraction of a Bragg stack can be described by the Bragg–Snell law which holds for normal incidence and non-absorbing materials [26]:

$$m\lambda = 2(n_l d_l + n_h d_h) \qquad \text{(Eqn. 2.12)}$$

where *m* is the diffraction order, n_l and n_h are the refractive indices of the low- and high-refractive-index materials, and d_l and d_h are the respective thicknesses. The reflectivity ∂ of the Bragg stack depends on the contrast of refractive index and the number of bilayers *N* comprising the stack [26]:

$$\partial = \left[\frac{n_0 - n_s(n_l/n_h)^{2N-2}}{n_0 + n_s(n_l/n_h)^{2N}}\right]^2 \qquad \text{(Eqn. 2.13)}$$

where n_0, and n_s are the refractive indices of surrounding medium and substrate respectively. If the central wavelength of photonic band is λ_0, then photonic stop band can be calculated as [26]:

$$\Delta\lambda_0 = \frac{4\lambda_0}{\pi} arcsin \frac{(n_h - n_l)}{n_h + n_l} \qquad \text{(Eqn. 2.14)}$$

From the Equations 2.13 and 2.14, the formation of 1D colloidal crystal depends on properties of individual particles and also the surroundings. For 3D colloidal crystal, it diffracts a specific wavelength as determined by Bragg's law:

$$m\lambda = 2nx\ sin\text{ø} \quad \text{(Eqn. 2.15)}$$

where m is the order of diffraction, λ is the wavelength of incident light, *n* is the mean refractive index of the system composed of colloids and voids, *x* is the spacing between the planes in lattice, and *ø* is angle of incident light. The colorful appearances of these materials are mainly ascribed to the interferences and reflections, which after a little mathematics gives rise to the Bragg-Snell equations [34].

$$\lambda = 2D(n_{eff}^2 - cos^2\text{ø})^{1/2} \quad \text{(Eqn. 2.16)}$$

where λ is the wavelength of the reflected light, n_{eff} is the average refractive index of the constituent photonic materials, *D* is the distance of diffracting plane spacing, and *ø* is the Bragg angle of incidence of the light falling on the nanostructures [34].

A common example is the Bragg quarter-wave stack, in which the high and low-refractive index areas allow the incident light interference to be both constructive and destructive, producing a wavelength-centric band of reflectiveness. When their stopbands fall into the visible range, the films show color [35]. Typical Bragg quart-wave reflectors consist of alternating stacks of the same optical thicknesses for high (n_h) and low (n_l) refractive index materials at some operating wavelength λ_0 [36].

$$n_l d_l = n_h d_h = \frac{\lambda_0}{4} \quad \text{(Eqn. 2.17)}$$

2.3.1 BRAGGS AND MIE THEORY

Mie and Bragg scattering are important optical phenomena, consisting of spherical or near-spherical particles, in photonic crystals. Mie's theory is used to explain the scattering of light from an isolated spherical object. In view of photonic crystal consisting of a periodic array of these

spheres, the interference of scattered waves results in the transformation of Mie into the Bragg scattering and the photonic belt structure is created [37].

Braggs law of diffraction describes constructive equation of interference, where *y* is the distance between particles planes, ø is the angle of the light of incident, m is the order of diffraction, and λ is the wavelength of the incident light. Combining Braggs law with Snell's law of refraction leads to Eqn. 2.19, where *y* is the distance between particle planes, n_{eff} is the mean effective refractive index, ø is the angle of incident light, m is the order of reflection, and λ is the wavelength of the reflected light. The reflected wavelength can also be calculated using the center-to-center distance *P* between the particles. The mean effective refractive index n_{eff} is defined as Eqn. 2.21, where $n_p$and n_m are the refractive indices of the particles and surrounding medium, respectively, and V_p and V_m are the respective volume fractions [37].

$$2y\,cos\text{ø} = m\,\lambda \qquad \text{(Eqn. 2.18)}$$

$$2y(n_{eff}^2 - \ sin^2\text{ø})^{\frac{1}{2}} = m\,\lambda \qquad \text{(Eqn. 2.19)}$$

$$\sqrt{(\tfrac{8}{3})}P\ (n_{eff}^2 - \ sin^2\text{ø})^{\frac{1}{2}} = m\,\lambda \qquad \text{(Eqn. 2.20)}$$

$$n_{eff}^2 = \ n_p^2 V_p + \ n_m^2 V_m \qquad \text{(Eqn. 2.21)}$$

The wavelengths λ of reflected light is determined by Bragg's law for periodic spheres with indices of refraction n_i of the spheres and the binding material: $\lambda = 2yn_{eff} = (\frac{8}{3})^2 P\ (\sum_i n_i\, V_i - \ sin^2\text{ø})^2$ where V_i is the volume fraction of the two materials, *y* is the characteristic spacing.

CHAPTER 3

EXPERIMENTAL DETAILS

Silica nanoparticles used in this study are monodisperse dry SiO_2 nanoparticles purchased from NANOCYM Inc., and three different diameters 200 nm, 300 nm, and 400 nm are studied which yielded bright blue, pinkish red, and green colors respectively. This study also includes multi-shelled nanoparticles having structures SiO_2/TiO_2, and $SiO_2/TiO_2/SiO_2$ with diameters 300 ± 11 nm, and 506 ± 13 nm respectively. The colloidal solution was prepared by mixing the nanoparticles in ethanol. The solution was then sonicated for 7 hours in a bath cooled by ice. About 0.025 µL of the prepared solution was dropped, using a pipette, on pre-cleaned soda-lime glass slide or on the solar cell glass cover and rolled using different wire wound roller rods. This process creates a thin coating with controlled thickness depending on the wire diameter and roller speed. Roll coating was performed using an Automatic Glass Bed Film Applicator (Part number AB3650) purchased from TQC Sheen. The samples were dried for 40-45 minutes and the same process was repeated for multiple coatings.

For the substrates coated using 200 nm particles, each coat gives three layers of nanoparticles and the coating thickness is about 600 nm. Similarly, for 300 nm each coat yields two layers (600 nm film thickness), and one single layer of closely packed nanoparticles with one coat of 400 nm nanoparticles (400 nm film thickness). The number of layers per each coat can be controlled either by diluting the solution by mixing more amount of ethanol (ml) or reducing the amount of nanoparticles by weight (mg) in the solution.

High resolution transmission electron microscopy (HRTEM, JEM-2100F, JEOL) was used to study the silica nanoparticle size uniformity and morphologies. The images of nanoparticles

from transmission electron microscope (TEM) were taken from the suspension that is drop coated on a TEM carbon-coated grid. The nanoparticle layer transmission and reflection spectra were characterized using a StellarNet BLACK-Comet spectrometer connected to a Nikon Ti-U inverted optical microscope where a pre-cleaned glass slide same as the one used to fabricate the thin films is used as reference.

For reflectance spectra, an aluminum mirror is used as the reference and another LED light source shines a light beam (~2 mm diameter) from the bottom; for which the sample is placed face down facing the light source to measure the reflectance. To make sure there are no secondary reflections, the glass slide after placing upside down is covered with a thick black cardboard sheet.

A thin layer of gold was deposited using polaron sputter coater equipment to make the samples conductive to study the layer morphology and stacking by a JEOL JSM-6060LV scanning electron microscope. An Oriel 150 W solar simulator equipped with an AM 1.5 spectral filter was used for solar cell testing under an irradiance of one sun. The solar cell I-V curves were obtained using a Keithley source meter and the data were collected using LabView software. The surface roughness of the samples was measured from the AFM images obtained by a Digital Instrument Dimension 3100 Atomic Force Microscope (AFM) operating in tapping mode.

CHAPTER 4

OPTIMIZATION OF COLLOIDAL SOLUTION

For the optimization of the colloidal solution only one size of nanoparticles (400 nm) was chosen to study the effects of viscosity on the assembly of the nanoparticles. As EtOH has low viscosity and is volatile in nature, the evaporation rate is too high (it takes the layer 10 s to dry at room temperature when deposited on a glass slide of 3 x 1 inch area), we add 0.2 % of poly-4-vinylphenol (PVPh) purchased from Sigma Aldrich (CAS ID 24979-70-2) by weight in solution to increase viscosity [9].

4.1 PREPARATION OF COLLOIDAL SOLUTION:

Two groups of solutions were mixed, one with 0.2 % PVPh, and the other without PVPh. Each group has three different dispersed concentrations of SiO_2/ EtOH in weight by volume. Table. 4.1 shows the basis of preparation of colloidal solution containing 0.2 % PVPh by weight in the solution, and Table. 4.2 shows the basis of preparation of colloidal solution without PVPh.

Table. 4.1. Preparation of colloidal solution with 0.2 % PVPh (Group 1).

Parameter	Silica nanoparticles by weight in the solution	0.2 % PVPh in solution	Ethanol
50g/L	50 mg	1.6 mg	1 ml
100g/L	100 mg	1.77 mg	1 ml
200g/L	100 mg	0.98 mg	0.5 ml

Table. 4.2. Preparation of colloidal solution without PVPh (Group 2).

Parameter	Silica Nanoparticles by weight in the solution	Ethanol
50g/L	50 mg	1 ml
100g/L	100 mg	1 ml
200g/L	100 mg	0.5 ml

After dispersing the solution according to the parameters in Table. 4.2., and Table. 4.3., the mixture was sonicated for 8 hours in an ice cooled sonic bath. The nanoparticles were spread on the surface of the substrate using roll-coating.

For a 3 x 1 in soda-lime glass slide ~0.025 µL nanoparticle suspension was dropped on the surface using a pipette, then roll-coated using an Automatic Glass Bed Film Applicator purchased from TQC Sheen (part number AB3650). The optimum speed used to coat was 0.5 inch/s.

3.2 RESULTS AND DISCUSSION:

A thin layer of gold was deposited for 60 s using Polaron sputter coater (E5100 Series II) at 0.09 mbar pressure, at a voltage of 2.5 kV, and 20 mA current to make the samples conductive to study the layer morphology and stacking by a JEOL JSM-6060LV scanning electron microscope.

Group 1 results:

50 g/L with 0.2 % PVPh:

The photographs and SEM images of soda-lime glass slide covered with 50 g/L of 400 nm particles containing 0.2 % PVPh (50 mg of nanoparticles and 1.6 mg of PVPh in 1 mL of EtOH) are shown in Fig. 4.1. The color of the coating is not visible in photographs taken with camera lens positioned at 30°, 45°, and 60°. But a slight green color can be seen at an angle of 90°. The SEM images of glass slide show hexagonal stacking of nanoparticles as islands with defects and empty spaces for both one coat and two coats of the solution.

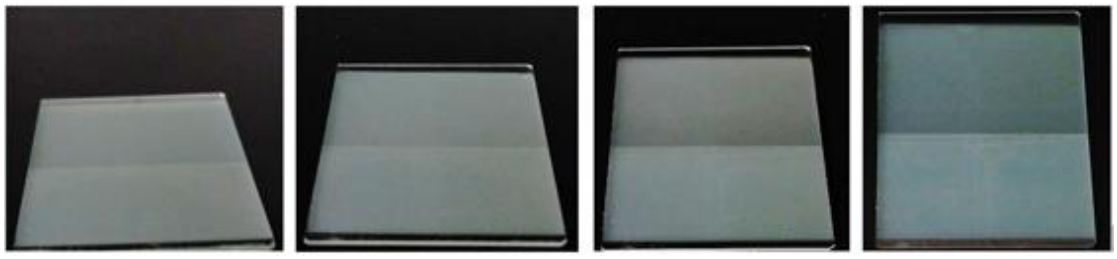

(a)

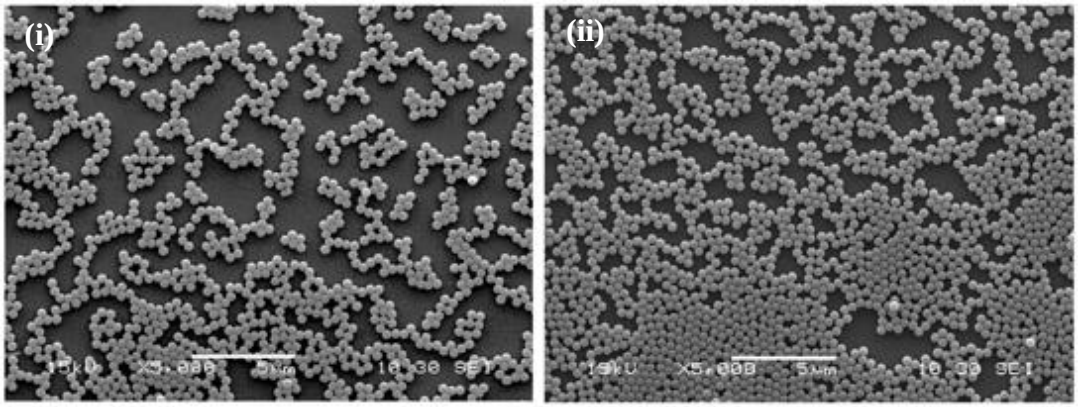

(b)

Fig. 4.1. (a) Photographs of a glass slide coated with 50 g/L of 400 nm particles (50 mg/ 1 mL of ethanol) with 0.2 % PVPh (1.6 mg) taken with camera lens axis positioned at 30°, 45°, 60°, and 90° (left to right). The glass slide was coated by one and two coats (top to bottom each covering half of the slide). (b) SEM images of soda-lime glass slide in which (i) has one coat, and (ii) has two coats showing the hexagonal stacking of silica nanoparticles as islands with defects and empty spaces.

100 g/L with 0.2 % PVPh

The photographs and SEM images of soda-lime glass slide covered with 100 g/L of 400 nm particles containing 0.2 % PVPh (100 mg of nanoparticles and 1.77 mg of PVPh in 1 mL of EtOH) are shown in Fig. 4.2. The color of the coating is not visible in photographs taken with camera lens positioned at 30°, and 45°. But, light green color can be seen when the camera lens is positioned at 60° and 90° angle. The SEM images of glass slide show hexagonal stacking of nanoparticles as islands with defects and empty spaces for glass slide having one coat. For glass slides having two coats of the solution, nanoparticles cover most of the surface but are not closely packed.

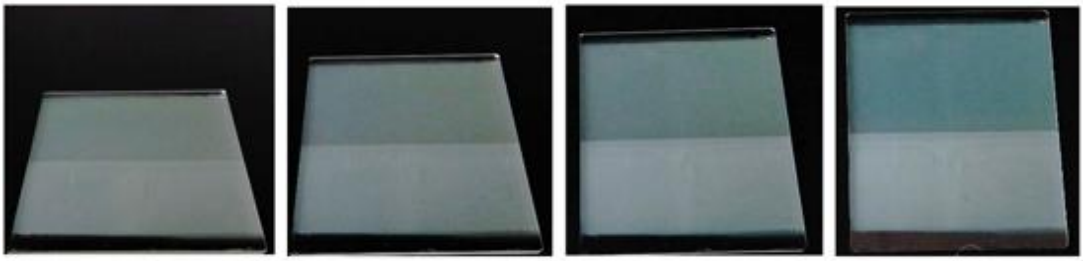

(a)

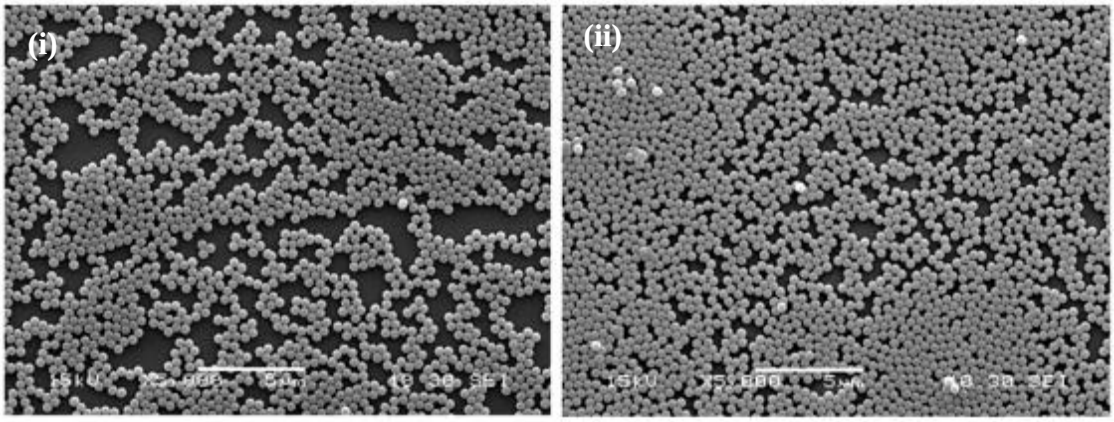

(b)

Fig. 4.2. (a) Photographs of a glass slide coated with 100 g/L of 400 nm particles (100 mg/ 1 mL of ethanol) with 0.2 % PVPh (1.77 mg) taken with camera lens axis positioned at 30°, 45°, 60°, and 90° (left to right). The glass slide was coated by one and two coats (top to bottom each covering half of the slide). (b) SEM images of soda-lime glass slide in which (i) has one coat, and (ii) has two coats showing the hexagonal stacking of silica nanoparticles as islands with defects and empty spaces for glass slide having one coat and loosely packed nanoparticles for glass slide having two coats.

200 g/L with 0.2 % PVPh

The photographs and SEM images of soda-lime glass slide covered with 200 g/L of 400 nm particles containing 0.2 % PVPh (100 mg of nanoparticles and 0.98 mg of PVPh in 0.5 mL of EtOH) are shown in Fig. 4.3. The color of the coating for part of glass slide covered in one coat (upper half of glass slide) is visible at all angles of 30°, 45°, 60°, and 90° but color of coating turns white for the area of glass slide covered with two coats (lower half of glass slide) of the solution. The SEM images of glass slide show hexagonal stacking of nanoparticles without any empty spaces for glass slide with both one and two coats.

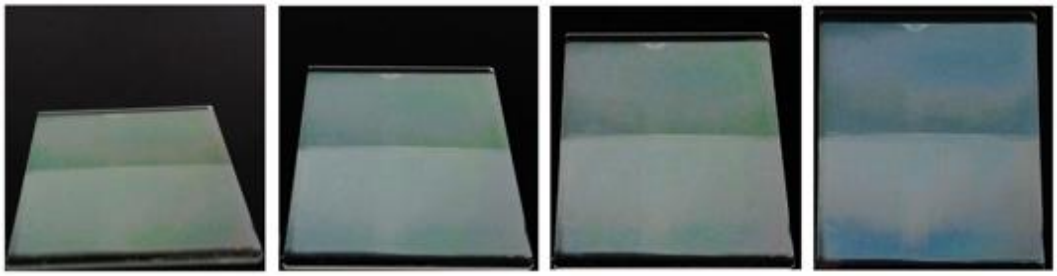

(a)

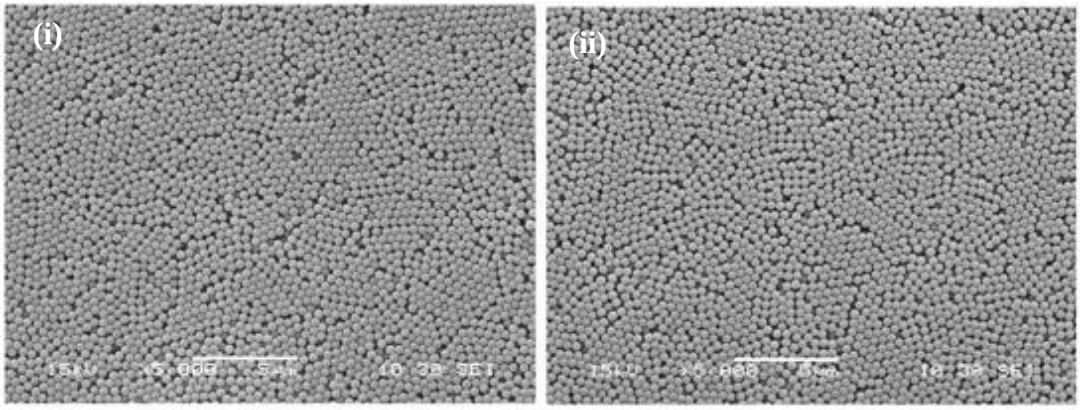

(b)

Fig. 4.3. (a) Photographs of a glass slide coated with 200 g/L of 400 nm particles (100 mg/ 0.5 mL of ethanol) with 0.2 % PVPh (0.98 mg) taken with camera lens axis positioned at 30°, 45°, 60°, and 90° (left to right). The glass slide was coated by one and two coats (top to bottom each covering half of the slide). (b) SEM images of soda-lime glass slide in which (i) has one coat, and (ii) has two coats showing the hexagonal stacking of silica nanoparticles without any empty spaces for glass slide having both one and two coats.

From the results in Figs 4.1, 4.2, and 4.3., we can see that the color of the coating changes with the concentration of the solution. For 50 g/L solution, the color is gray-green at most of the angles with the best green color seen at an angles of 60° and 90°. In this case, the nanoparticles are not closely packed. Poor packing is also observed for the glass slide coated by the 100 g/L solution with 0.2 % PVPh. In this case, the stacking is not good for a single coat but it improved for 2 coats. This is not the optimum required concentration as the present work is focused on developing a fast and scalable fabrication method and trying to get single layer of stacked nanoparticles in one coat application. For 200 g/L solution, the color is green for angles 30° through 60°, but the color changes to greenish-blue at 90° because of light scattering in multiple

directions from the nanoparticles. As the nanoparticles are closely packed, light can be scattered from one particle to another passing through the airgap between them. In group 1, the most vivid color among the three is obtained for 200 g/L with 0.2 % of PVPh.

Group 2 results:

50 g/L with no PVPh

The photographs and SEM images of soda-lime glass slide covered with 50 g/L of 400 nm particles without PVPh (50 mg of nanoparticles in 1 mL of EtOH) are shown in Fig. 4.4. The color of the coating is not visible in photographs taken with camera lens positioned at 30°, 45°, and 60°. But green color can be seen at an angle of 90°. The SEM images of glass slide show hexagonal stacking of nanoparticles as islands with defects and empty spaces for both one coat and two coats of the solution.

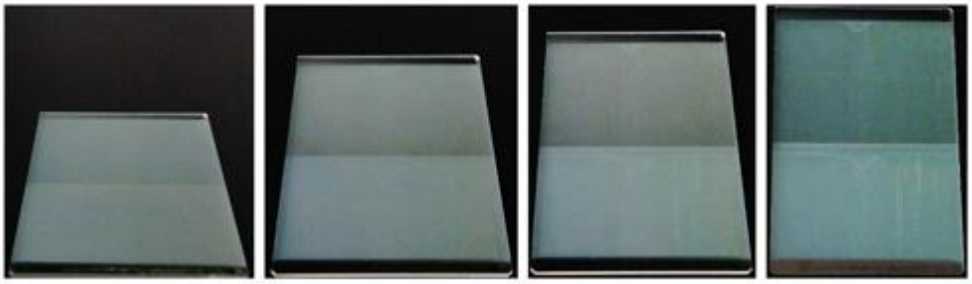

(a)

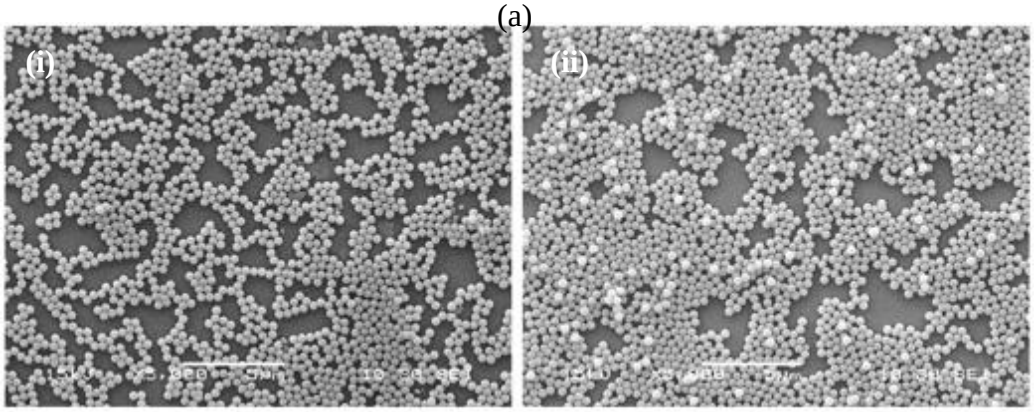

(b)

Fig. 4.4. (a) Photographs of a glass slide coated with 50 g/L of 400 nm particles (50 mg/ 1 mL of ethanol) without PVPh taken with camera lens axis positioned at 30°, 45°, 60°, and 90° (left to right). The glass slide was coated by one and two coats (top to bottom each covering half of the slide) showing bright green color when camera lens axis positioned at 90°. (b) SEM images of

soda-lime glass slide in which (i) has one coat, and (ii) has two coats showing the hexagonal stacking of silica nanoparticles as islands with defects and empty spaces.

100 g/L with no PVPh

The photographs and SEM images of soda-lime glass slide covered with 50 g/L of 400 nm particles without PVPh (100 mg of nanoparticles in 1 mL of EtOH) are shown in Fig. 4.5. The color of the coating in photographs taken with camera lens positioned at 30°, 45°, and 60° is not as bright as green color in photograph taken at an angle of 90°. The SEM images of glass slide show hexagonal stacking of nanoparticles with defects and empty spaces for glass slide covered with one coat and loosely packed nanoparticles for glass slide covered with two coats of the solution.

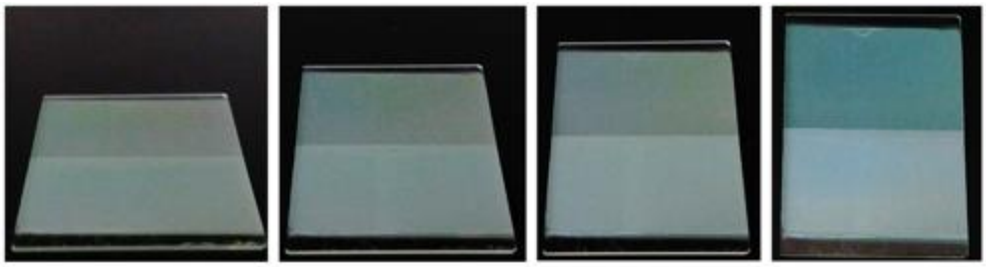

(a)

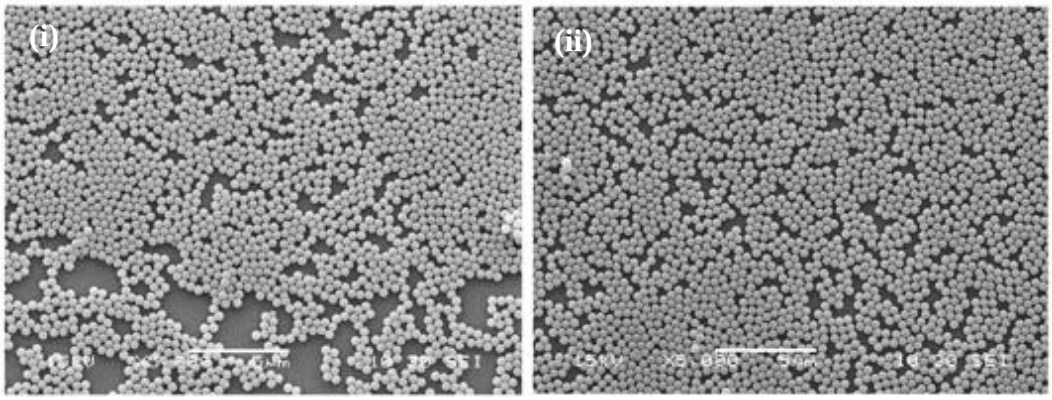

(b)

Fig. 4.5. (a) Photographs of a glass slide coated with 100 g/L of 400 nm particles (100 mg/ 1 mL of ethanol) without PVPh taken with camera lens axis positioned at 30°, 45°, 60°, and 90° (left to right). The glass slide was coated by one and two coats (top to bottom each covering half of the slide). (b) SEM images of soda-lime glass slide in which (i) has one coat, and (ii) has two coats showing the hexagonal stacking of silica nanoparticles with defects and empty spaces for glass slide having one coat and loosely packed nanoparticles for glass slide having two coats.

200 g/L with no PVPh

The photographs and SEM images of soda-lime glass slide covered with 200 g/L of 400 nm particles with no PVPh (100 mg of nanoparticles in 0.5 mL of EtOH) are shown in Fig. 4.6. The color of the coating for glass slides having one coat and two coats is bright green in the photographs taken with camera lens axis positioned at 30° and 45°. But color of coating changes to bluish-green / pale green in photographs taken at 60° and 90°. The SEM images of glass slide show hexagonal stacking of nanoparticles with some defects for one coat and without any empty spaces for glass slide with two coats.

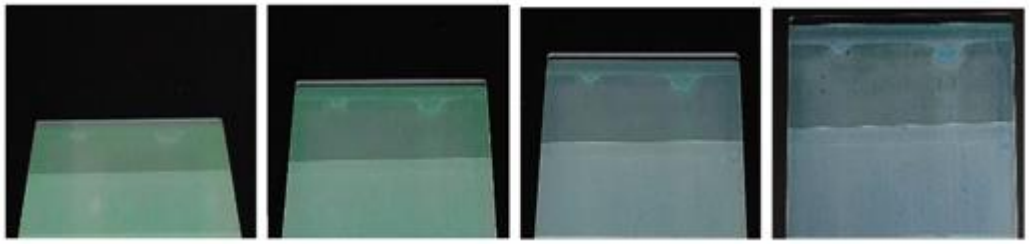

(a)

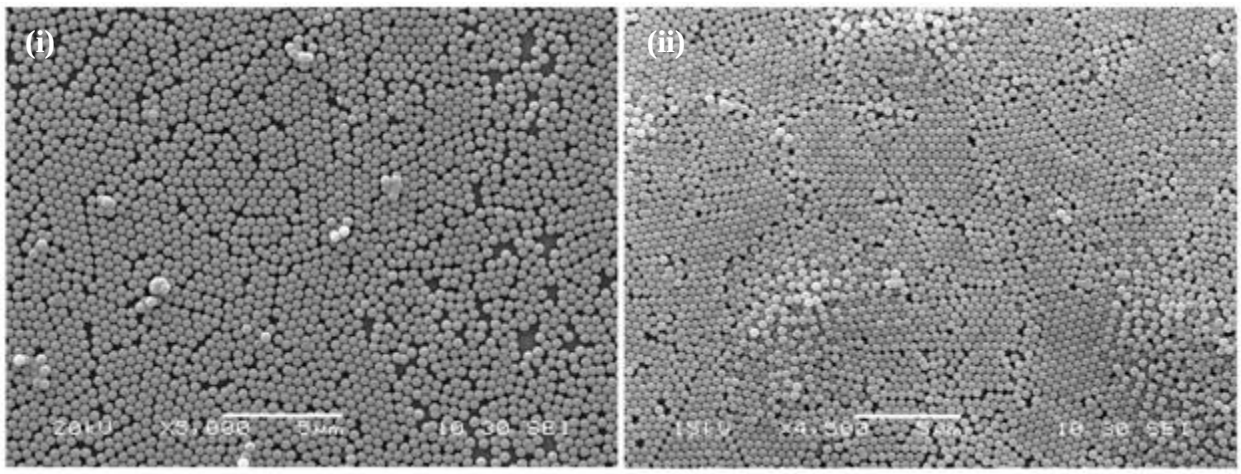

(b)

Fig. 4.6. (a) Photographs of a glass slide coated with 200 g/L of 400 nm particles (100 mg/ 0.5 mL of ethanol) without PVPh taken with camera lens axis positioned at 30°, 45°, 60°, and 90° (left to right). The glass slide was coated by one and two coats (top to bottom each covering half of the slide). (b) SEM images of soda-lime glass slide in which (i) has one coat, and (ii) has two coats showing the hexagonal stacking of silica nanoparticles without any empty spaces for glass slide having both one and two coats.

From the above results we can observe that the glass slides coated with solution concentrations of 50 and 100 g/L have significant defects in the stacking of the nanoparticles. However, slides coated with the 200 g/L show better staking with and without the addition of 0.2 % PVPh, which does not affect the quality of nanoparticle stacking. Therefore, the solution that provided best nanoparticle stacking was 200 g/L with no additional viscosity increasing agent. Therefore, the study continued with this solution.

CHAPTER 5

FABRICATION OF COATINGS USING DIFFERENT NANOPARTICLES

Silica Nanoparticles used in this study are monodisperse dry SiO_2 nanoparticles purchased from NANOCYM Inc., with 3 different diameters of 200, 300, and 400 nm are studied. The colloidal solution was prepared by mixing the nanoparticles in ethanol with 200 g/L concentration and sonicated for 7 hours in a bath cooled with ice. Roll coating was performed using an Automatic Glass Bed Film Applicator. These samples were dried for 40-45 minutes and the same process was repeated for multiple coatings.

5.1 PARTICLE CHARACTERIZATION

Commercial SiO_2particles with diameter ranging from 200 - 400 nm synthesized by NANOCYM were analyzed by Dr. Wei Cao at the Applied Research Center, Old Dominion University, using JEM-2100F TEM having accelerating voltage of 200 kV and magnification up to 800,000 X equipped with an Oxford INCAx-sight EDS detector, a 11-megapixel Gatan SC1000 ORIUS CCD camera, and a Gatan 626 single tilt liquid nitrogen cryo transfer holder. The TEM images of different particle sizes is shown in Fig. 5.1.

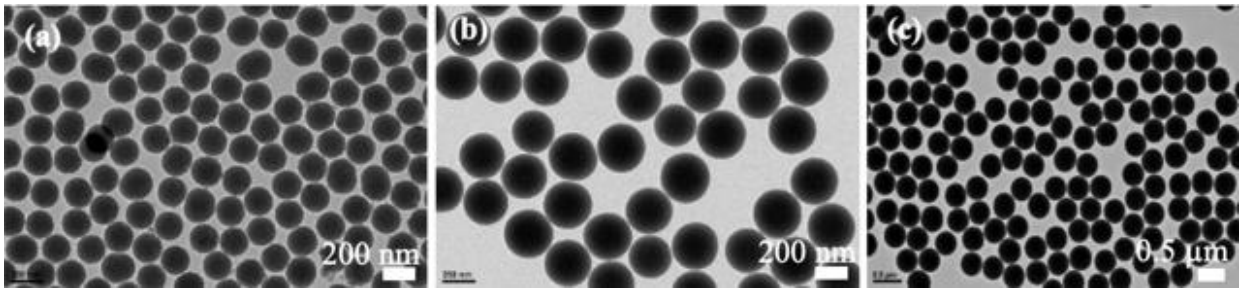

Fig. 5.1. Transmission electron microscope (TEM) images of nanoparticles taken from the suspension that is drop-coated on a carbon-coated TEM grids. (a) 200-nm, (b) 300-nm, and (c) 400-nm nanoparticles.

5.2 PREPARATION OF COLLOIDAL SOLUTION AND FABRICATION PROCEDURE

The dispersion of nanoparticles in ethanol according to their diameter is described in Table. 5.1. After dispersing the nanoparticles in ethanol, the solution was sonicated for 8 hours in a sonicator bath cooled by ice. About 0.025 µL of the prepared solution was dropped, using a pipette, on pre-cleaned soda-lime glass slide or on the solar cell glass cover and rolled using different wire wound roller rods. This process creates a thin coating with controlled thickness depending on the wire diameter and roller speed.

Table. 5.1 Preparation of commercial nanoparticle colloidal solution according to NP size.

Nanoparticle diameter (nm)	Weight of nanoparticles (mg)	Quantity of ethanol in (mL)
200	200	1
300	200	1
400	200	1.5

For even spreading of the solution and for uniform coating on the substrate using a roller rod we used a commercial roller coating applicator machine, Automatic Glass Bed Film Applicator to apply the thin coating on the glass slide. Different rods, varying from plain rod (without grooves) to rods having groove separation of 5 µm were used for the coating of the nanoparticles. A drop of solution of 0.025 µL was dropped on to the substrate and the rod was then pulled at a uniform speed of 0.5 inch/s. The schematic of the commercial film applicator is shown in the Fig. 5.2.

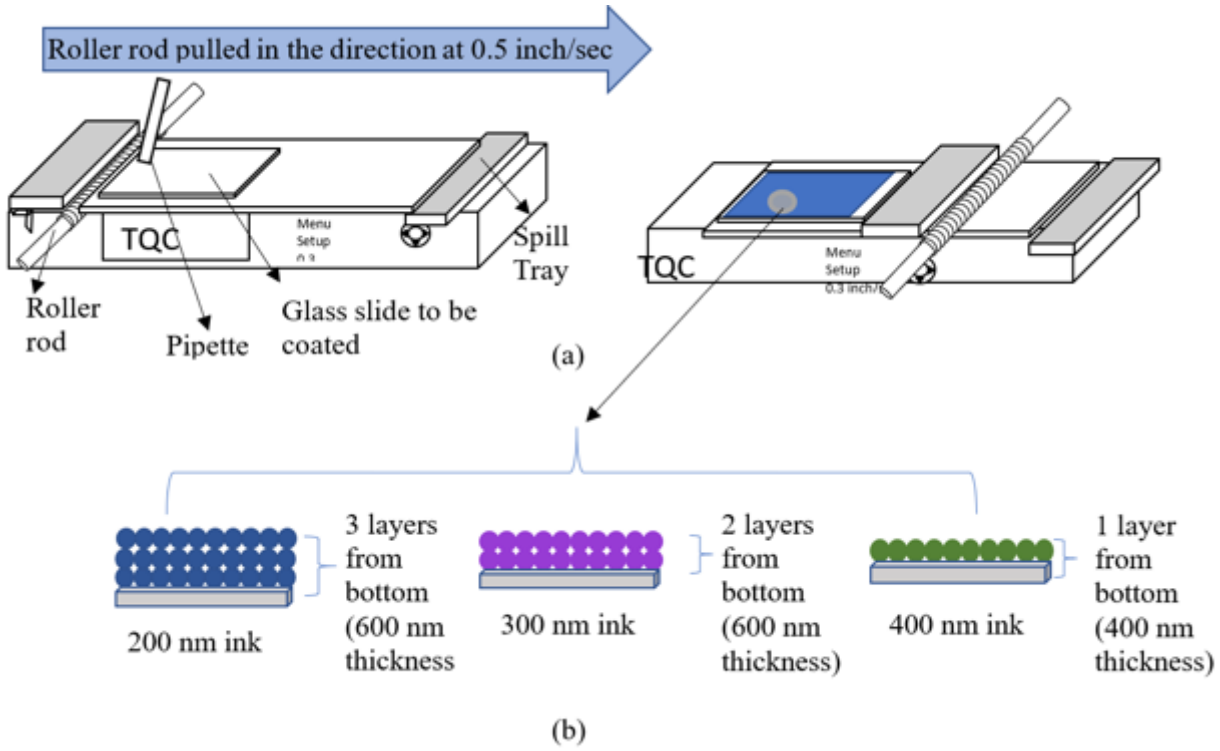

Fig. 5.2. (a) left image illustrates the operation of the automatic glass bed film applicator machine purchased from TQC Sheen, where the roller rod is pulled at the speed of 0.5 in/s in the direction shown in the schematic. Right image shows the coated glass slide having uniform coating over the entire slide. (b) (left to right) shows the number of layer of nanoparticles formed for one coat of solution for 200 nm, 300 nm, and 400 nm respectively.

5.3 RESULTS AND DISCUSSION

The nanoparticle layer transmission and reflection spectra were characterized using a StellarNet BLACK-Comet spectrometer connected to a Nikon Ti-U inverted optical microscope where a pre-cleaned glass slide the same as the one used to fabricate the thin films is used as reference. For transmission measurements, a LED light (~1 mm diameter) coupled to the spectrometer via an optical fiber is incident on the sample and is then plotted using OriginLab software to compare the transmission loss. For reflectance, an aluminum mirror is used as the reference and another LED light source shines a light beam (~2 mm diameter) from the bottom; for which the sample is placed upside down to measure the reflectance and is plotted using

OriginLab software. A thin layer of gold was deposited using Polaron sputter coater to make the samples conductive to study the layer morphology and stacking by a JEOL JSM-6060LV scanning electron microscope. The surface roughness of the samples was measured by the AFM images obtained from a Digital Instrument Dimension 3100 Atomic Force Microscope (AFM) operating in tapping mode.

Soda- lime glass slides coated with 200 nm:

Fig. 5.3 shows the photographs of 200 nm nanoparticle coated glass slide taken with camera lens axis positioned at 30°, 45°, 60°, and 90° (left to right). The glass slide was coated by one, two, and three coats (top to bottom each covering one third of the slide). The optical measurements, layer morphology and stacking of nanoparticles on the glass slides with one, two, and three coats are shown in Fig 5.4, Fig. 5.5, and Fig. 5.6, respectively.

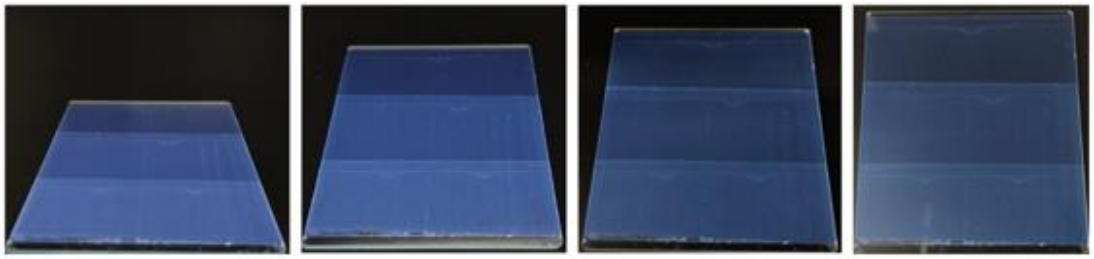

Fig. 5.3. Photographs of 200 nm nanoparticles coated glass slide taken with camera lens axis positioned at 30°, 45°, 60°, and 90° (left to right). The glass slide was coated by one, two, and three coats (top to bottom each covering one third of the slide).

From Fig. 5.3, the color of the slide becomes more vivid as the number of layers is increased. For the film to have a uniform color, glass slides must be dried for a 40 - 45 minutes before applying another coat on it. The optical transmission of the substrates was observed at 30°, 45°, 60°, and 90°, and reflectance was done with the slide positioned at normal to the incident light. An increase in the transmission loss with the number of layers is observed. The loss also increases with the size of nanoparticles.

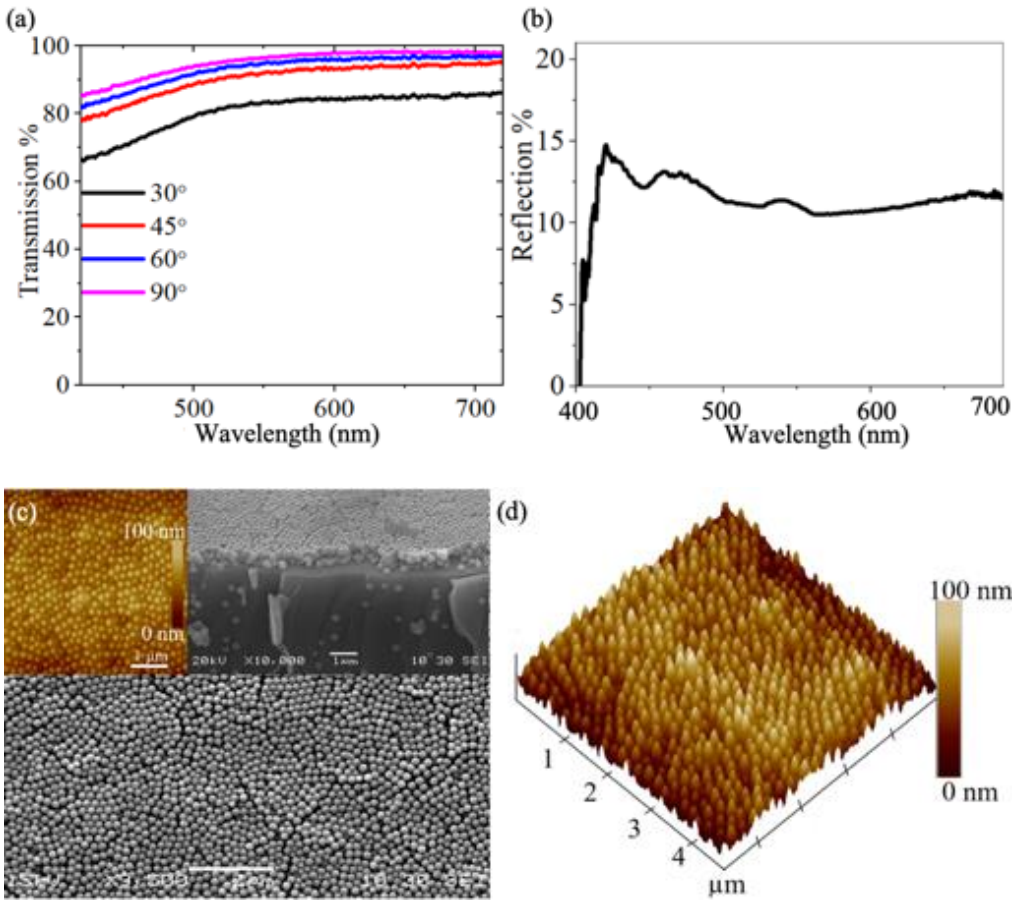

Fig. 5.4. (a) Optical transmission of the coated glass slide having one coat of 200-nm silica nanoparticles. The transmission was observed for the slides positioned at 30°, 45°, 60°, and 90° to the incident light beam. (b) The optical reflection spectra of the coated glass slide having one coat. The reflection was observed for the slide normal to the incident beam. (c) SEM image of the glass slide covered with 200 nm silica nanoparticles. Inset on the top left corner is 2D AFM and on top right corner is cross-sectional SEM image. (d) 3D AFM image of the substrate showing the roughness of the sample with a scale from 0 nm to 100 nm.

The transmission spectra of the coated glass slide was done by taking the uncoated slide as a reference. Results show that the transmission loss when the sample is incident to light beam is negligible and it increases as the angle with respect to the incident beam changes to more inclination. The reflection spectra is observed by taking an aluminum mirror with ~99% reflectance as a reference, and then the reflection is measured for the glass slide with the coating facing the light source and adding an extra layer of black sheet on the other side of the glass slide to make sure there are no secondary reflections. The reflection peak around 420 nm corresponds

to blue light in the electromagnetic spectra, and the reflection percentage observed here is less than 15%. Also, from SEM images it can be observed that the silica nanoparticles are closely packed with some defects, and the cross-sectional SEM image shows three layers of nanoparticles stacked upon one another from the surface of the glass slide. By altering the concentration of solution, the number of layers can be controlled.

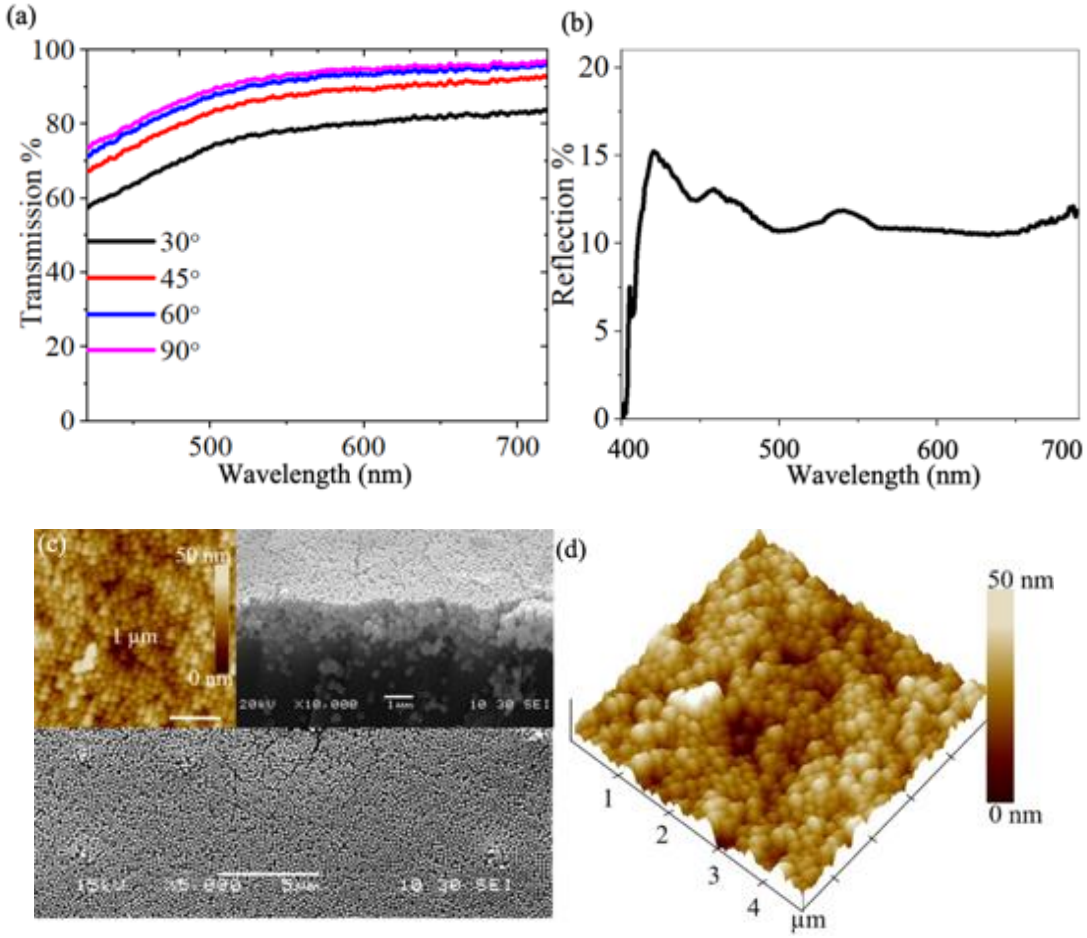

Fig. 5.5. (a) Optical transmission of the coated glass slide having two coats of 200-nm silica nanoparticles. The transmission was observed for the slides positioned at 30°, 45°, 60°, and 90° to the incident light beam. (b) The optical reflection spectra of the coated glass slide having two coats. The reflection was observed for the slide normal to the incident beam. (c) SEM image of the glass slide covered with 200 nm silica nanoparticles. Inset on the top left corner is 2D AFM and on top right corner is cross-sectional SEM image. (d) 3D AFM image of the substrate showing the roughness of the sample with a scale from 0 to 50 nm.

Fig. 5.5 is analysis of the soda lime glass coated with two coats of 200 nm nanoparticles. The transmission loss at 90° is negligible (~1% loss), and the maximum loss occurs at 30° (16-17 %). The intensity of the blue color as can be observed from the reflection spectra is enhanced. From Fig. 5.4 we can observe that one coat gives three layers of nanoparticles, while from Fig. 5.5 we can observe six layers of nanoparticles.

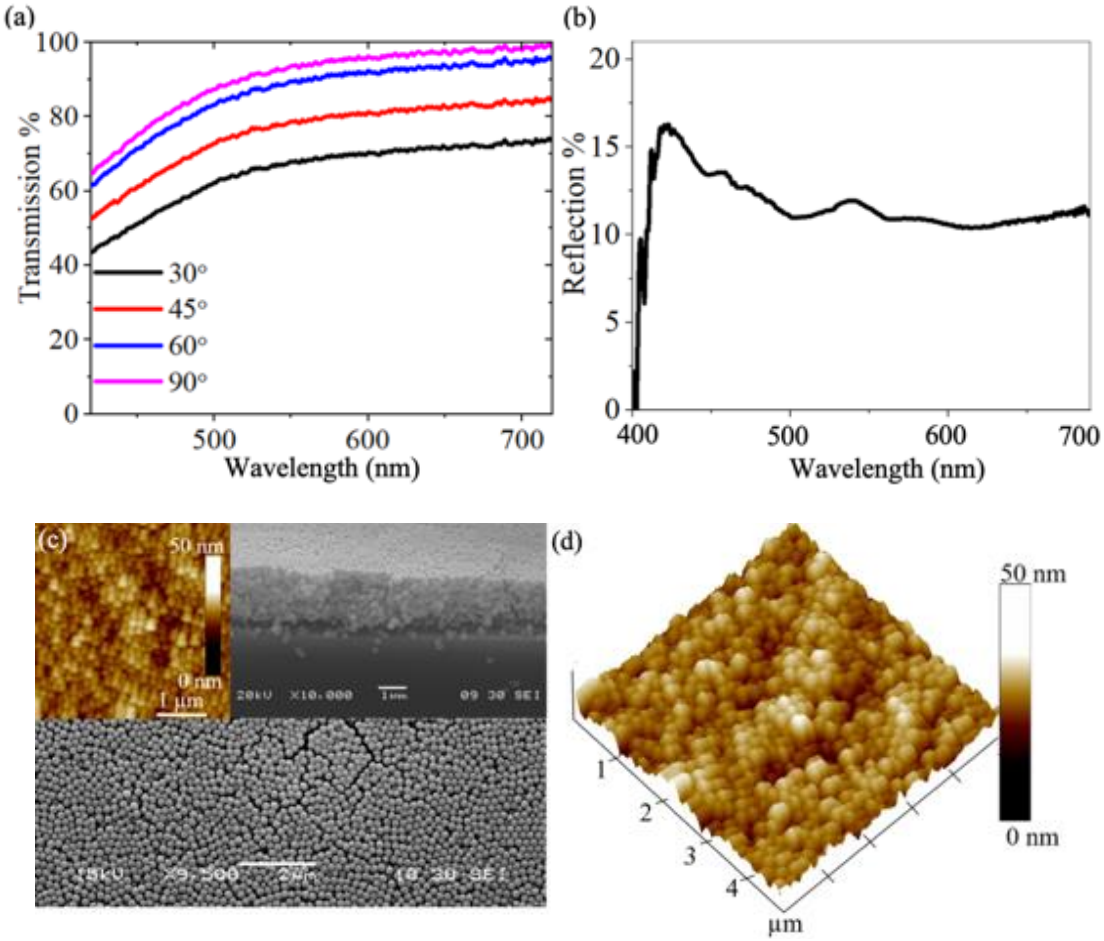

Fig. 5.6. (a) Optical transmission of the coated glass slide having three coats of 200-nm silica nanoparticles. The transmission was observed for the slides positioned at 30°, 45°, 60°, and 90° to the incident light beam. (b) The optical reflection spectra of the coated glass slide having three coats. The reflection was observed for the slide normal to the incident beam. (c) SEM image of the glass slide covered with 200 nm silica nanoparticles. Inset on the top left corner is 2D AFM and on top right corner is cross-sectional SEM image. (d) 3D AFM image of the substrate showing the roughness of the sample with a scale from 0 to 50 nm.

Fig. 5.6 is analysis of the soda lime glass coated with three coats of 200 nm nanoparticles. The transmission loss of the soda lime glass slides having three coats of 200 nm nanoparticles

shows increased loss at 30°, and 45°. The reflection peaks at 420 nm with 18-19% reflected around 420 nm. The SEM images show closely packed nanoparticles with a total of nine layers. Comparing the AFM images of Fig. 5.4, Fig. 5.5, and Fig. 5.6 we observe that the roughness grows for two and three coats when compared to one coat.

Soda- lime glass slides coated with 300 nm nanoparticles:

Fig. 5.7 shows the photographs of 300 nm nanoparticles coated glass slide taken with camera lens axis positioned at 30°, 45°, 60°, and 90° (left to right). The glass slide was coated by one, two, and three coats (top to bottom each covering one third of the slide). The optical results, morphology and stacking of nanoparticles on glass slides having one, two, and three coats are shown in Figs. 5.8, 5.9, and 5.10, respectively.

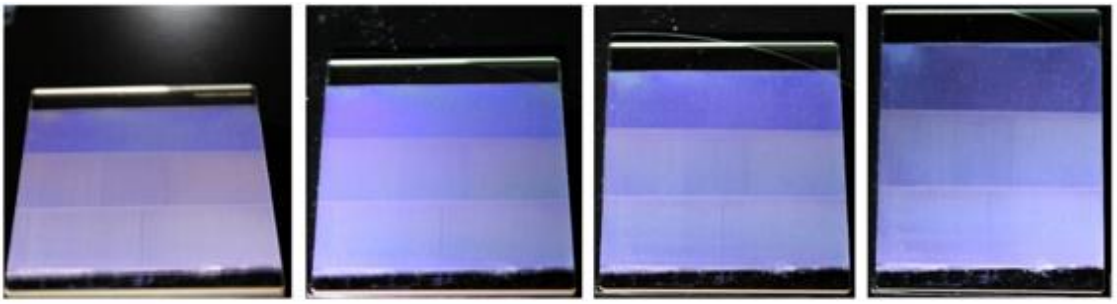

Fig. 5.7. Photographs of 300 nm nanoparticles coated glass slide taken with camera lens axis positioned at 30°, 45°, 60°, and 90° (left to right). The glass slide was covered with one, two, and three coats (top to bottom each covering one third of the slide).

From Fig. 5.7, the color of the slides becomes more vivid as the number of layers increase. For the film to have a uniform color, the glass slides must be dried for a 40 - 45 minutes before applying another coat on it. The transmission loss increases with the number of layers.

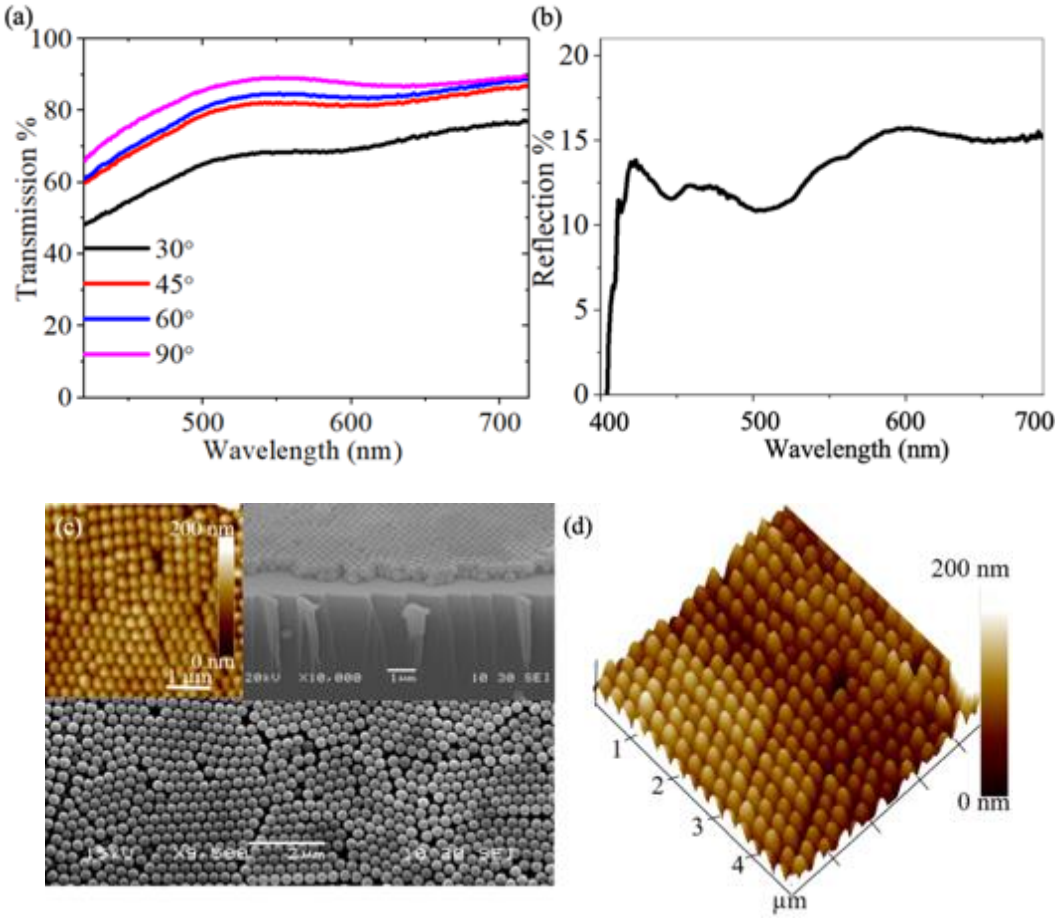

Fig. 5.8. (a) Optical transmission of the coated glass slide having one coat of 300-nm silica nanoparticles. The transmission was observed for the slides positioned at 30°, 45°, 60°, and 90° to the incident light beam. (b) The optical reflection spectra of the coated glass slide having one coat. The reflection was observed for the slide normal to the incident beam. (c) SEM image of the glass slide covered with 300 nm silica nanoparticles. Inset on the top left corner is 2D AFM and on top right corner is cross-sectional SEM image. (d) 3D AFM image of the substrate showing the roughness of the sample with a scale from 0 to 200 nm.

Fig. 5.8. is analysis of the soda lime glass coated with one coat of 300 nm nanoparticles. The transmission loss when the sample is 90° with respect to light beam is negligible and it increases as the angle with respect to incident beam is increased. The reflection peak around 600 - 680 nm corresponds to red light in electromagnetic spectrum, and the reflection percentage observed here is ~18%. From the SEM image, it can be observed the silica nanoparticles are closely packed and the cross-sectional SEM image shows two layers of nanoparticles stacked upon one another.

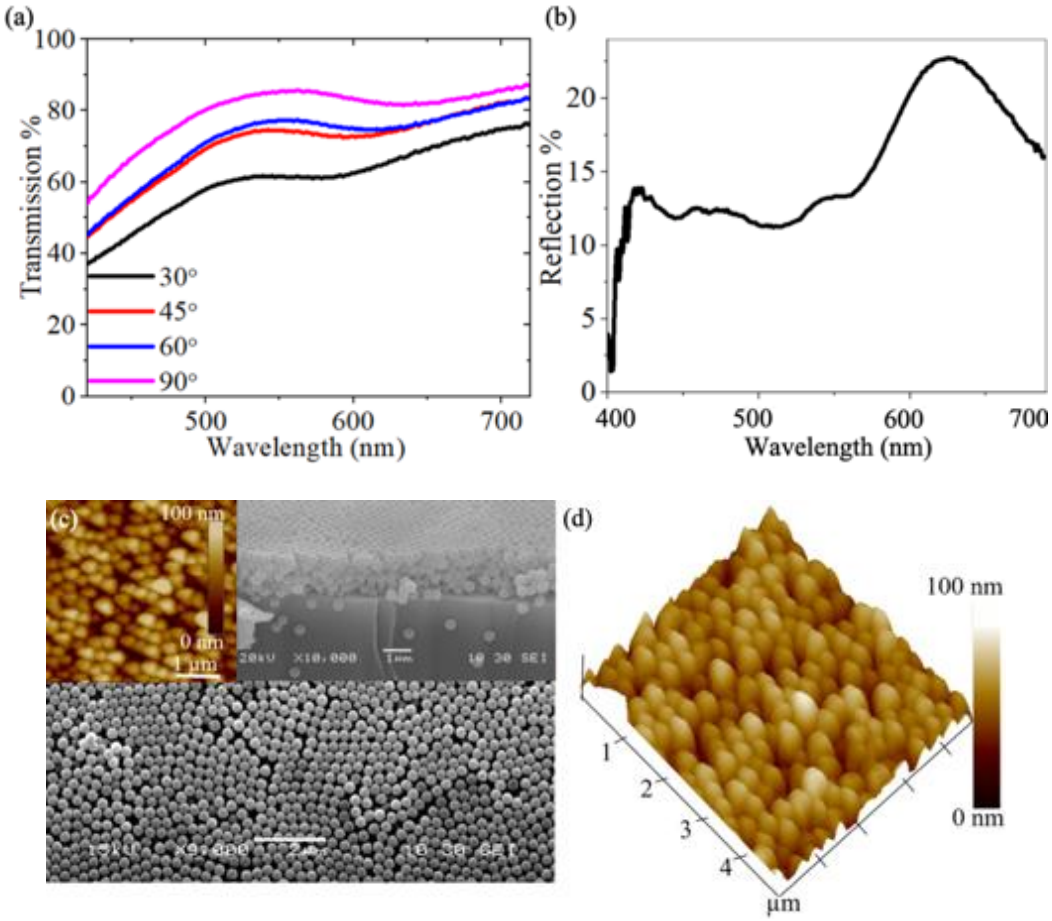

Fig. 5.9. (a) Optical transmission of the coated glass slide having two coats of 300-nm silica nanoparticles. The transmission was observed for the slides positioned at 30°, 45°, 60°, and 90° to the incident light beam. (b) The optical reflection spectra of the coated glass slide having two coats. The reflection was observed for the slide normal to the incident beam. (c) SEM image of the glass slide covered with 300 nm silica nanoparticles. Inset on the top left corner is 2D AFM and on top right corner is cross-sectional SEM image. (d) 3D AFM image of the substrate showing the roughness of the sample with a scale from 0 to 100 nm.

Fig. 5.9 shows results for the soda lime glass slide coated with two coats of 300 nm nanoparticles. The transmission loss at 90° is ~15 %, and the maximum loss occurs at 30°, which is ~20%. From Fig. 5.8 we can observe that one coat gives two layers of nanoparticles, and from Fig. 5.9 we can observe four layers of nanoparticles from the surface.

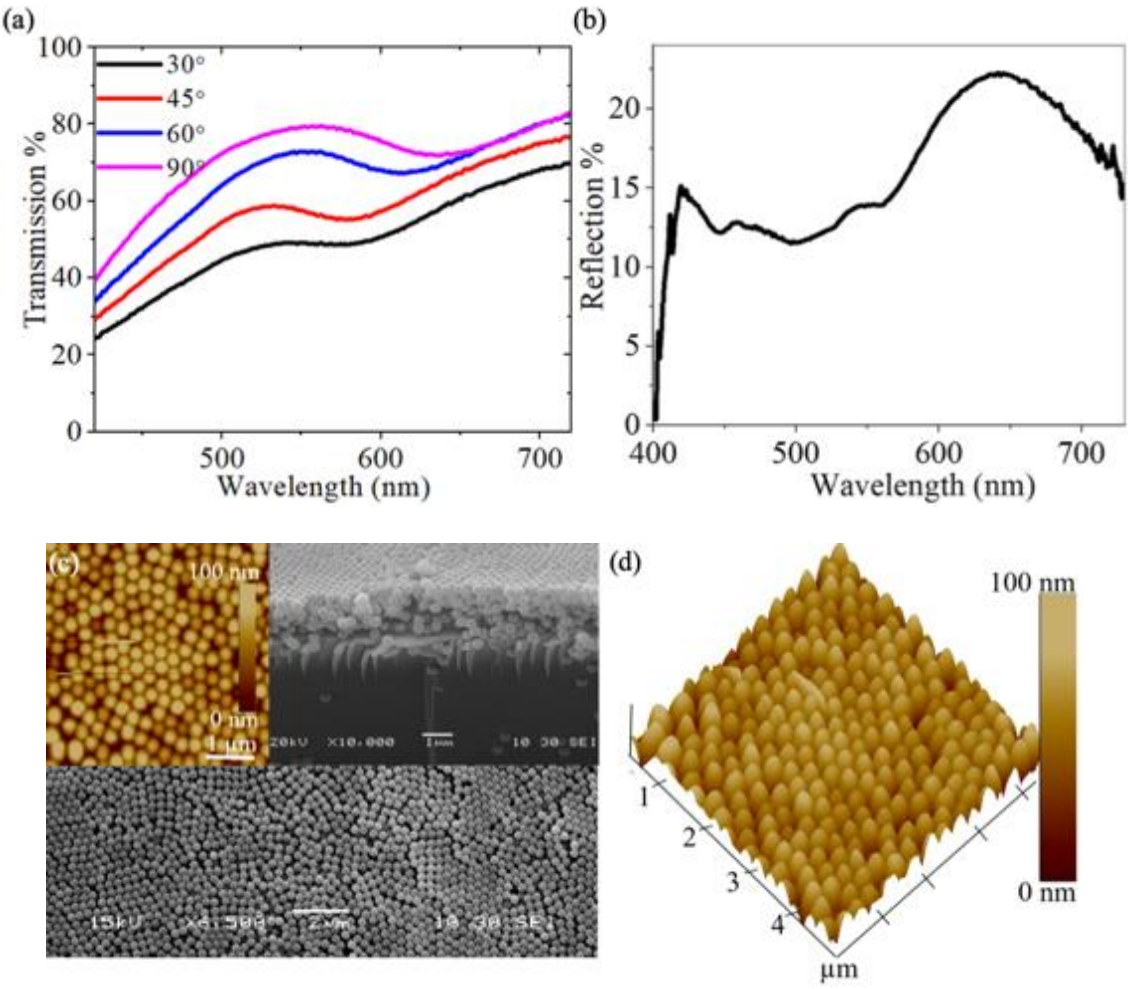

Fig. 5.10. (a) Optical transmission of the coated glass slide having three coats of 300-nm silica nanoparticles. The transmission was observed for the slides positioned at 30°, 45°, 60°, and 90° to the incident light beam. (b) The optical reflection spectra of the coated glass slide having three coats. The reflection was observed for the slide normal to the incident beam. (c) SEM image of the glass slide covered with 300 nm silica nanoparticles. Inset on the top left corner is 2D AFM and on top right corner is cross-sectional SEM image. (d) 3D AFM image of the substrate showing the roughness of the sample with a scale from 0 to 100 nm.

Fig. 5.10 is analysis of the soda lime glass coated with three coat of 300 nm nanoparticles. The transmission loss of the soda lime glass slides having three coats of 300 nm nanoparticles have increased loss at 30°, and 45°, the reflection peak has intensity of ~25 % at 630 nm. SEM images show closely packed nanoparticles with a total of 6 layers.

Soda- lime glass slides coated with 400 nm:

Fig. 5.11. shows the photographs of 400 nm nanoparticle coated glass slide taken with camera lens axis positioned at 30°, 45°, 60°, and 90° (left to right). The glass slide was coated by one, two, and three coats (top to bottom each covering one third of the slide). The optical measurements, layer morphology and stacking of nanoparticles on the glass slides with one, two, and three coats are shown in Fig 5.12, Fig. 5.13, and Fig. 5.14, respectively

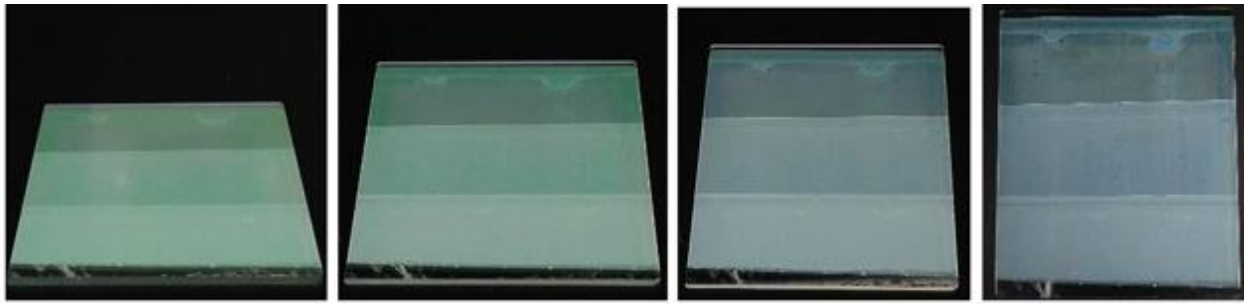

Fig. 5.11. Photographs of 400 nm coated glass slide taken with camera lens axis positioned at 30°, 45°, 60°, and 90° (left to right). The glass slide was covered with one, two, and three coats (top to bottom each covering one third of the slide).

For the glass slides coated using 400 nm, the color when observed with camera angle positioned at 30°, and 45° is green but when the angle is increased to 60° and 90°, the color looks bluish green because of the angle dependence of sub-micrometer nanoparticles which show angular dependence of color when the particles size approaches 500 nm or ½ a micron (0.5 μm). There can be seen increase in the transmission loss % as the number of layers increase.

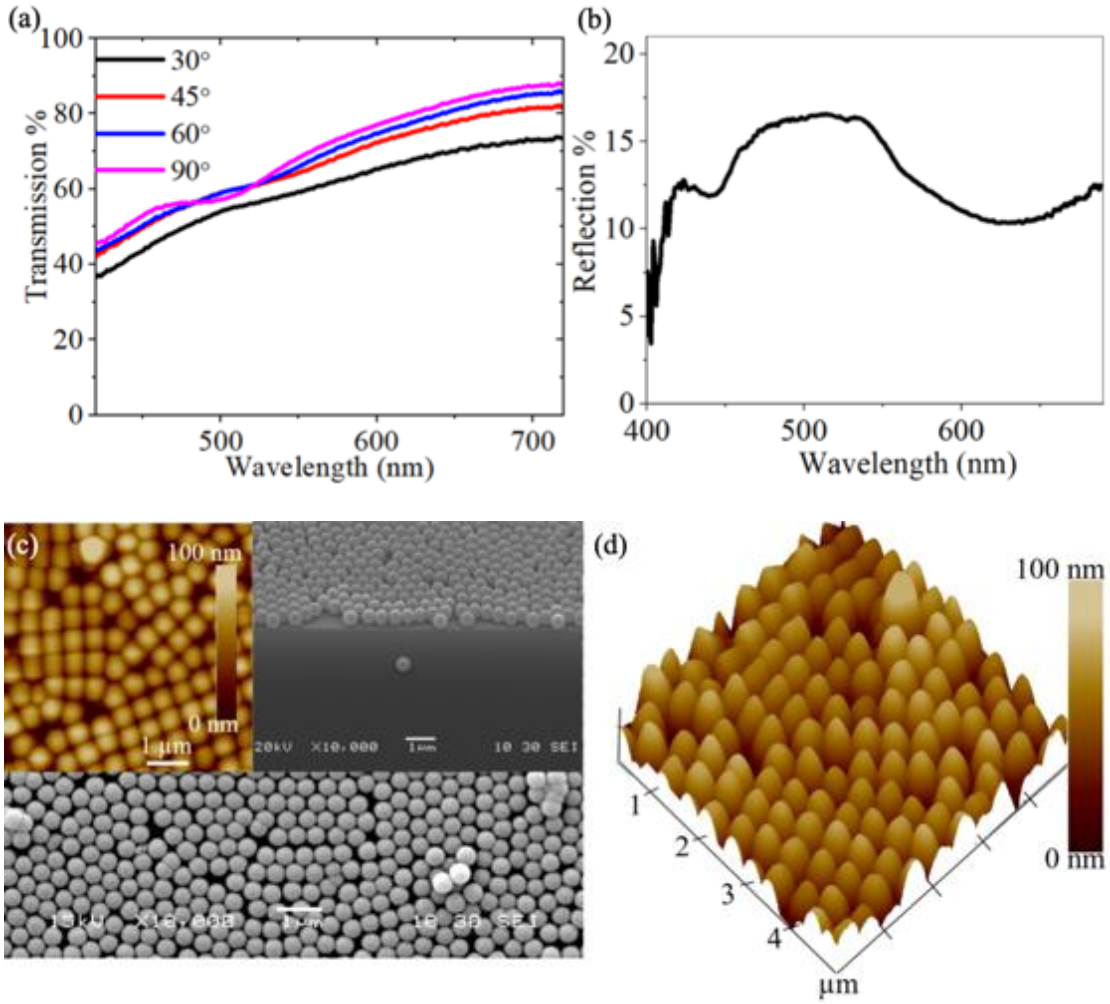

Fig. 5.12. (a) Optical transmission of the coated glass slide having one coat of 400-nm silica nanoparticles. The transmission was observed for the slides positioned at 30°, 45°, 60°, and 90° to the incident light beam. (b) The optical reflection spectra of the coated glass slide having one coat. The reflection was observed for the slide normal to the incident beam. (c) SEM image of the glass slide covered with 400 nm silica nanoparticles. Inset on the top left corner is 2D AFM and on top right corner is cross-sectional SEM image. (d) 3D AFM image of the substrate showing the roughness of the sample with a scale from 0 to 100 nm.

Fig. 5.12 is analysis of the soda lime glass coated with one coat of 400 nm nanoparticles. The reflection peak around 470-540 nm corresponds to green light in electromagnetic spectrum, and the reflection percentage observed here is ~18 %. SEM images show closely packed silica nanoparticles and the cross-sectional SEM image shows layers of nanoparticles from the surface of the glass slide

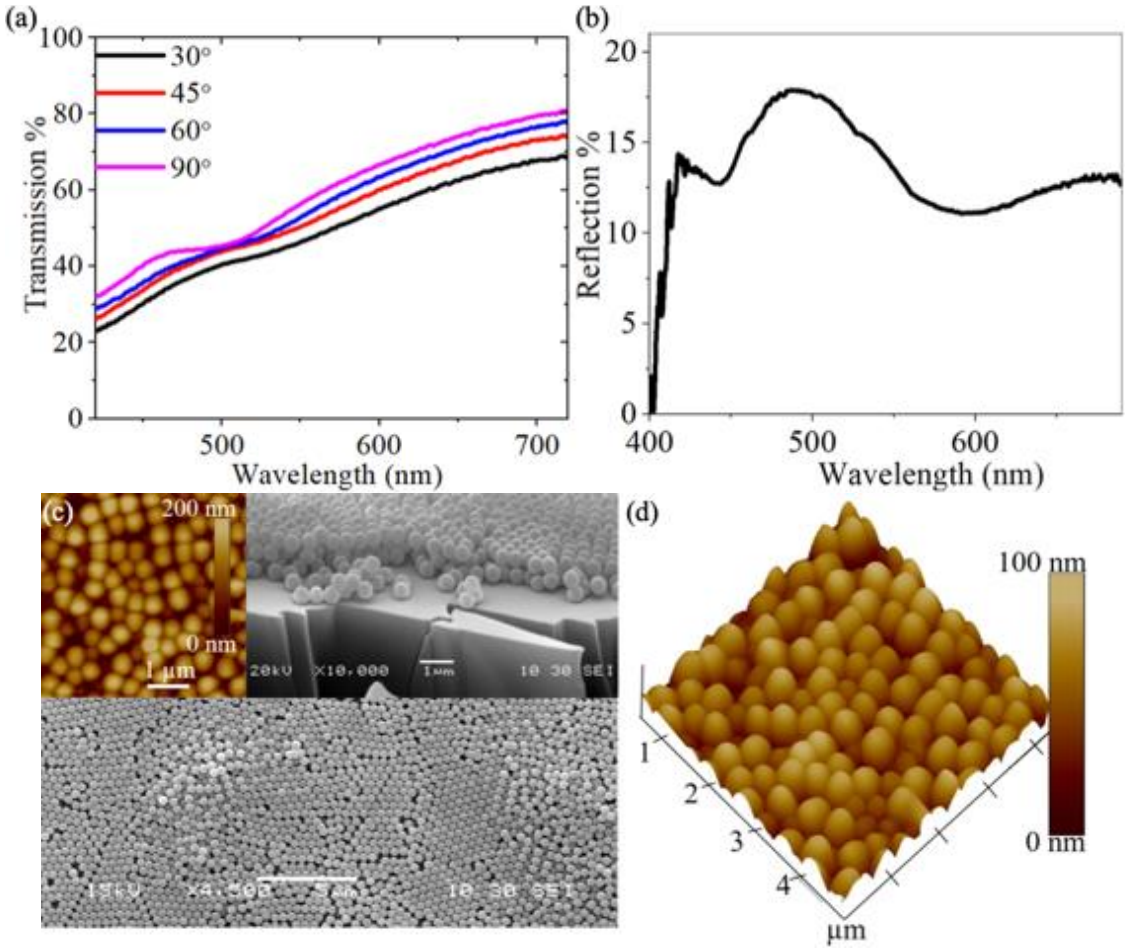

Fig. 5.13. (a) Optical transmission of the coated glass slide having two coats of 400-nm silica nanoparticles. The transmission was observed for the slides positioned at 30°, 45°, 60°, and 90° to the incident light beam. (b) The optical reflection spectra of the coated glass slide having two coats. The reflection was observed for the slide normal to the incident beam. (c) SEM image of the glass slide covered with 400 nm silica nanoparticles. Inset on the top left corner is 2D AFM and on top right corner is cross-sectional SEM image. (d) 3D AFM image of the substrate showing the roughness of the sample with a scale from 0 to 100 nm.

Fig. 5.13 is analysis of the soda lime glass coated with two coats of 400 nm nanoparticles. The transmission loss at 90° is ~20 %, and the maximum loss occurs at 30° (~25 %). The intensity of color as can be observed from the reflection spectra is enhanced. From the Fig. 5.12 we can observe that one coat gives one layer of nanoparticles from the surface of glass slide, and from Fig. 5.13 we can observe two layers of nanoparticles from the surface.

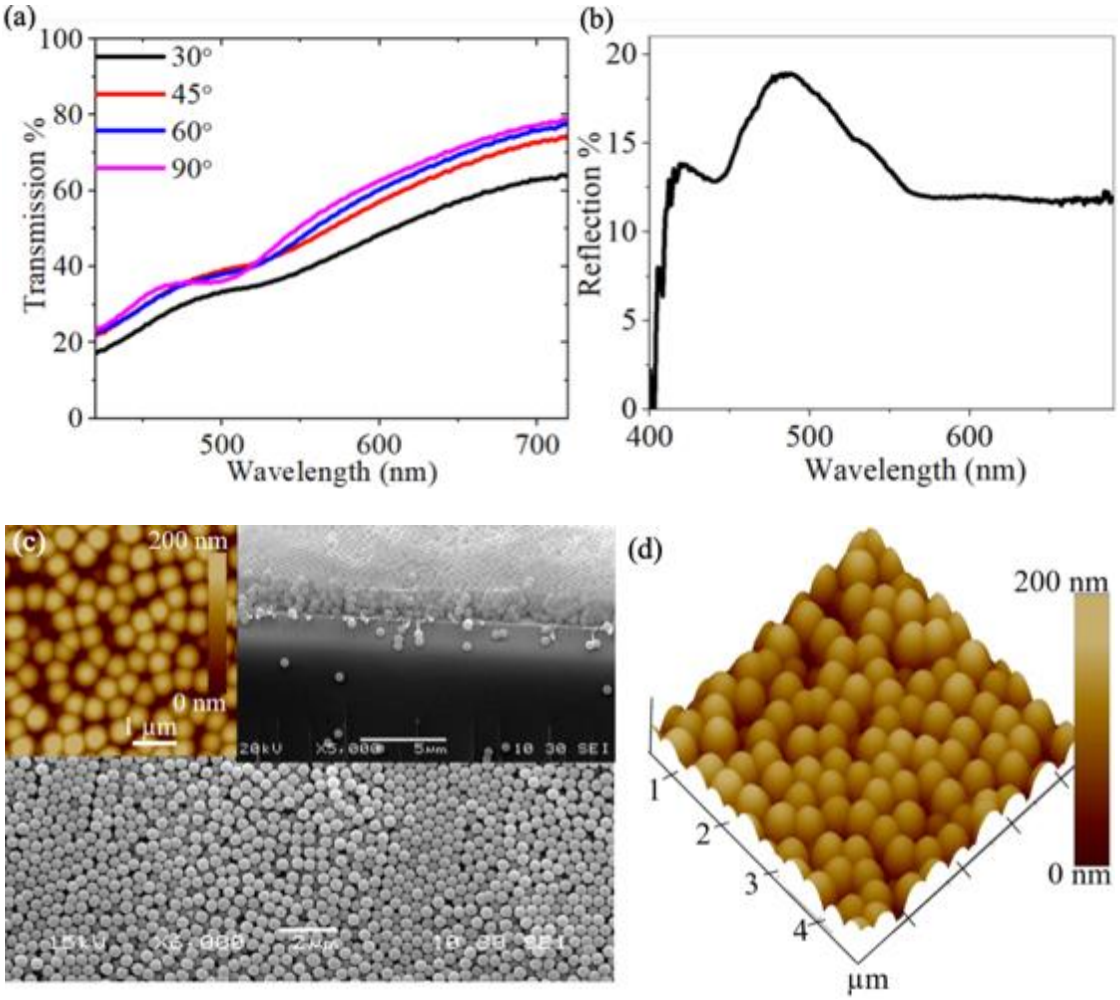

Fig. 5.14. (a) Optical transmission of the coated glass slide having three coats of 400-nm silica nanoparticles. The transmission was observed for the slides positioned at 30°, 45°, 60°, and 90° to the incident light beam. (b) The optical reflection spectra of the coated glass slide having three coats. The reflection was observed for the slide normal to the incident beam. (c) SEM image of the glass slide covered with 400 nm silica nanoparticles. Inset on the top left corner is 2D AFM and on top right corner is cross-sectional SEM image. (d) 3D AFM image of the substrate showing the roughness of the sample with a scale from 0 to 200 nm.

Fig. 5.14 is analysis of the soda lime glass coated with three coats of 400 nm nanoparticles. From the reflection spectra it is clear that vividness of color increases with the number of coats, so as the transmission loss. The reflection spectra show peak intensity ~20 % at corresponding 490 nm.

The color of the coating changes depending on the size of the nanoparticles. This is due to the phenomenon of incident light scattering in the coating. For every nanoparticle size the light

absorption differs, similarly the scattering of light due to nanoparticles changes. The reflected λ is determined by the geometry of the unit cell and the indices of refraction of the periodic structure and surrounding medium. For applications as a transparent colored coating, the structure of the spheres is not sensitive to defects. The wavelengths λ of reflected light is determined by Bragg's law for periodic spheres with indices of refraction n_i of the spheres and the binding material: $\lambda = 2dn_{eff} = (\frac{8}{3})^2 D\ (\sum_i n_i V_i - \ sin^2\theta)^2$ where V_i is the volume fraction of the two materials, d is the characteristic spacing, D the particle size, and θ the angle between the incident beam with the surface. The coating transmission depends on wavelength, coating thickness, and angle of light incidence. For λ above 700 nm, where Si solar cells operate with maximum efficiency, it is possible to achieve >80% for substrates coated by 3 layers of 200 and 300 nm nanoparticles. However, for the substrates coated by 400 nm nanoparticles, the one and two coats have transmission ~80%, but the substrates with three coats have transmission <80% for λ above 700 nm.

CHAPTER 6

COATED SOLAR CELL PERFORMANCE

6.1 INTRODUCTION

The work has the goal of demonstrating the use of roll coating to apply a transparent colored coating on commercial solar cells. Commercial polycrystalline silicon solar cells were used for this purpose. The aim of this work is to test the change in solar cell performance as different coating is applied to them. Silicon solar cells were chosen because they remain widely used in photovoltaic power generation. Since different PV material has different bandgaps, the results presented here apply only to the silicon solar cells, and in particular polycrystalline silicon.

6.2 EXPERIMENTAL DETAILS

Polycrystalline silicon solar cells were used to test the solar cell performance with the colored nanoparticle coating. The solar cells used were AOSHIKE 2V, 130 mA Micro Solar panels of size 45x45 mm^2. The nanoparticle coating was applied directly to the glass cover of the solar cell without any surface treatment except cleaning with ethanol. Two drops of the same nanoparticle solution used in CHAPTER 5 (0.025 µL) were dropped onto the surface to be rolled at 0.5 in/s. The coating was allowed to dry in air. Each solar cell performance was tested prior to and after applying the coating. An Oriel 150 W solar simulator equipped with an AM 1.5 spectral filter was used for solar cell testing under an irradiance of one sun. The solar cell *I-V* curves were obtained using a Keithley source meter and the data were collected using LabView software. This data was then used to plot the graphs in OriginLab software. Fig. 6.1 shows image of uncoated solar cell.

The total area of solar cell including the frame is 45 x 45 mm^2, but the solar cell area encapsulated in the frame is 35 x 35 mm^2. The solar cell area encapsulated in the frame has four

cells soldered to the terminals based on which the active solar cell area is approximately calculated to be 676 mm2.

Fig. 6.1. Photograph of uncoated AOSHIKE Micro Solar cell.

The maximum power loss P_{max} in % is calculated from;

$$P_{max}\ Loss\ (\%) = 1 - \frac{P_{max_{Coated}}}{P_{max_{Uncoated}}} \quad where\ P_{max} = (V_m)(J_m) \qquad \text{(Eqn. 6.1)}$$

Input power for AM 1.5 can be given as 1 kW/m2. So according to the calculations the total input power of AOSHIKE Micro solar cell is 676 mW/cm2 i.e., input power P_{in} = 676 mW/cm2.

P_{max} loss is equivalent to loss of solar cell efficiency tested under a solar simulator, $P_{max_{Coated}}$ is the coated solar cell maximum power, and $P_{max_{Uncoated}}$ is the maximum power of the solar cell prior to coating it. In order to eliminate any effects due to differences in solar cell performance from one unit to another, each solar cell used was characterized prior to applying the nanoparticle, then the characterization was performed on the solar cell after coating and its performance compared to that prior to coating it. The fill factor FF in % for both coated and uncoated solar cell is calculated using;

$$FF = \frac{(V_m)(J_m)}{(V_{OC})(Jsc)}\ X\ 100 \qquad \text{(Eqn. 6.2)}$$

Where J_m and J_{sc} are maximum power density and short circuit power density in mA/cm^2 respectively.

6.3 RESULTS AND DISCUSSION

The solar simulator was turned on and left for 5 minutes before turning the lamp on, to make sure the lamp was stabilized to provide the intensity of 1 sun. The solar cell terminals were

connected to the positive and negative terminals of multimeter which is programmed in LabView software to collect the data. The results below contain solar cells tested with coatings of 200, 300, and 400 nm nanoparticles each containing one coat, two coats, and three coats, respectively. The table for each set of results represents the associated $V_{OC}, J_{SC}, V_m, J_m, P_{max},$ Fill Factor %, and $P_{max}\ loss$ % for coated and uncoated solar cells respectively.

Solar cell coated with 200 nm nanoparticles:

Fig. 6.2 shows the *I-V* curves of solar cells without and with coats of 200 nm silica nanoparticles applied to the solar cell glass cover. The coated solar cell is shown in the insets of each figure taken at 30°, 45°, 60°, and 90°, left to right, respectively. The solar cell *I-V* curve was first obtained without applying the coating, then, the nanopartices were applied followed by measuring the *I-V* curves.

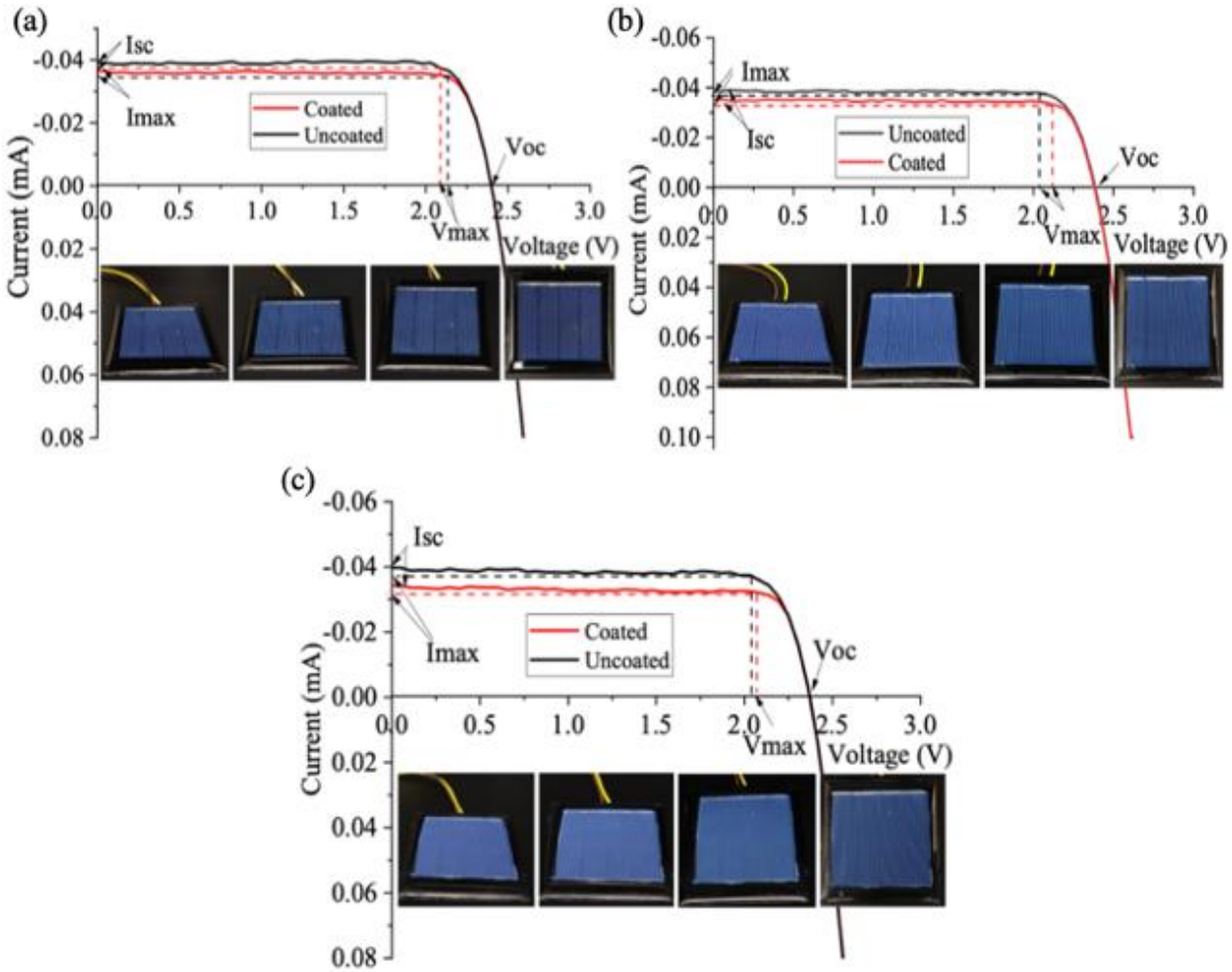

Fig. 6.2. *I-V* curves of the AOSHIKE Micro Solar without and with (a) one coat, (b) two coats, and (c) three coats of 200 nm silica nanoparticles (a single coat gives three layers of nanoparticles) applied to the solar cell glass cover. The coated solar cell is shown in the photographs taken at 30°, 45°, 60°, and 90°, left to right respectively. For the 200 nm coating, the color shows little variation with viewing angle.

Table. 6.1 below, summarizes the results from the *I-V* curves in Fig. 6.2. There are small color variation in the solar cell, when the angle of observation changes from 60° to 90°. Also, blue color on the solar cell becomes more vivid with the number of coats and the underlying solar cell features, such as boarders and connections, become less visible. Each gives three layers of nanoparticles. The power loss is minimum for one coat ~2.01 % loss, and the maximum loss is for the solar cell with three coats ~7.83 %.

Table. 6.1. Solar cell *I-V* characteristics before and after coating with 200 nm silica nanoparticles.

No. of coats	**Coating**	V_{OC}	V_m	J_{SC} (mA/cm^2)	J_m (mA/cm^2)	P_{max} (mW /cm^2)	**Fill factor** %	P_{max} *Loss* %
1	Uncoated	2.41	2.03	5.75	5.37	10.91	78.72	2.01
	Coated	2.41	2.08	5.75	5.14	10.69	77.17	
2	Uncoated	2.33	2.03	5.41	5.50	11.16	88.57	3.58
	Coated	2.41	2.03	5.23	5.30	10.76	85.39	
3	Uncoated	2.36	2.03	5.64	5.16	10.47	78.64	7.83
	Coated	2.36	2.08	5.64	4.64	9.65	72.47	

Solar cell coated with 300 nm nanoparticles:

Fig. 6.3. shows the *I-V* curves of solar cells without and with coats of 300 nm silica nanoparticles applied to the solar cell glass cover. The same procedure used to apply the 200 nm nanoparticles in Fig. 6.2 was followed. The solar cell color for the 300 nm nanoparticle coat is almost pink with some dependence on angle of observation, particularly for the single coat.

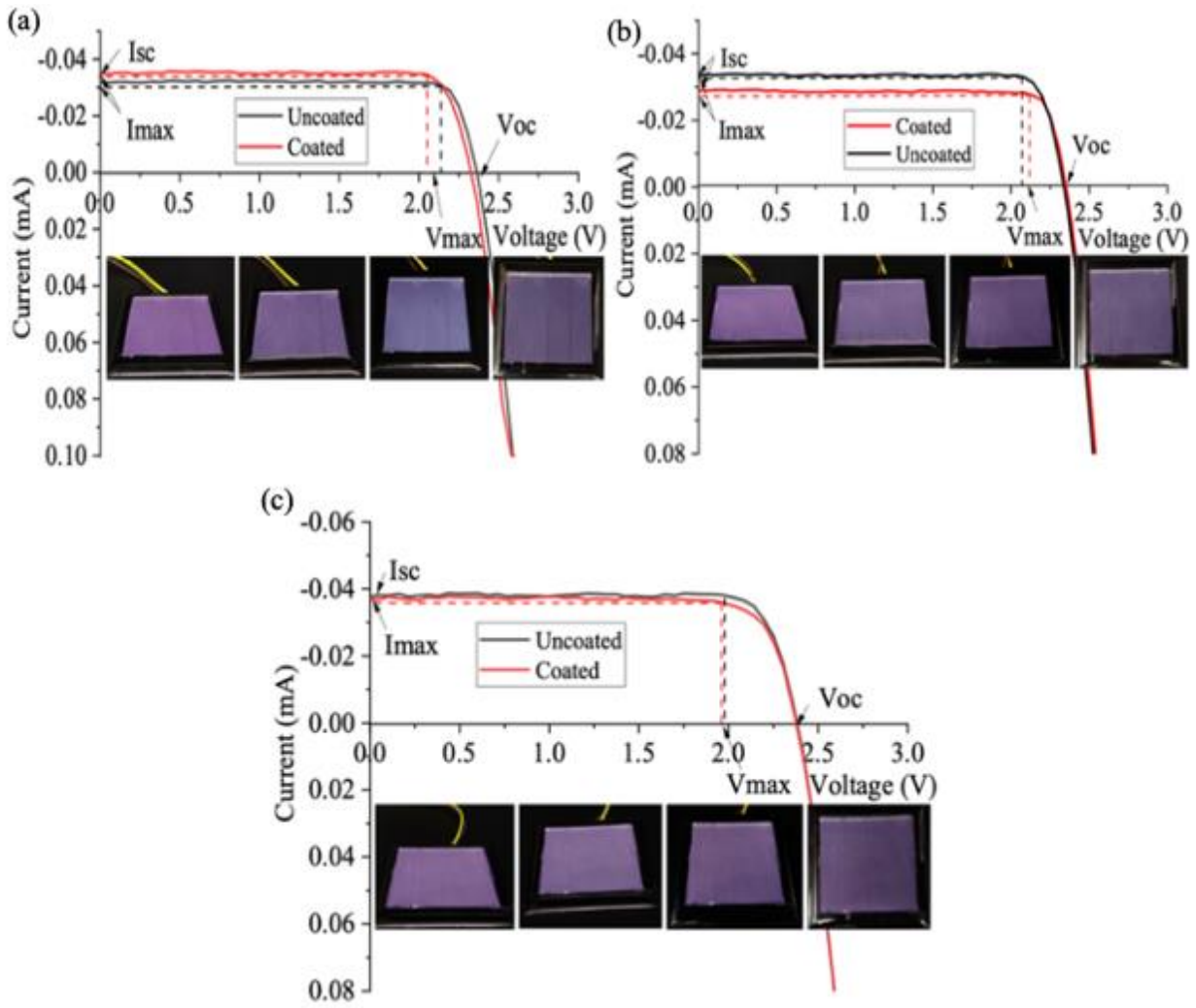

Fig. 6.3. *I-V* curves of the AOSHIKE Micro Solar without and with (a) one coat, (b) two coats, and (c) three coats of 300 nm silica nanoparticles (a single coat gives two layers of nanoparticles) applied to the solar cell glass cover. The coated solar cell is shown in the photographs taken at 30°, 45°, 60°, and 90°, left to right respectively.

Table. 6.2, summarizes the results from the *I-V* curves of Fig. 6.3. The pink color of the solar cell increases with the increase in the number of coats. The solar cell power loss also increases with the number of coats. Each coat on the solar cell gives two layers of nanoparticles. The power loss for one coat is ~4.11 % loss, and the loss for the solar cell with three coats ~9.63 %.

Table. 6.2. Solar cell *I-V* characteristics before and after coating with 300 nm silica nanoparticles.

No. of coats	**Coating**	V_{OC}	V_m	J_{sc} (mA/cm^2)	J_m (mA/cm^2)	P_{max} (mW /cm^2)	**Fill factor** %	P_{max} $Loss$ %
1	Uncoated	2.36	2.03	5.09	5.14	10.44	86.93	4.11
	Coated	2.30	2.14	5.21	4.68	10.01	83.45	
2	Uncoated	2.36	1.97	5.00	5.05	9.95	84.37	7.23
	Coated	2.39	2.22	4.94	4.16	9.23	78.08	
3	Uncoated	2.41	2.03	5.43	5.63	11.42	87.29	9.63
	Coated	2.41	1.92	5.43	5.37	10.32	78.88	

Solar cell coated with 400 nm nanoparticles:

Fig. 6.4 shows the *I-V* curves of solar cells without and with coats of 400 nm silica nanoparticles applied to the solar cell glass cover. The same procedure was followed. The solar cell color for the 400 nm nanoparticle coat is green with small dependence on angle of observation for the single coat.

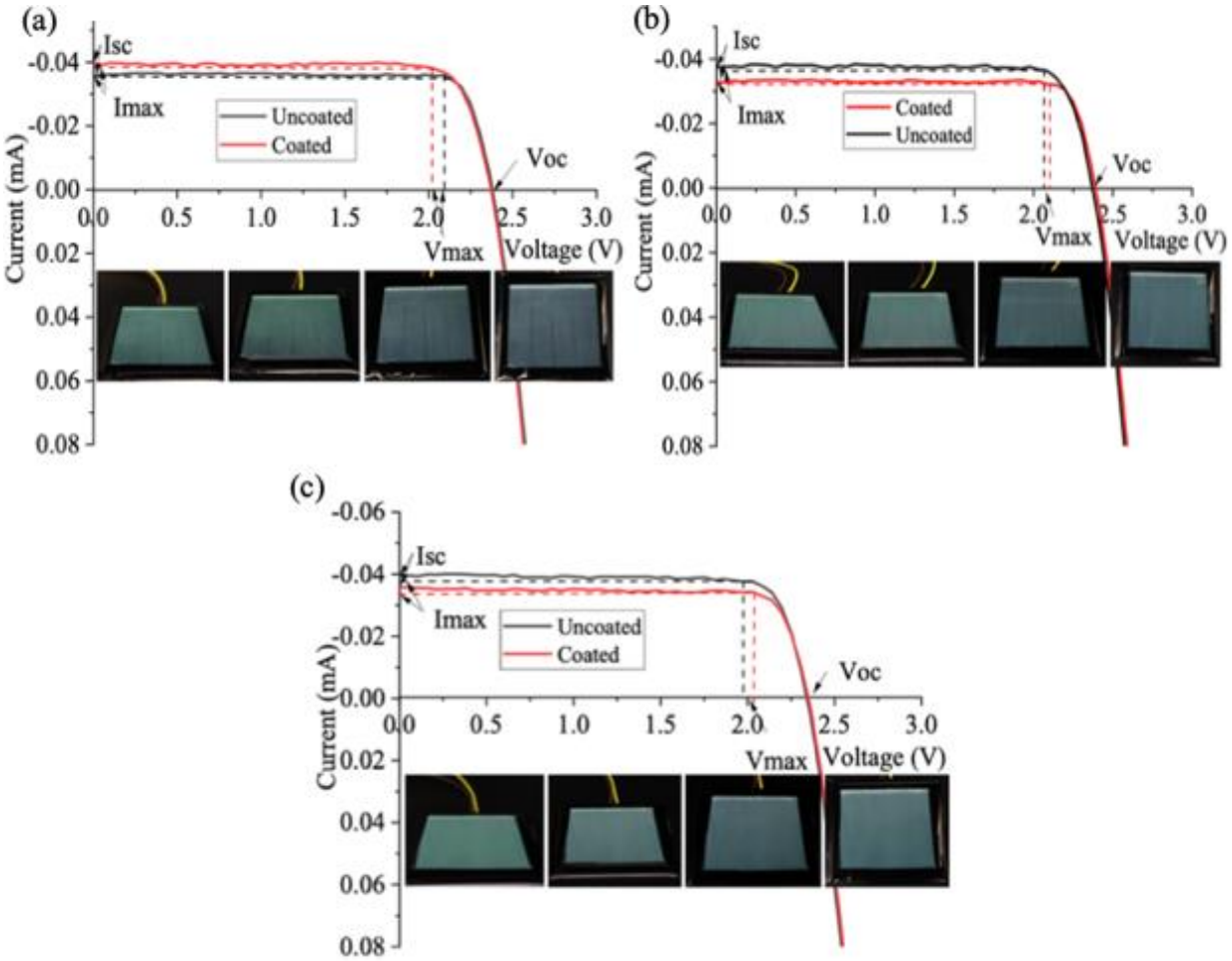

Fig. 6.4. *I-V* curves of the AOSHIKE Micro Solar without and with (a) one coat, (b) two coats, and (c) three coats of 400 nm silica nanoparticles (a single coat gives one layer of nanoparticles) applied to the solar cell glass cover. The coated solar cell is shown in the photographs taken at 30°, 45°, 60°, and 90°, left to right, respectively.

Table. 6.3, summarizes the results from the *I-V* curves of Fig. 6.4. The green color becomes more vivid with the increase in the number of coats, but the solar cell power loss also increases. Each coat application on the solar cell gives two layers of nanoparticles. From Table. 5.3, it can be observed that the power maximum difference for one coat and uncoated solar cell has a gain of 3.39 %. This can be explained by the antireflective property of the coating formed by the thin layer of nanoparticles which traps some of the incident light. Therefore, for a single 400-nm nanoparticle layer the solar cell becomes green and the power output is increased due to better coupling of the

incident light on the solar cell. The power loss for two coats is ~4.97 % loss and for the solar cell with three coats is ~8.63 %.

Table. 6.3. Solar cell I-V characteristics before and after coating with 400 nm silica nanoparticles.

No.of coats	**Coating**	V_{OC}	V_m	J_{SC} **(mA/**cm^2**)**	J_m **(mA/** cm^2**)**	P_{max} **(mW** $/cm^2$**)**	**Fill factor %**	P_{max} $Loss$ **%**	P_{max} $Gain$ **%**
1	Uncoated	2.41	2.08	5.45	5.43	11.29	86.02	--	3.39
	Coated	2.39	2.03	5.50	5.75	11.67	88.81		
2	Uncoated	2.35	2.03	4.91	4.85	9.86	85.44	4.97	--
	Coated	2.30	2.05	5.02	4.57	9.36	81.17		
3	Uncoated	2.36	1.98	5.59	5.55	11.00	83.36	8.63	--
	Coated	2.43	2.01	5.41	5.00	10.05	76.42		

Anti-reflective coating

To further study the effect of fabricating a thin layer of nanoparticles on the solar cell as an antireflection coating, we have tested the application of a diluted solution of 200 nm nanoparticles mixed at 65g/L in w/v with EtOH to form one layer of the 200-nm nanoparticles. The solution is diluted as to form a concentration of 65 g/L in w/v with EtOH. The solution was made by dispersing 200 mg of commercial 200 nm SiO_2 nanoparticles in 3 mL of the EtOH. After sonication, a drop of solution ~0.025 µL is dropped on the solar cell and roll-coated following the same procedure used. Fig. 6.5.(a) shows the *I-V* curves of the solar cell without and with one coat of 200 nm silica nanoparticles. The coated solar cell is shown in the photographs taken at 30°, 45°, 60°, and 90°, left to right respectively. The SEM image shows that one layer of nanoparticles is coated on the surface, with exception of a few areas of island formation. This single 200-nm nanoparticle layer results in a highly transparent blue shade on the solar cell.

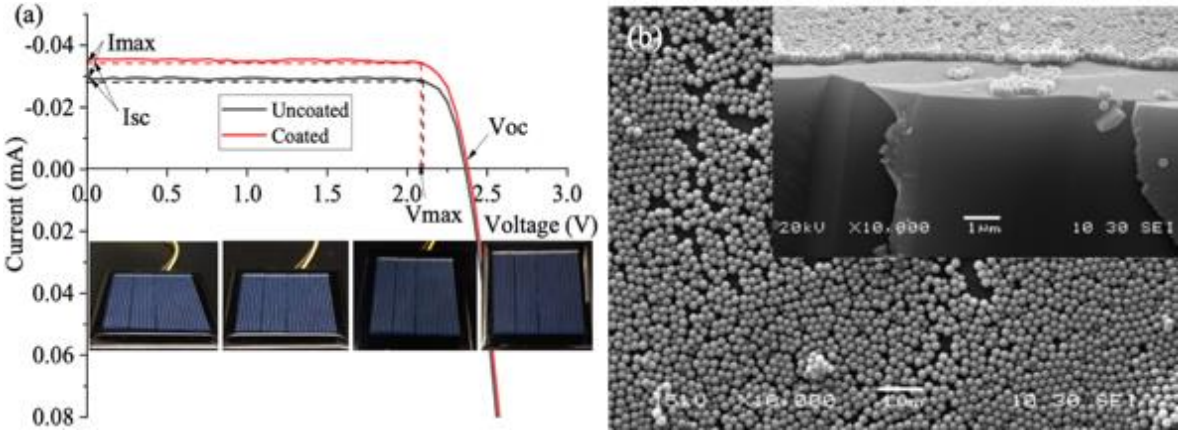

Fig. 6.5. (a) *I-V* curves of the AOSHIKE Micro Solar without and with one coat of 200 nm silica nanoparticles (a single coat gives one layer of nanoparticles) applied to the solar cell glass cover. The coated solar cell is shown in the photographs taken at 30°, 45°, 60°, and 90°, left to right respectively. (b) SEM image of glass slide coated with 200 nm silica nanoparticles with an inset of cross section SEM image on top right corner showing one layer of nanoparticles on the surface.

Table. 6.4 summarizes results of the measurement in Fig. 6.5, which shows a solar cell power gain of 3.21 % as a result of the application of one layer of 200-nm nanoparticles. The results show that if the nanoparticles are fabricated on the surface of the solar cell such that a single layer is formed on the surface, then the film acts as anti-reflective coating. For both 200 and 400-nm silica nanoparticles, the polycrystalline Si solar cell tested had a power gain of ~3.21 %.

Table. 6.4. Solar cell *I-V* before and after coating with a single layer of 200 nm silica nanoparticles.

No. of coats	**Coating**	V_{OC}	V_m	J_{sc} (mA/cm^2)	J_m (mA/cm^2)	P_{max} (mW /cm^2)	**Fill factor** %	P_{max} $Gain$ %
1	Uncoated	2.55	2.08	4.71	4.55	9.46	78.78	3.21
	Coated	2.36	2.05	5.11	4.77	9.77	81.07	

CHAPTER 7

MULTISHELLED NANOPARTICLES

7.1 INTRODUCTION

Color generation by multilayers of transparent materials are common in nature and man-made materials [34, 36]. To create vividly structured colors, materials with high index of refraction n are used such as ZnS, TiO_2, or ZrO_2. TiO_2 is an important photocatalytic material due to its high stability and efficiency, low toxicity, and low cost and availability [40].

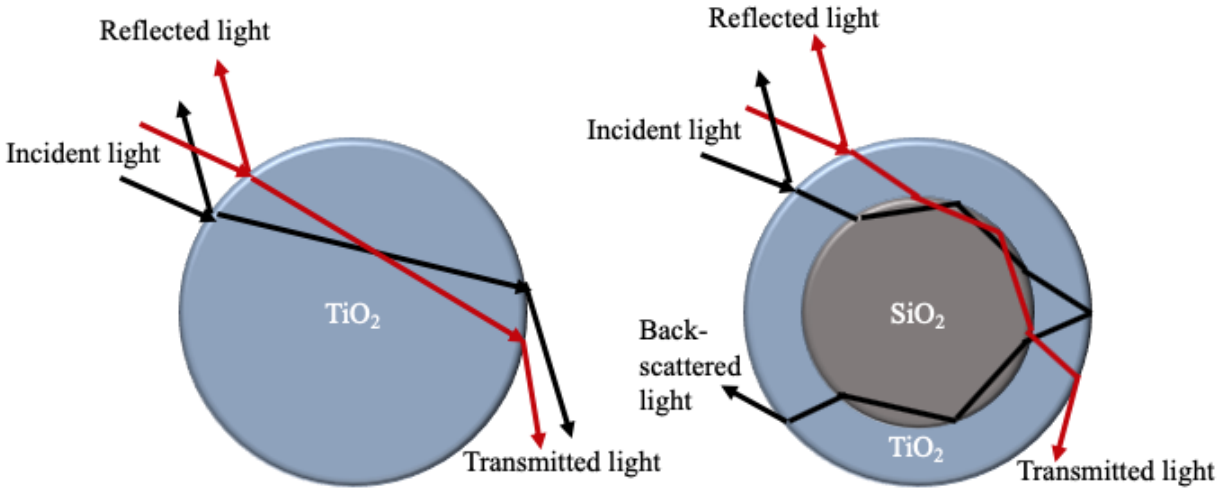

Fig. 7.1. Schematic showing light scattering path inside TiO_2 and core-shell (SiO_2/TiO_2) nanoparticle based on [45].

Fig. 7.1 illustrates the light scattering path inside the TiO_2 and core-shell nanoparticle in which the light undergoes scattering based on geometric plane of incident light. Light undergoes modified internal reflection when it passes through core SiO_2 layer and emerges as reflected light in backward direction resulting in stronger backscattering. When the light passes through the TiO_2 layer it does not backscatter [45,46].

Photonic crystals can only reflect a portion of the visible light in a number of layers on the surface of the TiO_2 after it has passed through the SiO_2 layer of the nanometer, thus enhancing the interaction between air and matter in the nanometer TiO_2 layer. The location of the reflectance spectra for the SiO_2/TiO_2 PCs can be estimated by the ultraviolet visible absorption spectrum. This process was explained by Bragg diffraction [39].

The movement of the position of the reflection peak can be explained by the Bragg equation:

$$\lambda = 2d_{hkl}(n_{eff}^2 - \ sin^2\beta)^{1/2} \quad \text{(Eqn. 7.1)}$$

where λ is the wavelength of the reflection peak, and $d_{hkl}$is the interplanar spacing of the photonic crystal in the [111] direction $d_{111} = \left(\frac{2}{3D}\right)^{1/2}$. D is the particle size, and β is the angle of incidence of light. For densely packed structures, the effective refractive index can be calculated by the following [39]:

$$n_{eff}^2 = n_{ST}^2 f + \ n_{air}^2(1 - f) \quad \text{(Eqn. 7.2)}$$

Where, f = 0.74 for fcc crystal, and n_{ST}, and n_{air} are refractive indices of silica@titania and air respectively. For the SiO_2/TiO_2 nanospheres, n_{ST} can be expressed by the following equation:

$$n_{ST} = \ n_{SiO_2}\frac{V_{SiO_2}}{V} + \ n_{TiO_2}\frac{V_{TiO_2}}{V} \quad \text{(Eqn. 7.3)}$$

Where n_{SiO_2}, and n_{TiO_2} are refractive indices of silica and titania respectively. Usually, refractive index of silica is 1.46, and titania is 2.46 which yields to the equation:

$$n_{eff} = 2.46 - (r/R)^3 \quad \text{(Eqn. 7.4)}$$

From the above equation it can be inferred that, the position of reflection peak is determined by n_{eff}. That is, with an increase in titania shell thickness, total size increases and as the refractive index of titania is higher than silica the total refractive index increases [39].

7.2 EXPERIMENTAL DETAILS

The multishell nanoparticles were prepared and analyzed using dynamic light scattering to determine the size by Dr. Bala Ramjee and his group, Department of Chemistry and Biochemistry, Old Dominion University. These nanoparticles were analyzed by Dr. Wei Cao, Applied Research Center, Old Dominion University, using JEM-2100F transmission electron microscope equipped with an Oxford INCAx-sight energy dispersive spectroscopy detector. The transmission and reflection spectra of the nanoparticle layer were characterized using a StellarNet BLACK-Comet spectrometer connected to a Nikon Ti-U inverted optical microscope where a pre-cleaned glass slide, similar to those used to fabricate the thin films, is used as a reference. For transmission measurements, a LED light (~1 mm diameter) from the spectrometer via optical fiber is incident on the sample and is then plotted using OriginLab software to compare the transmission loss. For reflectance, an aluminum mirror is used as the reference and another LED light source shines a light beam (~2mm diameter) from the bottom; for which the sample is placed, with the coated surface down, to measure the reflectance. A thin layer of gold was deposited using Polaron sputter coater to produce a conductive surface for scanning electron microscopy (JEOL JSM-6060LV). The TEM images of the nanoparticles used are shown below in Fig. 7.2.

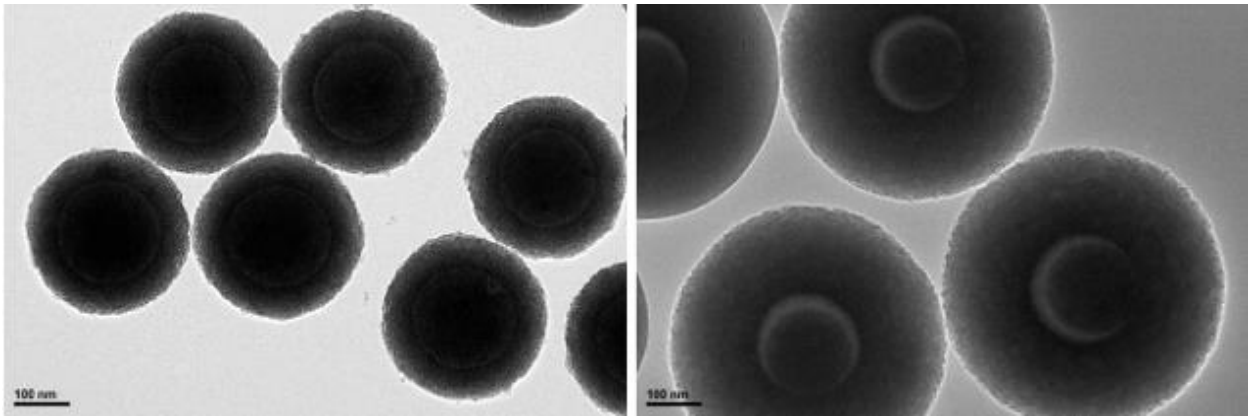

Fig. 7.2. TEM images of (a) SiO_2/TiO_2 nanoparticles labelled as AB3170 (300 ± 11 nm), and (b) $SiO_2/TiO_2/SiO_2$ nanoparticles labelled as AB 4064 (506 ± 13 nm).

The multishell nanoparticles were grown on the core of 200 nm silica nanoparticles with a TiO_2 shell of thickness ~100 nm for the SiO_2/TiO_2 nanoparticles. For $SiO_2/TiO_2/SiO_2$ nanoparticles, a shell of TiO_2 with ~120 nm thickness followed by 177 ± 13 nm SiO_2 outer shell. A schematic representing the core, core + shell, and core + shell + outer shell is shown in Fig. 7.3.

(a) (b) (c)

Fig. 7.3. Schematic of multi-shell nanoparticles showing (a) core (~209 nm) used to build shells, (b) core + shell (SiO_2/TiO_2) with core SiO_2 of ~209 nm and TiO_2 shell of ~100 nm with total diameter of 300 ± 11 nm, and (c) core + shell + outer shell ($SiO_2/TiO_2/SiO_2$) with core SiO_2 of ~209 nm, TiO_2 shell of ~120 nm, and SiO_2 outer shell of ~177 ± 13 nm with total diameter of 506 ± 13 nm.

The nanoparticles were dispersed in ethanol according to their diameter is as described in the Table. 7.1. The solution was then sonicated for 8 hours in a sonicator bath cooled by ice. About 0.025 µL of the prepared solution was dropped, using a pipette, on pre-cleaned glass slide or on the solar cell glass cover and rolled using different wire wound roller rods. This process creates a thin coating with controlled thickness depending on the wire diameter and roller speed.

Table. 7.1 Preparation of multishell nanoparticles colloidal solution according to nanoparticle size.

Nanoparticle diameter (nm)	Structure of nanoparticles	Weight of nanoparticles (mg)	Quantity of ethanol in (mL)
300 ± 11	SiO_2@TiO_2	200	1
506 ± 13	SiO_2@TiO_2@SiO_2	100	1

To uniformly coat the substrate using a roller rod, we used a commercial roller coating applicator machine “Automatic Glass Bed Film Applicator” purchased from TQC sheen to apply the thin coating on the glass slide. A drop of solution 0.025 µL was dropped on to the substrate and the rod was pulled at a uniform speed of 0.5 in/s.

7.3 RESULTS AND DISCUSSION

Soda lime glass slide coated with 300 ± 11 nm solution

Fig. 7.4. shows photographs of 300 ± 11 nm, SiO_2/TiO_2 nanoparticle coated glass slide taken with the camera lens axis positioned at 30°, 45°, 60°, and 90° (a-d), respectively. The glass slide was coated by one, two, and three coats (left to right in each set of images). The optical transmission and reflection, layer morphology and stacking of nanoparticles on glass slides having one, two, and three coats are shown in Fig. 7.5.

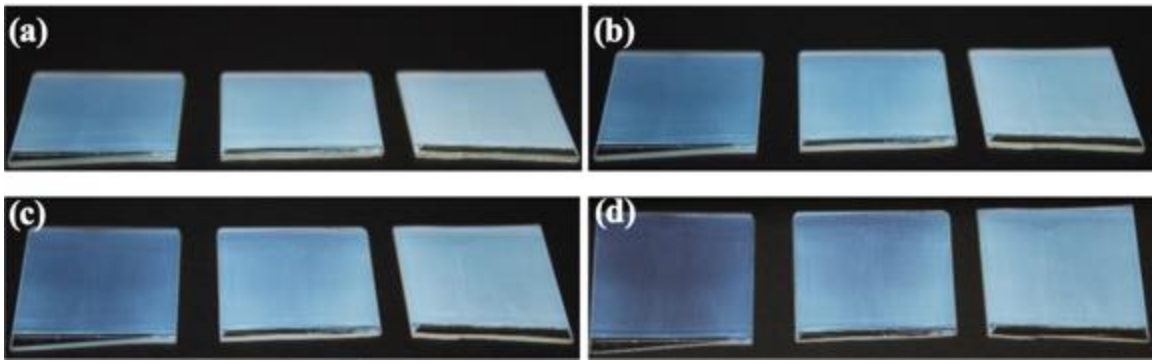

Fig. 7.4. Photographs of soda lime glass coated with 300 ± 11 nm solution taken with camera lens positioned at (a) 30°, (b) 45°, (c) 60°, and (d) 90° each image contains soda lime glass having one coat, two coats, and three coats (left to right) respectively.

The color vividness increases with the number of layers. For the film to have a uniform coating, the glass slides are dried for a minimum of 15 min. after each coat before applying another coat on to it. The optical transmission of the substrates was observed at 30°, 45°, 60°, and 90°, and the reflectance was measured with the slide positioned at normal to the incident light. Increasing the number of coats reduces the layer transmission.

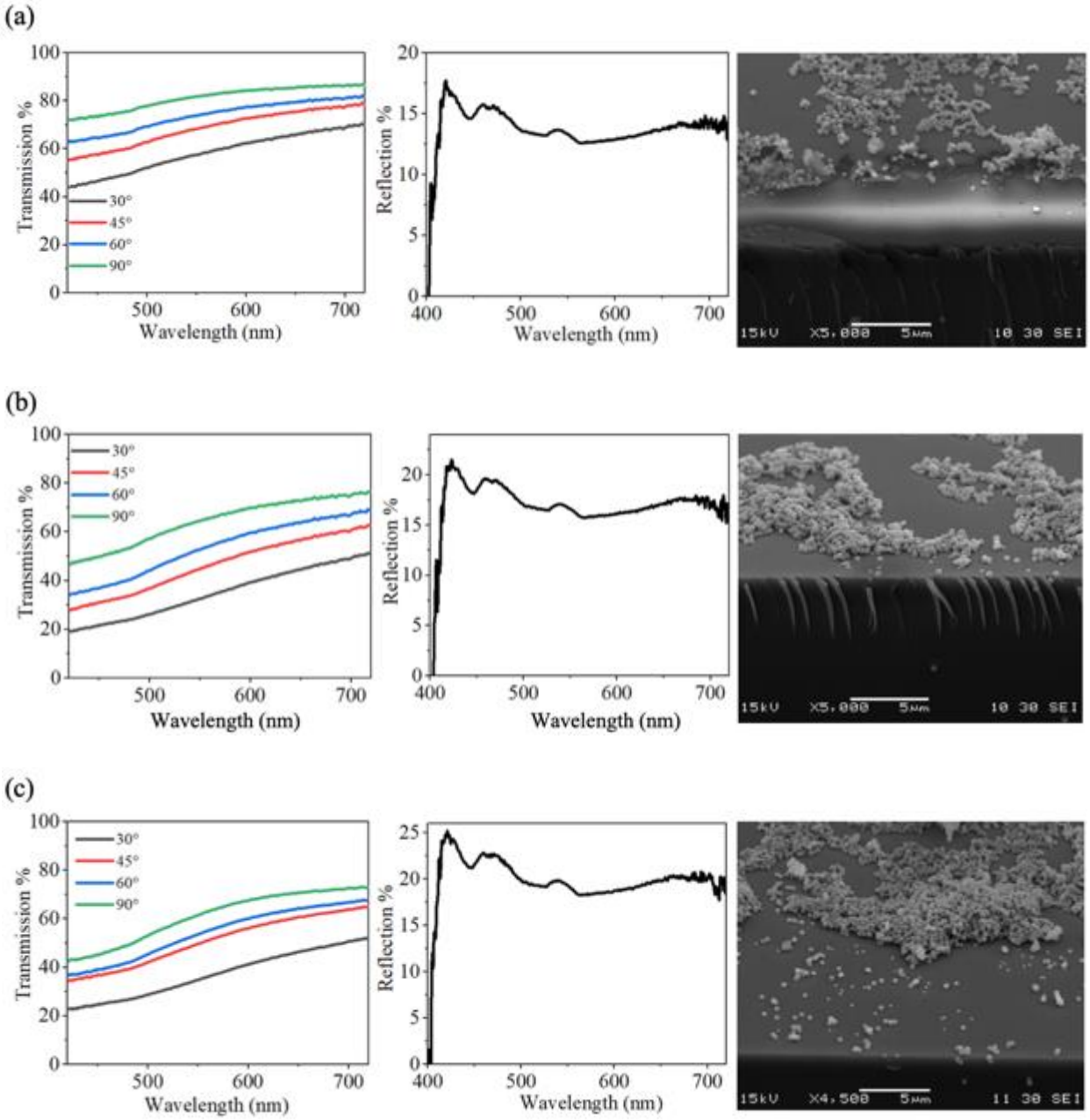

Fig. 7.5. (a) (left to right) Optical transmission of the coated glass slide with one coat. The transmission was observed for the slides positioned at 30°, 45°, 60°, and 90° to the incident light beam. The image in center is the optical reflection spectra of the coated glass slide with one coat. The reflection was observed for the slide normal to the incident beam, and the right image is SEM image of glass slide covered by 1 coat of 300 ± 11 nm. (b) and (c) are with two coats, and three coats respectively.

From the SEM figures, we observe that the nanoparticles are not stacked well and form islands or clusters of nanoparticles. This poor stacking is seen in the multishell nanoparticles terminated with TiO_2 outer shell.

Soda lime glass slide coated with 506 ± 13 nm solution

Fig. 7.6 shows photographs of 506 ± 13 nm of $SiO_2/TiO_2/SiO_2$ multi-shell coated glass slide taken with the camera lens axis positioned at 30°, 45°, 60°, and 90° (a-d), respectively. The glass slide was coated by one, two, and three coats (left to right in each set of images). The optical results. Fig. 7.7 shows SEM images of the stacking and surface morphology of three coats of 506 ± 13 nm on the glass slide.

The optical transmission of the substrates was observed at 30°, 45°, 60°, and 90°, and the reflectance was measured with the slide positioned at normal to the incident light. The transmission is reduced with the number of layers. To observe the stacking of nanoparticles, a thin layer of gold was sputtered on the glass slide to make it conductive and then observed using scanning electron microscopy, shown in Fig. 7.7.

(a)

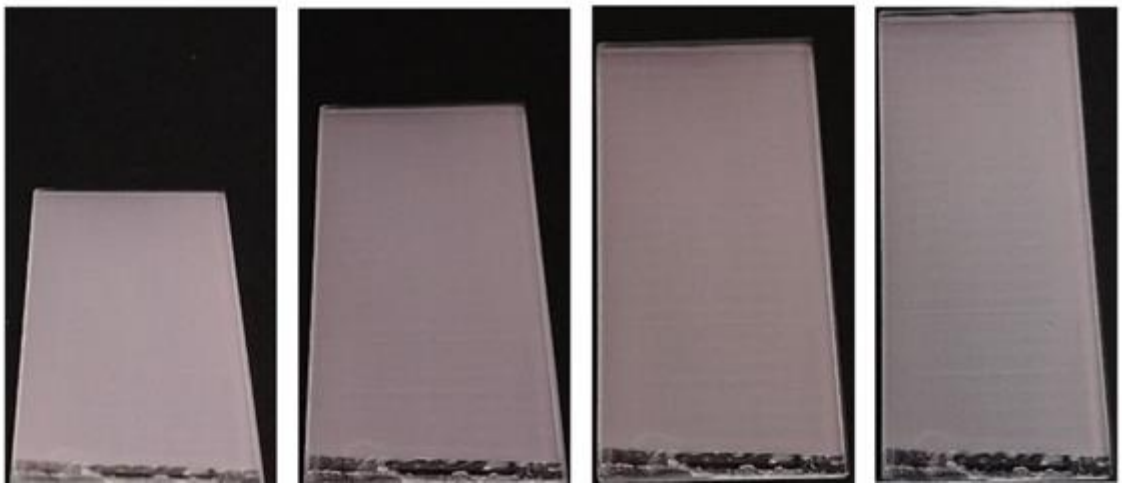

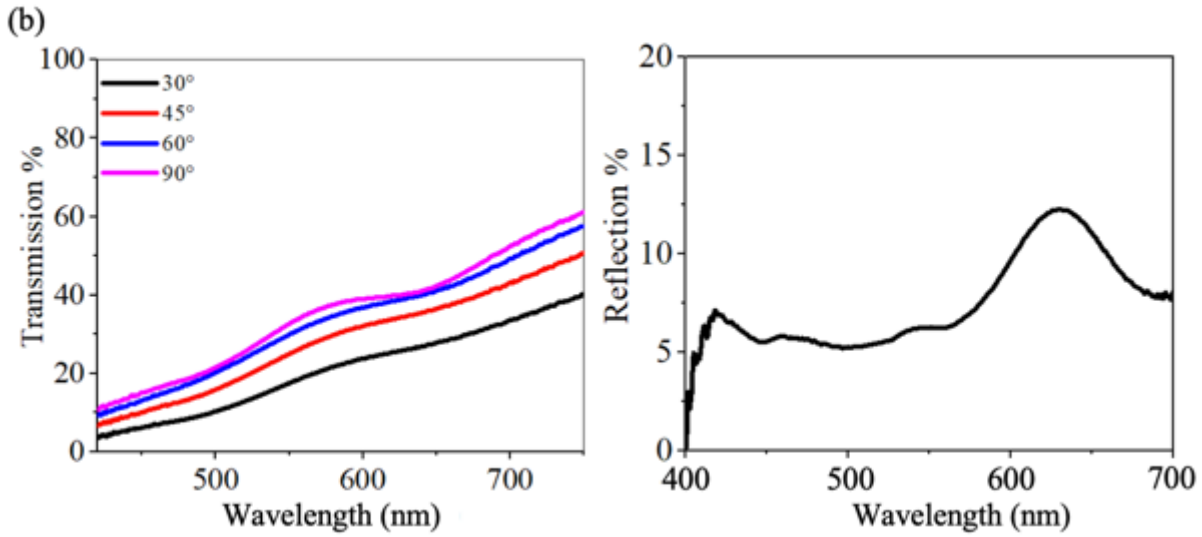

Fig. 7.6. (a) Photographs of soda lime glass slide having three coats of 506 ± 13 nm solution taken with camera lens positioned at (left to right) 30°, 45°, 60°, and 90°. (b) Optical transmission (left) and optical reflection spectra (right) of glass slide with 3 coats of 506 ± 13 nm solution.

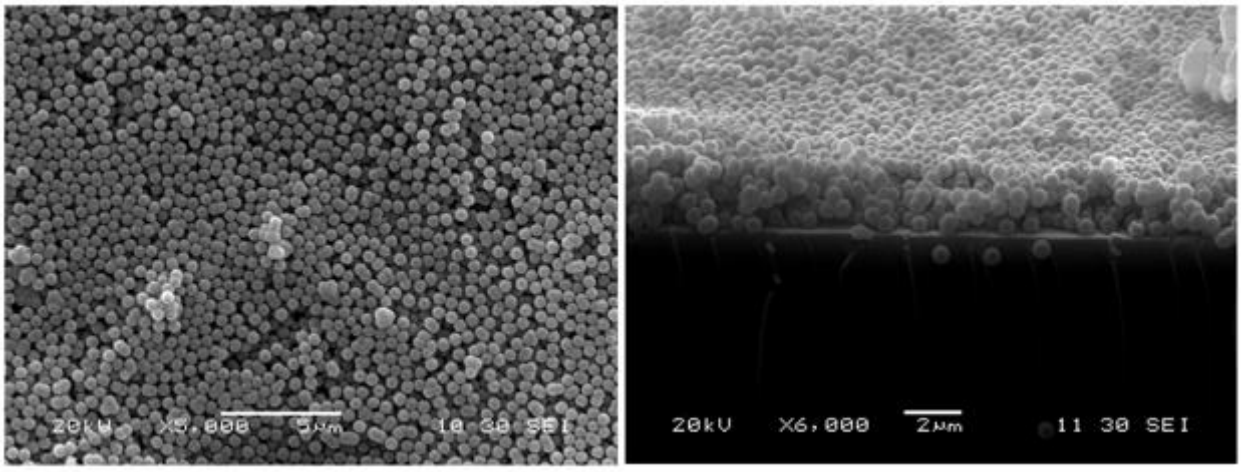

Fig. 7.7. (left) SEM image showing stacking of nanoparticles, and (right) is the cross-sectional SEM image showing the number of layers formed from the surface.

The SEM image shows stacking of nanoparticles with many defects. However, the stacking of these particles, which are terminated with SiO_2, is much better than the stacking of the 300 ± 11 nm particles that are terminated with TiO_2. Applying 3 coats of the 506 ± 13 nm nanoparticles leads to 3 layers of nanoparticles formed on the surface of the glass slide. There are many clusters and voids on the surface.

Solar cell performance with three coats of 506 ± 13 nm multishells

Fig. 7.8. shows the *I-V* curves of the solar cell without and with three coats of 506 ± 13 nm multi-shell nanoparticles, applied to the solar cell glass cover. The coated solar cells are shown in the insets of each figure taken at 30°, 45°, 60°, and 90°, left to right respectively. The solar cell operating parameters without and with the coating are given in Table 7.2. The three coats caused 10.92 % loss in power.

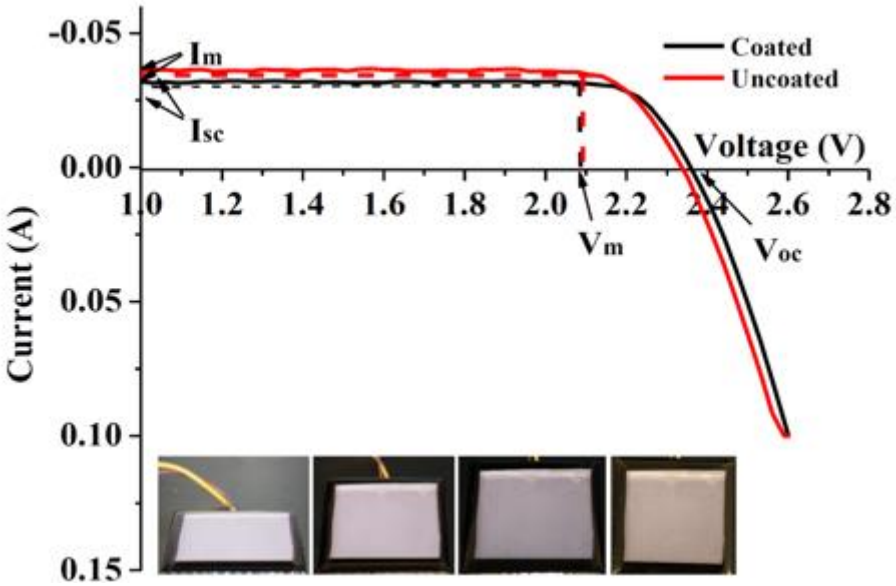

Fig. 7.8. *I-V* curve of the AOSHIKE Micro Solar without and with three coats of multishell silica-titania nanoparticles (a single coat gives one layer of nanoparticle) applied to the solar cell glass cover. The coated solar cell is shown in the photographs taken at 30°, 45°, 60°, and 90°, left to righ respectively. For the 506 ± 13 nm coating, the color shows some variation with viewing angle, particularly when the viewing angle was changed from 60° to 90°.

Table. 7.2. Solar cell *I-V* characteristics when uncoated and after multishell nanoparticles coating.

NP	Coating	V_{OC}	V_m	J_{SC} (mA/cm^2)	J_m (mA/ cm^2)	P_{max} (mW/cm^2)	Fill factor %	P_{max} $Loss$ %
506 ± 13 nm	Coated	2.32	2.08	4.71	4.68	9.73	88.97	10.92
	Uncoated	2.33	2.08	5.34	5.25	10.92	87.77	

CHAPTER 8

CONCLUSION AND FUTURE WORK

A layered micro/nanoparticle coating for selective spectral reflection, while providing high transmission to an underlying photovoltaic (PV) panel was developed. This coating is to maintain an attractive color appearance of the exterior surface for architecturally integrated PV. The study focused on controlled coating of glass surfaces by the nanoparticles to form crystalline structure on the surface with selective reflection with high transmission in the photon energy range needed for PV panels, while reflecting a selected part of the spectra to achieve a certain color. The major results are:

• Using layers of SiO_2 nanoparticles with different sizes to form a photonic crystal on Si solar cell with glass encapsulation is a relatively simple and effective method to produce colored solar cells with a loss of efficiency of ~ 2.08 – 9.54 %, depending on the color.

• A monolayer of silica nanoparticles on the solar cell cover such that was shown to increase the maximum power of the Si solar cells as the thin film acts as an antireflective coating.

• Multishell particles layered on the surface is an effective method to color solar cells with a demonstrated efficiency loss of ~11.1 % for three layers of the multishell particles, which is expected to be higher for one and two layers. This method is, however, more complicated due to the required steps in chemical synthesis.

• Roll-coating of layered nano/micro particles is a fast (10s of minutes to dry), cost effective, repeatable, and highly controllable method of fabricating layers of nanoparticles on solar cell glass encapsulation.

REFERENCES

[1] https://en.wikipedia.org/wiki/Building-integrated_photovoltaics , [Accessed April 1, 2020]

[2] S. John, "Strong localization of photons in certain disordered dielectric superlattices," *Phys. Rev. Lett.*, vol. 58, no. 23, pp. 2486–2489, Jun. 1987, doi: 10.1103/PhysRevLett.58.2486.

[3] M. Li, L. Zeng, Y. Chen, L. Zhuang, X. Wang, and H. Shen, "Realization of Colored Multicrystalline Silicon Solar Cells with SiO_2/SiN_x:H Double Layer Antireflection Coatings," *International Journal of Photoenergy*, vol. 2013, pp. 1–8, 2013, doi: 10.1155/2013/352473.

[4] https://www.albawaba.com/business/pr/dubai-investments%E2%80%99-coloured-solar-panels-dress-buildings-dubai-through-emirates-insolair, posted October 23rd, 2017, [Accessed March 30, 2020.]

[5] https://www.swissinso.com/technology, [Accessed March 30, 2020]

[6] https://www.solaxess.ch/en/photovoltaic-panels-pv/innovation-by-color/, [Accessed March 30, 2020.]

[7] V. Neder, S. L. Luxembourg, and A. Polman, "Efficient colored silicon solar modules using integrated resonant dielectric nanoscatterers," *Appl. Phys. Lett.*, vol. 111, no. 7, p. 073902, Aug. 2017, doi: 10.1063/1.4986796.

[8] L.-E. Perret *et al.*, Eds., "New challenges in solar architectural innovation," *Proceedings of CISBAT 2011 - CleanTech for Sustainable Buildings*, 2011.

[9] G. Peharz *et al.*, "Application of plasmonic coloring for making building integrated PV modules comprising of green solar cells," *Renewable Energy*, vol. 109, pp. 542–550, Aug. 2017, doi: 10.1016/j.renene.2017.03.068.

[10] O. L. Pursiainen, J. J. Baumberg, H. Winkler, B. Viel, P. Spahn, and T. Ruhl, "Nanoparticle-tuned structural color from polymer opals," *Opt. Express*, vol. 15, no. 15, p. 9553, 2007, doi: 10.1364/OE.15.009553.

[11] R. O. Prum, R. H. Torres, S. Williamson, and J. Dyck, "Coherent light scattering by blue feather barbs," *Nature*, vol. 396, no. 6706, pp. 28–29, Nov. 1998, doi: 10.1038/23838.

[12] V. Saranathan *et al.*, "Structure and optical function of amorphous photonic nanostructures from avian feather barbs: a comparative small angle X-ray scattering (SAXS) analysis of 230 bird species," *J. R. Soc. Interface*, vol. 9, no. 75, pp. 2563–2580, Oct. 2012, doi: 10.1098/rsif.2012.0191.

[13] R. O. Prum, "Structural colouration of mammalian skin: convergent evolution of coherently scattering dermal collagen arrays," *Journal of Experimental Biology*, vol. 207, no. 12, pp. 2157–2172, May 2004, doi: 10.1242/jeb.00989.

[14] B. Q. Dong *et al.*, "Structural coloration and photonic pseudogap in natural random close-packing photonic structures," *Opt. Express*, vol. 18, no. 14, p. 14430, Jul. 2010, doi: 10.1364/OE.18.014430.

[15] C. Pouya, D. G. Stavenga, and P. Vukusic, "Discovery of ordered and quasi-ordered photonic crystal structures in the scales of the beetle Eupholus magnificus," *Opt. Express*, vol. 19, no. 12, p. 11355, Jun. 2011, doi: 10.1364/OE.19.011355.

[16] S. Kinoshita, S. Yoshioka, and Y. Fujii, "Mechanisms of Structural Color in Nature," *J. Jpn. Soc. Colour Mater.*, vol. 75, no. 10, pp. 493–499, 2002, doi: 10.4011/shikizai1937.75.493.

[17] Austin Roorda, VS203B, Lecture Notes, Topic: “Thin Film Interference.” School of Optometry, Berkeley School of Optometry, University of California, Berkeley, California, Spring 2011.
[18] OpenStaxCollege, “Thin Film Interference,” in *College Physics*, 2012.
[19] “CAS PY 106 Study Guide - Spring 2014, - Superposition Principle, Geometrical Optics, Physical Optics,” *OneClass*. https://oneclass.com/study-guides/us/boston-u/cas-py/cas-py-106/338534-interference-py-106.en.html (accessed Apr. 01, 2020).
[20] B. Parida, S. Iniyan, and R. Goic, “A review of solar photovoltaic technologies,” *Renewable and Sustainable Energy Reviews*, vol. 15, no. 3, pp. 1625–1636, Apr. 2011, doi: 10.1016/j.rser.2010.11.032.
[21] H. Majaron, “Structural Coloration,” presented at the Seminar for the Department of Mathematics and Physics (University of Ljubljana), Ljubljana, December 2013.
[22] K. Koc, F. Z. Tepehan, and G. G. Tepehan, “Antireflecting coating from Ta2O5 and SiO2 multilayer films,” *J Mater Sci*, vol. 40, no. 6, pp. 1363–1366, Mar. 2005, doi: 10.1007/s10853-005-0566-2.
[23] A. Thelen, *Design of optical interference coatings*. New York: McGraw-Hill, 1989.
[24] F. L. Pedrotti, L. M. Pedrotti, and L. S. Pedrotti, *Introduction to optics*. 2018.
[25] S. Kinoshita, S. Yoshioka, and J. Miyazaki, “Physics of structural colors,” *Rep. Prog. Phys.*, vol. 71, no. 7, p. 076401, Jul. 2008, doi: 10.1088/0034-4885/71/7/076401.
[26] J. Ge and Y. Yin, “Responsive Photonic Crystals,” *Angew. Chem. Int. Ed.*, vol. 50, no. 7, pp. 1492–1522, Feb. 2011, doi: 10.1002/anie.200907091.
[27] O. L. Pursiainen, J. J. Baumberg, H. Winkler, B. Viel, P. Spahn, and T. Ruhl, “Nanoparticle-tuned structural color from polymer opals,” *Opt. Express*, vol. 15, no. 15, p. 9553, 2007, doi: 10.1364/OE.15.009553.
[28] Xia, Y., Gates, B. and Li, Z.-Y, “Self-Assembly Approaches to Three-Dimensional Photonic Crystals,” *Advanced Materials*, vol. 13, no. 6, 2001, pp. 409-413. 2001, https://doi.org/10.1002/1521-4095(200103)
[29] E. Yablonovitch, “Inhibited Spontaneous Emission in Solid-State Physics and Electronics,” *Phys. Rev. Lett.*, vol. 58, no. 20, pp. 2059–2062, May 1987, doi: 10.1103/PhysRevLett.58.2059.
[30] S. John, “Strong localization of photons in certain disordered dielectric superlattices,” *Phys. Rev. Lett.*, vol. 58, no. 23, pp. 2486–2489, Jun. 1987, doi: 10.1103/PhysRevLett.58.2486.
[31] Gates, B., Park, S.H. and Xia, Y., “Tuning the Photonic Bandgap Properties of Crystalline Arrays of Polystyrene Beads by Annealing at Elevated Temperatures,” *Advanced Materials*, vol. 12, no. 9, pp. 653-656, 2000,. https://doi.org/10.1002/(SICI)1521-4095(200005)12:9<653::AID-ADMA653>3.0.CO;2-3
[32] A. Blanco, H. Míguez, F. Meseguer, C. López, F. López-Tejeira, and J. Sánchez-Dehesa, “Photonic band gap properties of CdS-in-opal systems,” *Appl. Phys. Lett.*, vol. 78, no. 21, pp. 3181–3183, May 2001, doi: 10.1063/1.1370981.
[33] Ozin, G.A. and Yang, S.M. ,”The Race for the Photonic Chip: Colloidal Crystal Assembly in Silicon Wafers.” Adv. Funct. Mater., 11: 95-104. 2001, doi:10.1002/1616-3028(200104)11:2<95::AID-ADFM95>3.0.CO;2-O
[34] Y. Zhao, Z. Xie, H. Gu, C. Zhu, and Z. Gu, “Bio-inspired variable structural color materials,” *Chem. Soc. Rev.*, vol. 41, no. 8, p. 3297, 2012, doi: 10.1039/c2cs15267c.

[35] Y. Si, Z. Dong, and L. Jiang, “Bioinspired Designs of Superhydrophobic and Superhydrophilic Materials,” *ACS Cent. Sci.*, vol. 4, no. 9, pp. 1102–1112, Sep. 2018, doi: 10.1021/acscentsci.8b00504.

[36] P. Kurt, D. Banerjee, R. E. Cohen, and M. F. Rubner, “Structural color via layer-by-layer deposition: layered nanoparticle arrays with near-UV and visible reflectivity bands,” *J. Mater. Chem.*, vol. 19, no. 47, p. 8920, 2009, doi: 10.1039/b912211g.

[37] C. Fenzl, T. Hirsch, and O. S. Wolfbeis, “Photonic Crystals for Chemical Sensing and Biosensing,” *Angew. Chem. Int. Ed.*, vol. 53, no. 13, pp. 3318–3335, Mar. 2014, doi: 10.1002/anie.201307828.

[38] S. Jeong, L. Hu, H. R. Lee, E. Garnett, J. W. Choi, and Y. Cui, “Fast and Scalable Printing of Large Area Monolayer Nanoparticles for Nanotexturing Applications,” *Nano Lett.*, vol. 10, no. 8, pp. 2989–2994, Aug. 2010, doi: 10.1021/nl101432r.

[39] F. Wang, L. Feng, Y. Qin, T. Zhao, H. Luo, and J. Zhu, “Dual functional SiO_2@TiO_2 photonic crystals for dazzling structural colors and enhanced photocatalytic activity,” *J. Mater. Chem. C*, vol. 7, no. 38, pp. 11972–11983, 2019, doi: 10.1039/C9TC03426A.

[40] C. Xie, T. Fan, A. Wang, and S.-L. Chen, “Enhanced Visible-Light Photocatalytic Activity of a TiO_2 Membrane-Assisted with N-Doped Carbon Quantum Dots and SiO_2 Opal Photonic Crystal,” *Ind. Eng. Chem. Res.*, vol. 58, no. 1, pp. 120–127, Jan. 2019, doi: 10.1021/acs.iecr.8b05101

[41] A. Kafizas, S. Kellici, J. A. Darr, and I. P. Parkin, “Titanium dioxide and composite metal/metal oxide titania thin films on glass: A comparative study of photocatalytic activity,” *Journal of Photochemistry and Photobiology A: Chemistry*, vol. 204, no. 2–3, pp. 183–190, May 2009, doi: 10.1016/j.jphotochem.2009.03.017.

[42] S. Nishimura *et al.*, “Standing Wave Enhancement of Red Absorbance and Photocurrent in Dye-Sensitized Titanium Dioxide Photoelectrodes Coupled to Photonic Crystals,” *J. Am. Chem. Soc.*, vol. 125, no. 20, pp. 6306–6310, May 2003, doi: 10.1021/ja034650p.

[43] L. I. Halaoui, N. M. Abrams, and T. E. Mallouk, “Increasing the Conversion Efficiency of Dye-Sensitized TiO_2 Photoelectrochemical Cells by Coupling to Photonic Crystals,” *J. Phys. Chem. B*, vol. 109, no. 13, pp. 6334–6342, Apr. 2005, doi: 10.1021/jp044228a.

[44] A. Mihi, M. E. Calvo, J. A. Anta, and H. Míguez, “Spectral Response of Opal-Based Dye-Sensitized Solar Cells,” *J. Phys. Chem. C*, vol. 112, no. 1, pp. 13–17, Jan. 2008, doi: 10.1021/jp7105633.

[45] S. Son, S. H. Hwang, C. Kim, J. Y. Yun, and J. Jang, “Designed Synthesis of SiO_2/TiO_2 Core/Shell Structure As Light Scattering Material for Highly Efficient Dye-Sensitized Solar Cells,” *ACS Appl. Mater. Interfaces*, vol. 5, no. 11, pp. 4815–4820, Jun. 2013, doi: 10.1021/am400441v.

[46] Y. Takano and K.-N. Liou, “Phase matrix for light scattering by concentrically stratified spheres: comparison of geometric optics and the ‘exact’ theory,” *Appl. Opt.*, vol. 49, no. 20, p. 3990, Jul. 2010, doi: 10.1364/AO.49.003990.

APPENDIX A

Roller Coating Procedure

The image of TQC roller is as shown in Fig. A.1., taken from official website of TQC sheen. The parts are described as per the labelled numbers.

Fig. A.1. Image of TQC automatic glass bed film applicator machine present at ODU, showing the part numbers (Image taken from official TQC website).

Part names as per the numbering in the image

1. Power switch
2. Emergency stop knob
3. Clamp
4. Applicator weight
5. Glass bed
6. Navigation keys
7. Display
8. Traverse

Procedure

1.) Turn on the power supply using power switch, and the roller coat applicator will turn on with a message of positioning the applicator. Press Yes on the display screen using OK key from the Navigator keys, and it calibrates itself.

2.) The display shows the current set limits of speed. Eg. 55 mm/s, with options of SETUP, RUN, and MENU on the display which you can select using navigator keys.

3.) To change the speed, or the notation of speed (from mm/s to inch/s) navigate to SETUP option on display and press OK, where you can change the speed or notation using the navigator keys.

4.) After setting up the desired value of speed, go to RUN option and press OK, from where the display will show the RUN MENU with the START option.

5.) To roll coat a sample, press the clamp down to open, and then place the substrate to be coated all the way under the clamp position, and release the clamp to make sure the substrate is held in place.

6.) Now place the roller rod below the applicator weight, and on to the substrate to be coated.

7.) Drop the solution using a pipette on to the roller rod (rather than on to the substrate itself) to eliminate any non-uniform drying of the solution.

8.) After dropping the solution, press START using OK button from the navigation keys, and the traverse will start moving at the set speed, coating the substrate with the solution.

9.) After the coating is done, press BACK option using the OK button, and the traverse will return to its calibrated position.

10.) Remove the substrate by releasing the clamp (Press down the clamp).

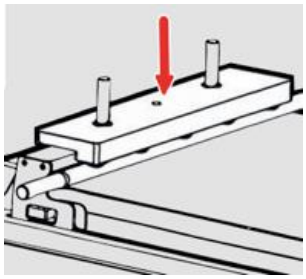

Fig. A.2. Image showing the applicator weight, where extra weight can be added (Image taken from TQC website).

If needed extra weight can be added on the Applicator weight as shown in the Fig. A.2., to make sure the rod doesn't rotate, but rather drags the solution on the substrate to create a uniform coating.

APPENDIX B

Optical Spectroscope

StellarNet BLACK-Comet spectrometer connected to a Nikon Ti-U inverted optical microscope, is used to perform the transmission and reflection spectra on the coated glass slide.

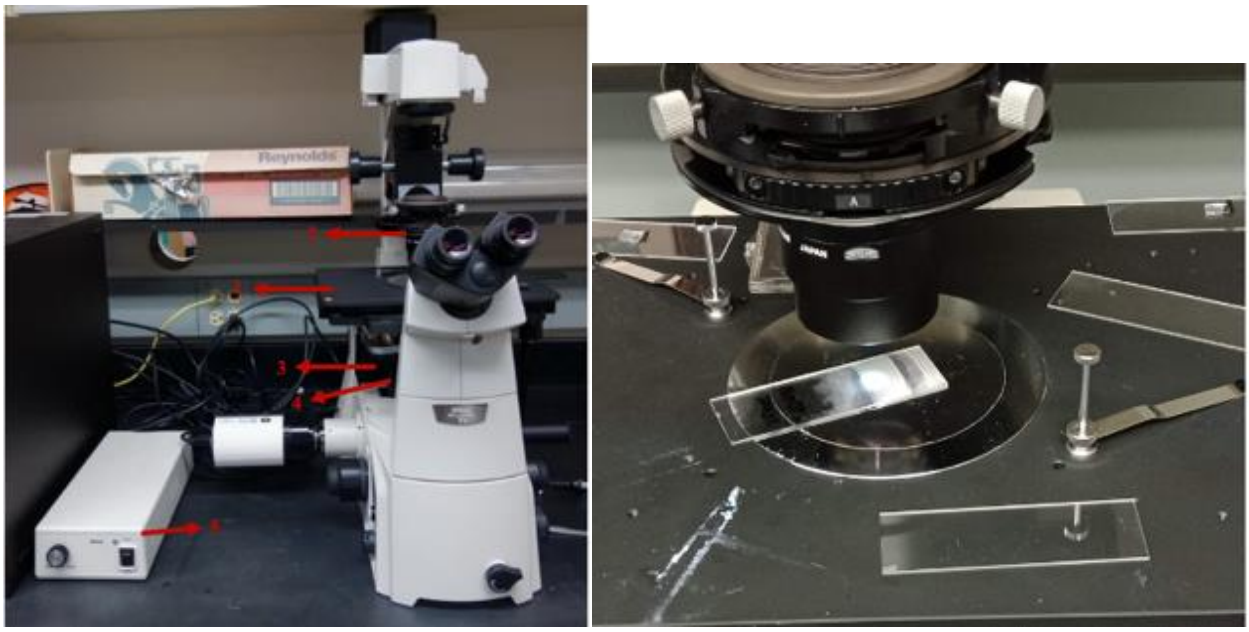

Fig. B.1. (left) Image of Optical Spectrometer connected to microscope at ODU, (right) sample space showing light irradiation from the top for transmission spectra.

The Fig. B.1. shows, 1.) Sample space, 2.) optical fiber cable from light source for transmission spectra, 3.) Optical fiber cable from light source for reflection spectra, 4.) Detector, and 5.) Light source for reflection spectra

Fig. B.2. shows, schematic of spectrometer connected to Nikon TI-U inverted microscope, showing the path of light for transmission measurement on glass slides. The light source intensity can be varied using the knob, and the adapter tube contains a lens that focuses the transmitted light to the optical fiber connected to spectrometer.

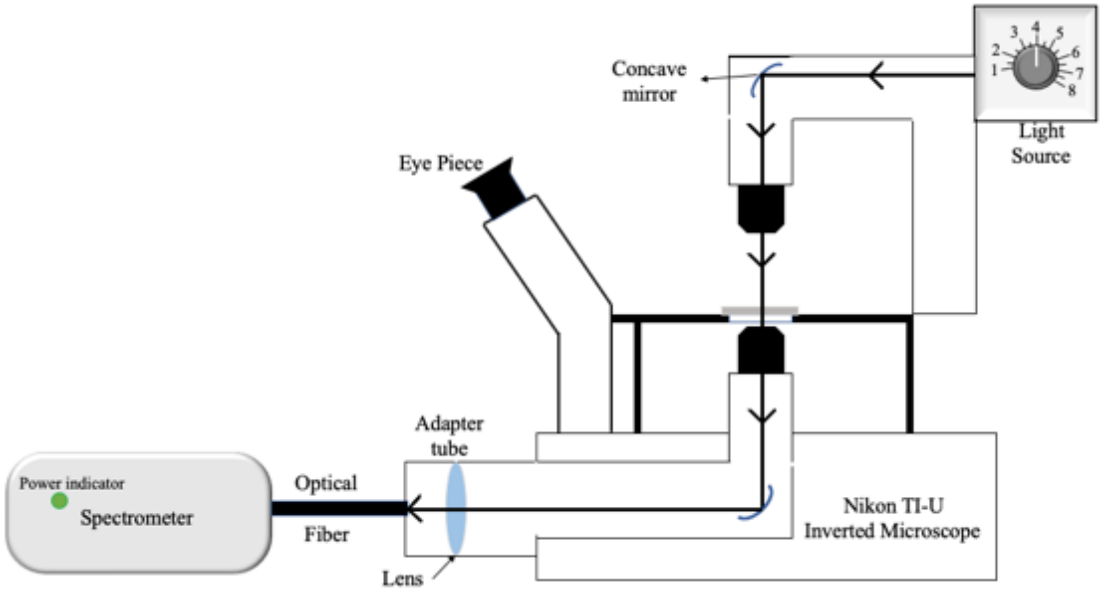

Fig. B.2. Schematic of spectrometer connected to Nikon TI-U inverted optical microscope.

The optical spectroscope is connected to a spectroscopy software StellarNet. Inc, corresponding to stellarnet detector which detects the electromagnetic spectrum ranging from 200 nm to 800 nm. The software shows the spectra only from 400 nm to 750 nm (<400 nm and > 750 nm is junk value).

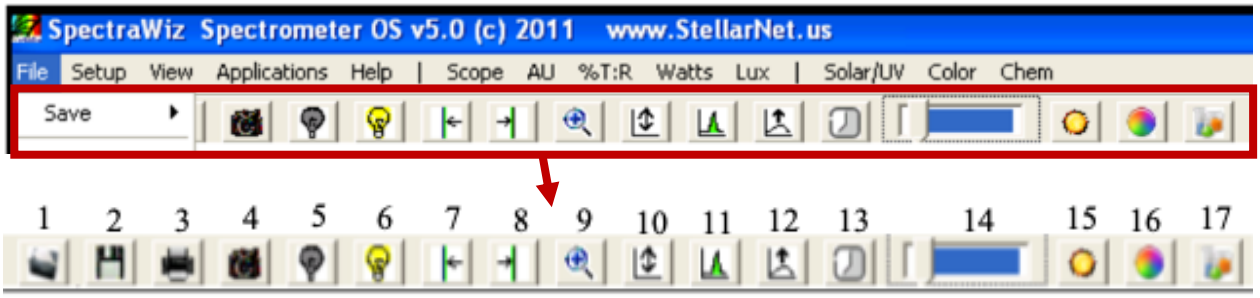

Fig. B.3. Image of Stellarnet spectrometer software showing Toolbar options (Image taken from manual).

1.) File open
2.) Save sample spectrum
3.) Print graph
4.) Snapshot spectra
5.) Save dark spectrum
6.) Save light reference
7.) Move data cursor left
8.) Move data cursor right
9.) Zoom wavelength
10.) Re-scale Y axis
11.) Compute area
12.) Auto-integration
13.) Detector integration time
14.) Integration time bar
15.) Solar Monitor
16.) CIE color measurement
17.) ChemWiz Chemistry

15.), 16.), and 17.) are Application Icons

Procedure

For transmission spectra:

1.) Turn off the lights in the room for accurate spectroscopy measurements, turn on the system connected to the stellarnet detector and press Save dark spectrum, to save the minimum transmission value.

2.) Now, turn on the light source for transmission analysis, and a light of around 1 mm diameter is irradiated from the top of the optical spectrometer (from point 2 in Fig.B.1).

3.) Place an uncoated slide in the sample space similar to the glass slide used for fabricating the thin film to set it as a 100 % reference, and make sure the light is passing through the glass slide towards the detector. Press Save Light reference from the tool bar in the software.

4.) Now place the coated glass slide in the sample space with the coated side facing upwards towards the light irradiation, and select File --> Save --> Save Spectrum, and save the spectrum in .TRM format to use it again to plot using Origin software.

5.) To do transmission analysis at different angles, repeat the same steps but hold the sample at the required angle with respect to the light irradiation direction.

For reflectance spectra:

1.) Follow steps 1 and 2 from the procedure for transmission spectra, but the light in this case is irradiated from the bottom of the optical spectroscope (from point 3 in Fig. B.1)

2.) Place the uncoated glass slide, with an aluminum mirror on top of it covering the glass slide in the sample space and press Save light spectrum to save the 100 % reflection reference.

3.) Now place the coated glass slide with face down towards the light irradiation and place a dark sheet (in our case we used a black cardboard) to eliminate any secondary reflections. Now select File ---> Save ---> Save spectrum, and save the spectrum in .TRM format to use it again to plot using Origin software.

APPENDIX C

Atomic Force Microscope

A Digital Instrument Dimension 3100 Atomic Force Microscope (AFM) operating in tapping mode connected to a NanoScope IIIa Scanning Probe Microscope Controller, and NanoScope Dimension 3100 Controller operating with NanoScope SPM software. The AFM machine is setup on a vibration resistant bench as it is a vibration sensitive equipment.

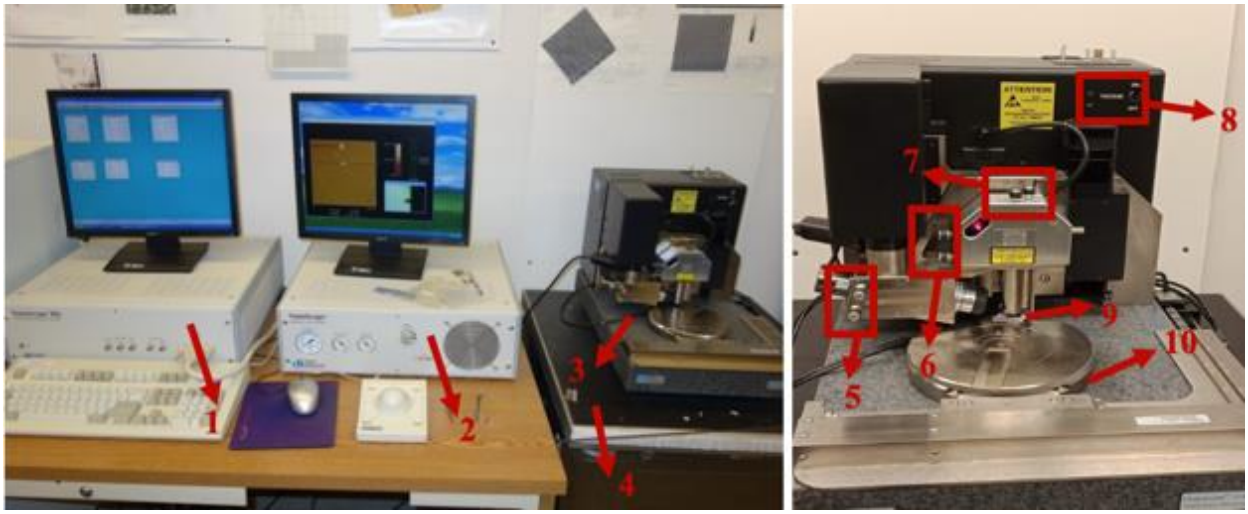

Fig. C.1. Image of Atomic Force Microscope at ODU facility showing different parts.

1.) NanoScope IIIa Scanning Probe Microscope Controller
2.) NanoScope Dimension 3100 Controller
3.) Atomic Force Microscope
4.) Vibration resistant bench
5.) Camera Adjustment knobs
6.) Photodetector adjustment knobs
7.) Laser adjustment knobs
8.) Vacuum Switch
9.) Tip head
10.) Sample stage

Procedure

1.) Turn on the system and turn on the switches behind Nanoscope Scanning Probe microscope, and Nanoscope Dimension controllers.

2.) Click on the Nanoscope SPM software icon on desktop and go into imaging mode by clicking on the imaging icon in toolbar.

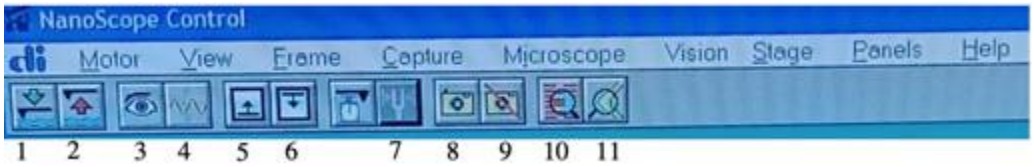

Fig. C.2. Nanoscope SPM control software tool bar.

1.) Tip Engage
2.) Tip retract
3.) Image mode
4.) Scope mode
5.) Extend tip
6.) Retract tip
7.) Auto-tune
8.) Capture on
9.) Capture off
10.) Focus surface
11.) Locate tip

3.) Imaging mode of the software opens, and the above controls are available to start the scan for surface roughness. Make sure that the AFM is operating in Tapping mode.

4.) If the operating mode is in Tapping mode, then turn off the vacuum switch, and place the sample on the sample stage. After placing the sample on the stage turn the vacuum switch back to ON, and manually rotate the sample stage such that the sample is approximately under the tip head.

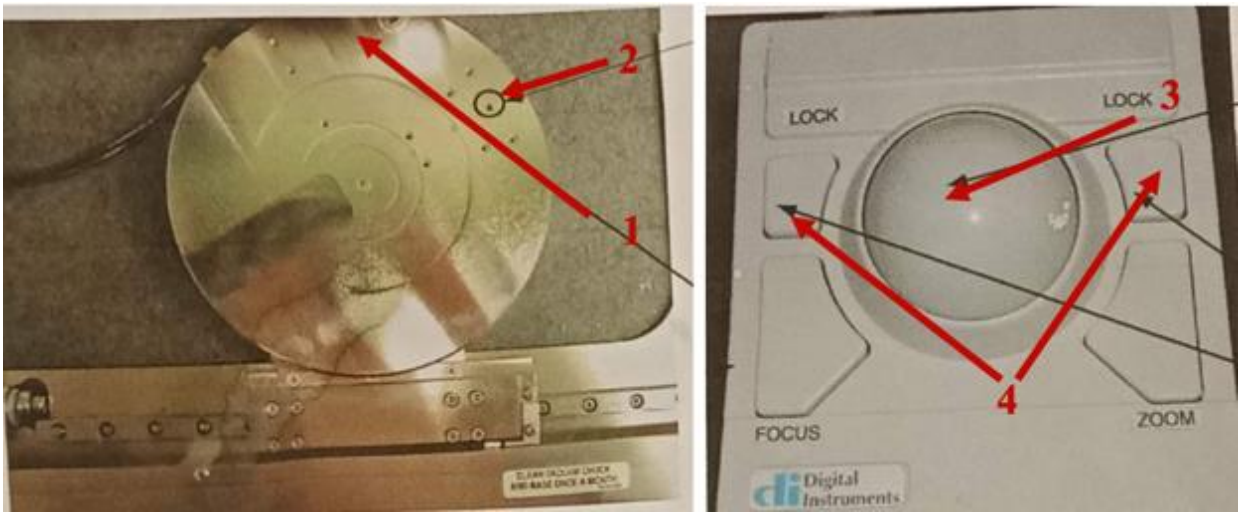

Fig. C.3. Image showing the sample stage, and track ball showing the parts for operating.

1.) Sample holder space for larger samples
2.) Sample holder space for small samples
3.) Track ball
4.) Lock button to keep stage moving

5.) Now, click on the focus surface icon (point 10 in Fig. C.2.), and use the trackball to move the sample precisely under the tip head.

6.) After moving the sample under the tip head, click the locate tip icon to locate the tip and use the camera adjustment knobs to center the tip on the screen as shown in the Fig. C.4. below.

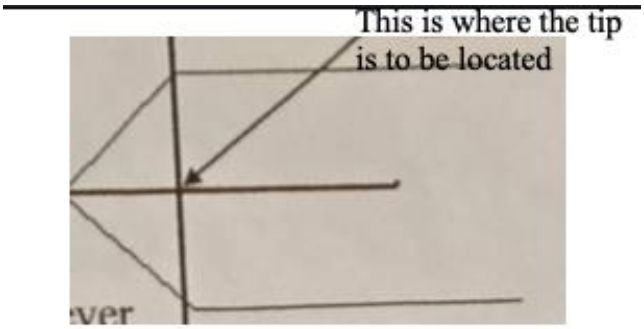

Fig. C.4. Image of schematic of cantilever and tip position.

7.) After locating the tip and centering the tip position using the camera knobs, click on the focus surface icon and focus the surface by holding the focus button and using the trackball on trackball control.

8.) Now as the surface is focused, click on the auto-tune icon to see if the tip is tuned to the frequency to operate in the tapping mode and the sweep should appear as seen below.

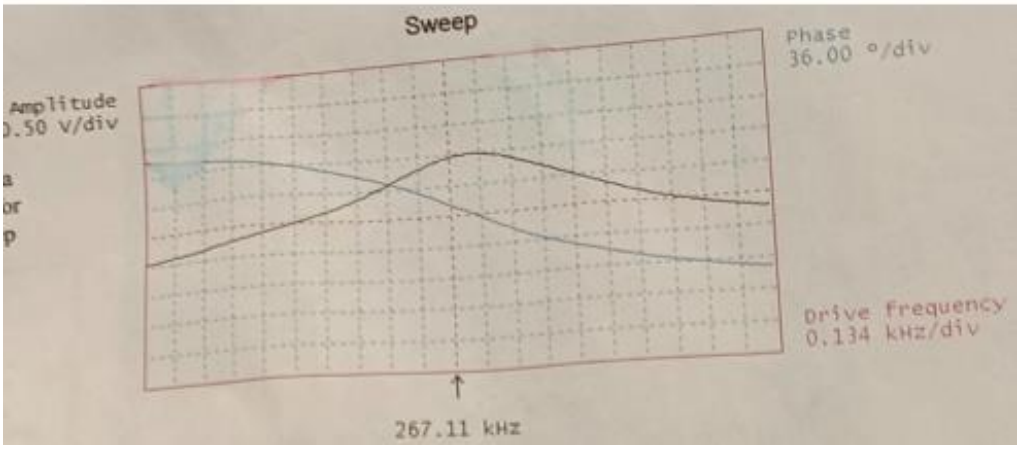

Fig. C.5. Example of a good trace for tuning sweep.

9.) After the tune sweep is as shown in the Fig. C.5., click on Engage tip icon to lower the tip in-order to start a scan.

10.) After starting the scan, click on the scope mode to check the trace and retrace signals if they're overlapping one another as shown in Fig. C.6.

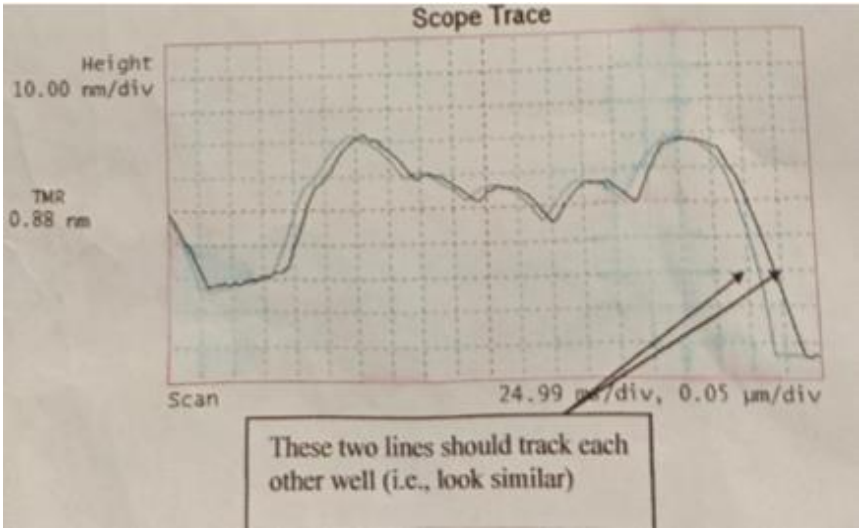

Fig. C.6. Image showing how the trace and retrace line should appear.

11.) If the trace and retrace lines are not as shown in the image, there are many parameters that can be changed such as the Integral gain, Proportional gain, and Amplitude setpoint. The Proportional gain should be twice that of integral gain, and if the trace lines are tracking each other well but not perfectly you can reduce the Amplitude setpoint by factor of one or two. If the trace lines are not tracking at all in the worst case, you can use the extend and retract tip but should be very cautious as it may break the tip if it is extended more than it should be.

12.) If the scan is good, and the image is looking clear, click on the Capture ON icon to capture the image of the sample, and make sure there are no vibrations caused from closing the door or so.

13.) After the capturing is done, the software automatically saves the image and the image can be viewed and any corrections needed can be done using the Nanoscope software.

APPENDIX D

Sample preparation for Scanning Electron Microscope:

A thin layer of gold is deposited using polaron sputter coater equipment to make the samples conductive to study the layer morphology and stacking by a JEOL JSM-6060LV scanning electron microscope.

Fig. D.1. Polaron sputter coater equipment at ODU.

1.) Voltage supply to target
2.) Specimen chamber
3.) Target holder
4.) Vent valve
5.) Mode control
6.) Leak valve
7.) Voltage control
8.) Time setting knob

Procedure

1.) Make sure that the vent valve and leak valve are closed and open the chamber lid.

2.) Place your samples to be coated in the specimen chamber and close the lid.

3.) Turn the mode control knob to PUMP position and the pump starts to vacuum the chamber.

4.) When the vacuum pressure reaches 0.1 mbar, open the Argon gas valve, and then using the leak valve- leak the chamber for 30 seconds, then close the leak valve and wait for the vacuum pressure to reach 0.01 mbar. (Repeat this step for 3 times)

5.) Now, after flushing the chamber with argon gas, turn the MODE selector knob to SET HT, and turn the voltage control slowly to 2.5 KV.

6.) Open the leak valve slowly, such that the current reading shows ~20 mA. At this point you will observe plasma generated in the specimen chamber.

7.) Turn the MODE knob to control and use the timer knob to set time for say 60 seconds, and then press the button on timer. At this point the deposition starts. Maintain the current at 20 mA by using leak valve.

8.) After the timer ends, the deposition process will automatically stop. Bring the voltage back to zero slowly. Close the leak valve completely and bring the MODE to OFF position.

9.) Open the vent valve to vent the chamber and close the Argon gas valve. Your samples will be coated with thin film of Au/Pd depending on the target you use.

The coating film thickness is determined by this simple equation:

$$X = 7.5\ It \qquad \text{(at V= 2.5 kV, and target to specimen distance of 50 mm)}$$

Where, I = current in mA

t = time in minutes

X = Thickness in A^o

APPENDIX E

Scanning Electron Microscope

JEOL JSM 6060 Scanning Electron Microscope is used to study the morphology of samples after coating them with thin layer of Au/Pd using Polaron sputter coater.

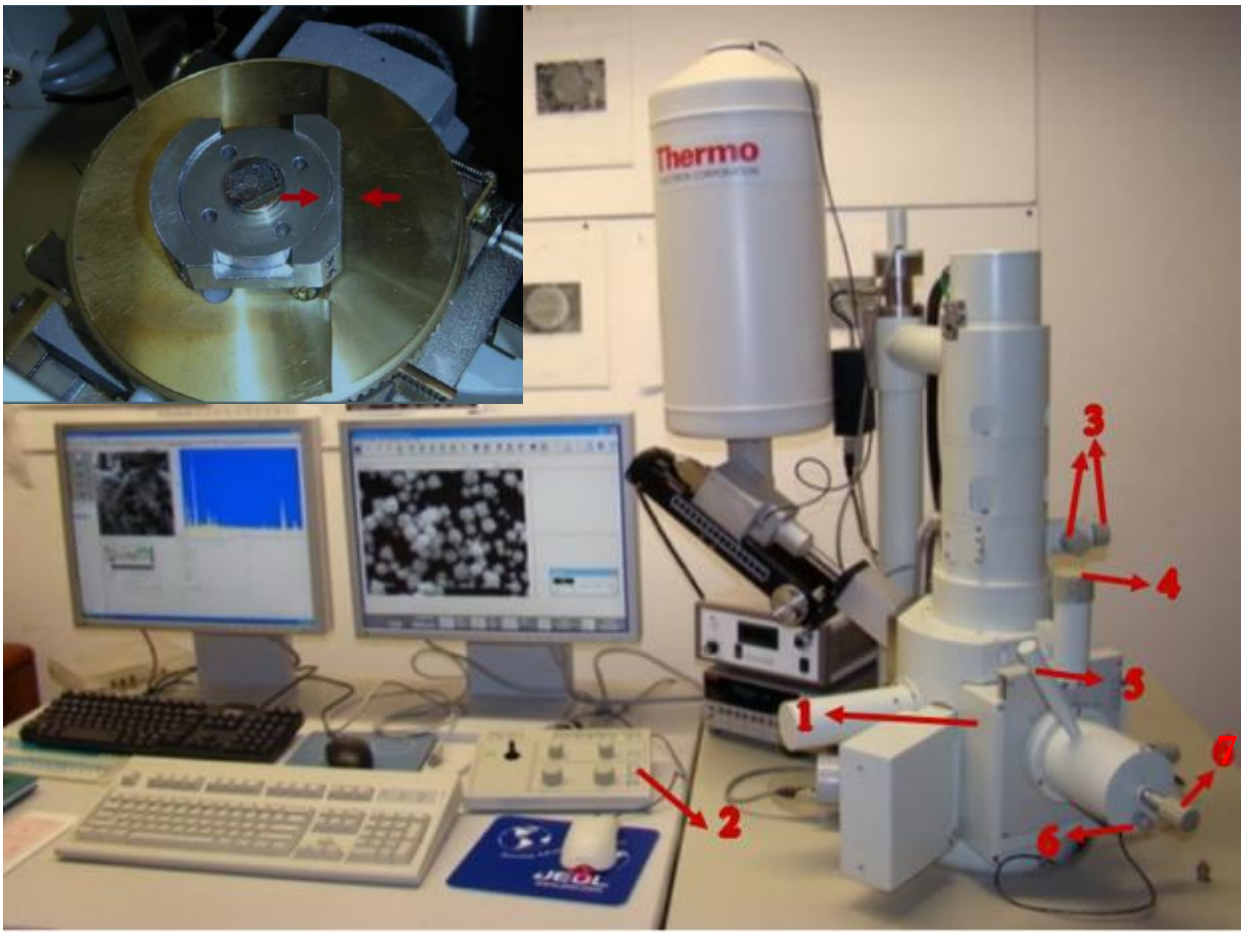

Fig. E.1. Photograph of Scanning Electron Microscope at ODU facility with an inset of sample substrate holder on top left corner.

1.) Stage drawer
2.) Controls for image adjustment
3.) Objective aperture
4.) Working distance knob
5.) Sample stage tilting
6.) Stage rotation
7.) Knob to move stage in X direction (left or right)

Procedure

1.) Turn on the system connected to Scanning Electron Microscope, and then click on the sample icon, a dialogue box appears with VENT and EVAC options. Click on the VENT option and wait for 10 minutes till the chamber vents.

2.) After the chamber is vented, put on gloves and slide the stage drawer out to keep the prepared sample on the sample stage in the direction of dove tail making sure the sample doesn't move inside the chamber.

(a)

(b)

Fig. E.2. (a) Image of tool bar showing options available in SEM software, (b) Image of controls available in the software to control electron beam.

3.) Making sure the sample height is below the detector, slowly slide the stage drawer inside. The sample height should be less than the detector position as it may knock down the detector and will cost >3000$ if done so.

4.) After the stage drawer is closed completely, click on the SAMPLE icon, and click on EVAC option from the dialogue box. This will again evacuate the chamber and vacuum it.

5.) After EVAC is done, click on the READY icon that appears on the top left corner of the software's toolbar. At this point, the electrons are emitted by the cathode, and you can see your sample at a magnification of 30X.

6.) You can change the Acceleration voltage, by clicking on the Acc. Volt icon and select the desired voltage. Generally, to analyze samples deposited with silica nanoparticles acceleration voltage of 15 – 20 KV is used.

7.) Also, the spot size can be changed by clicking on the SPOTSIZE icon and selecting the desired spot size (diameter of electron beam). The trade-off for high acceleration voltage and large spot size is that the image looks clear but doesn't show each and every detail. In my case, the spot size used was 30.

8.) Set the optimum working distance to 10 mm (Specimen to target distance). The working distance can be set by clicking on WD icon and selecting 10 mm. If the specimen is too close to the detector (<10 mm) the image you see is blurred and you should increase the size by turning the working distance knob in clockwise direction. If the distance is large (>10 mm), then the image appears blurry and the working distance knob is to be rotated anti-clockwise direction slowly till the image appears to be focused.

9.) Using the controls, you can zoom the surface, focus, and also set brightness-contrast/ XY stigmatism by selecting the STIG mode on the control.

10.) After magnifying to the desired value (Eg. 5000X), focus the surface till you observe a clear image of the nanoparticles. After focusing the sample, you should check the beam stability in XY direction by clicking on WOBB icon in toolbar. If the beam is not consistent and is moving, then the image although is focused, has its edges blurred.

11.) After clicking on WOBB icon, use the objective aperture lens in XY direction to make the beam constant. After setting the objective aperture lens, click on SCAN 2 icon to go to scanning mode and then click on the STIG button on the control and use the X knob to set stigmatism in the X direction. After correcting the stigmatism in X direction, once again FOCUS the surface by using the FOCUS knob on control. After the surface is focused at its best, correct stigmatism in Y direction and again focus the surface.

12.) After wobbling and stigmatism are corrected, you can now use SCAN 4 (High resolution image scan) to freeze your surface and SAVE it in the desired folder on computer.

13.) After scanning is done reduce the magnification to 30X (or to the minimum) and then click on SAMPLE icon and select VENT option from the dialogue box. Wait for 10 minutes till the chamber vents and pull out the stage drawer and remove the sample holder.

14.) Make sure to close the stage drawer and again EVAC the system before leaving the room.

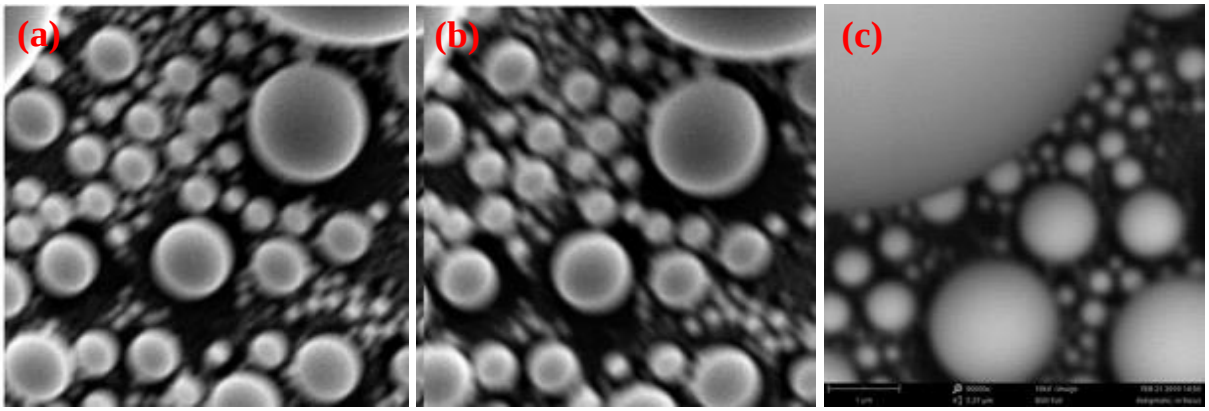

Fig. E.3. Images of Scanning electron microscopy showing (a) over-focused image, (b) under-focused image, (c) astigmatic image of the sample.

APPENDIX F

Solar simulator operation and active area of AOSHIKE solar cell

An Oriel 150 W solar simulator equipped with an AM 1.5 spectral filter was used for solar cell testing under an irradiance of one sun. The solar cells used in this report are purchased from AOSHIKE, and every solar cell has dimensions of 45 mm x 45 mm including frame encapsulating the 4 solar cells which have dimensions ~ 35 mm x 7.6 mm. The schematic of AOSHIKE solar cell is shown in Fig. F.1 (a) One sun is given as input power of 100 mW/cm^2. The schematic of solar simulator is shown in Fig. F.1 (b). with ARC power supply where the intensity of power provided to lamp is set to be 100.

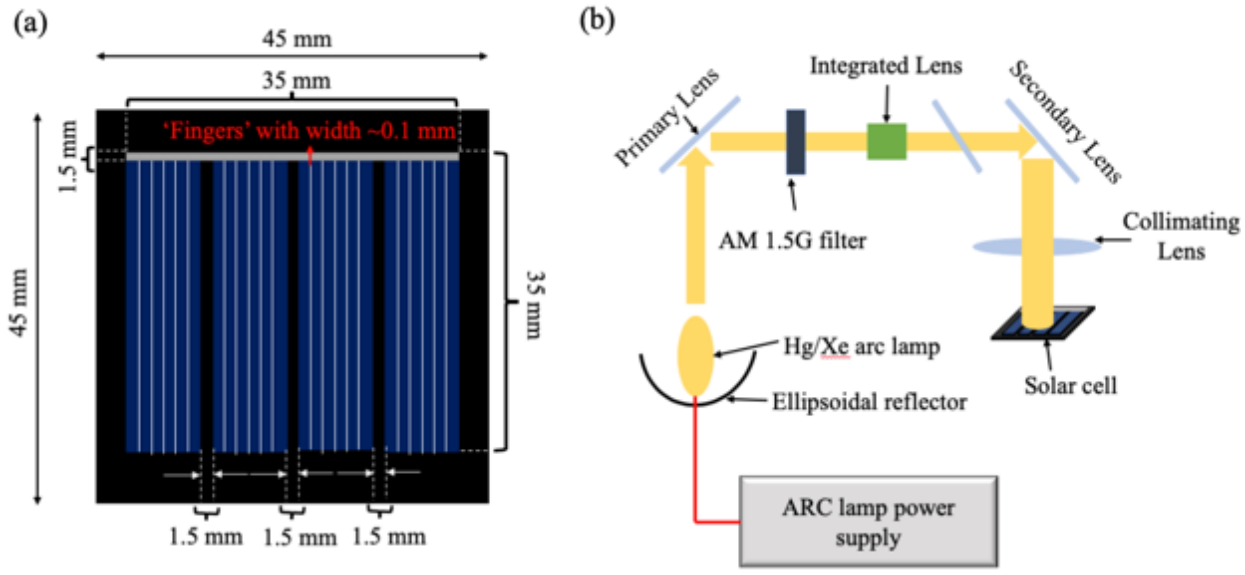

Fig. F.1. (a) Schematic of AOSHIKE solar cell showing the dimensions of actual solar cell and frame encapsulating the solar cells, (b) schematic of AM 1.5 solar simulator showing the ARC lamp power supply connected to Hg/Xe arc lamp

Solar simulator uses a F/1 single element fused silica condenser as collimating lens for a 33 mm diameter collimated light beam at the target. This means that the diameter of light beam coming out from the solar simulator is ~33 mm in diameter (D) and it covers $2\pi r^2$ of the solar cells area; where r = D/2 = 16.5 mm.

The calculations are made based on the area of solar cell covered by light to get the actual efficiency of solar cells. For better understanding we've divided the total area of solar cell into active area and non- active area.

The non- active solar cell areas include ~35 mm x 1.5 mm gap between individual solar cells, and white lines (indicated as 'FINGER' in solar cell terminology) which are ~35 mm x 0.1 mm dimensions. All these non- active region areas are calculated based on the area of light incident on the solar cell. This calculation is done as explained in Fig. F.2.

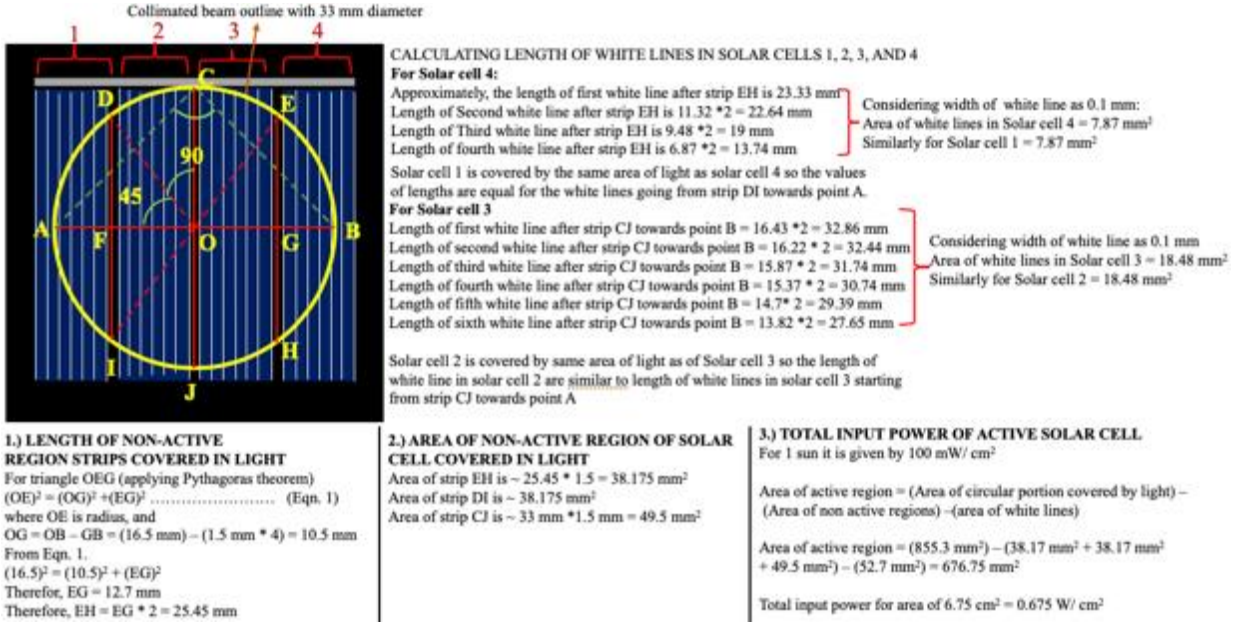

Fig. F.2. Schematic showing the outline of collimated beam (33 mm diameter) covering the surface of solar cell including non-active areas and active areas, and calculations to determine total input power of solar cell.

The solar cell is placed under the light such that the collimated beam is centered on the solar cell as shown in Fig. 2. The calculations are done based on the geometric and Pythagoras theorem. An example is illustrated considering one part of the solar cell covered in light in Fig. F.3. Considering the collimated light beam having its center at 'O', and the length 'OC' is 'r' which is equal to 16.5 mm.

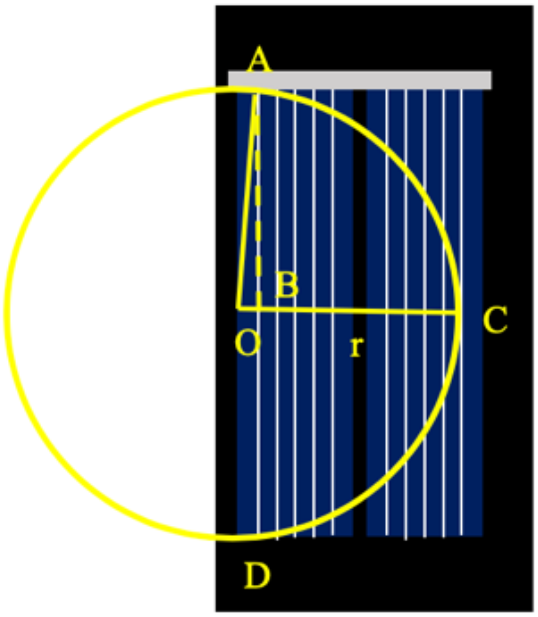

To determine the length of white line 'AD', according to Pythagoras theorem;

$(OA)^2 = (AB)^2 + (OB)^2$
Where, OA = radius, OB = active solar cell width = 1.5 mm, and AD = 2 * AB.

$(16.5)^2 = (AB)^2 + (1.5)^2$
$(AB)^2 = 270$
$AB = 16.43\ mm$

Therefore, length of AD = 2 * AB = 32.86 mm

Fig. F.3. Schematic showing the collimated light beam covering two individual solar cells to calculate the length of first line covered inside the collimated beam.

Similarly, the length of all other white lines is calculated as per addition of width of active solar cell in between the white lines.

After calculating each and every line area, and gaps between the individual solar cells – these areas are removed from the total area of solar cell covered under the beam as shown in point 3 in Fig. F.2. and the active area covered under solar cell responsible for input power is 676.75 mm^2.

To calculate the total input power:

The input power for efficiency calculations is given as 100 mW/ cm^2. So, for 6.76 cm^2 the input power is 676 mW/cm^2.

Let us calculate the efficiency of uncoated solar cell from Table. 6.1.;

$$\eta = V_{oc} I_{sc}\ FF/\ P_{in} \qquad \text{(Eqn. F.1)}$$

η = 10.92 % = ~ 11 %

VITA

Akbar Ali Syed

2117 Engineering Systems Building
ECE Department
Old Dominion University
Norfolk, VA 23529

Education

2020	**M.S.**	Electrical & Computer Engineering	Old Dominion University, VA
2017	**B.TECH.**	Electronics & Communication Engineering	JNTU Kakinada, India